EUROPEAN ORGANISATION FOR NUCLEAR RESEARCH

CERN-PPE/92-126
01 July 1992

THE CRYSTAL BARREL SPECTROMETER AT LEAR

THE CRYSTAL BARREL COLLABORATION

E Aker[12,(a)], C Amsler[12], I Augustin[5], C A Baker[10], B M Barnett[12,(b)], C J Batty[10], R Beckmann[4], P Birien[1], J Bistirlich[1], P Blüm[5], R Bossingham[1], H.Bossy[1], K Braune[8], D V Bugg[9], M Burchell[3], T Case[1], S Cierjacks[6], K M Crowe[1], K Dederichs[8], M Doser[3], W Dünnweber[8], H Emerich[8], D Engelhardt[5], M A Faessler[8], C Felix[8], G Folger[8], J Friedrich[4], R Hackmann[7], R Haddock[2], H Hammer[7], F Heinsius[4], N P Hessey[10], P Illinger[8], D Jamnik[8], H Kalinowsky[7], B Kämmle[4], T Kiel[4], E Klempt[7], H Koch[5,(c)], C Kolo[8], K Königsmann[8], F Krennrich[8], M Kunze[5,(c)], R Landua[3], J Lüdemann[7,(c)], H Matthaey[5,(c)], M Merkel[7], J P Merlo[7], C A Meyer[12], U Meyer-Berkhout[8], L Montanet[3], A Noble[12], K Peters[7,(c)], W Rohrbach[5], A H Sanjari[9], E Schäfer[7], B Schmid[12], W Schott[5], K Sidiropoulos[4], S Spanier[7], A Staude[8], Chr. Strassburger[7], U Strohbusch[4], M Suffert[11], C Sutton[5], D Urner[12], C Völcker[8], D Walther[5,(c)], S Walther[7], Ch. Weddigen[6], U Wiedner[4], N Winter[5], J Zoll[3], C Zupancic[8].

[1]University of California, LBL, Berkeley, CA 94720, USA
[2]University of California, Los Angeles, CA 90024, USA
[3]European Laboratory for Particle Physics, CERN, CH-1211 Genève, Switzerland
[4]Universität Hamburg, D-2000 Hamburg, Germany
[5]Universität Karlsruhe, D-7500 Karlsruhe, Germany
[6]Kernforschungszentrum Karlsruhe, D-7500 Karlsruhe, Germany
[7]Universität Mainz, D-6500 Mainz, Germany
[8]Universität München, D-8000 München, Germany
[9]Queen Mary and Westfield College, London E1 4NS, UK
[10]Rutherford Appleton Laboratory, Chilton, Didcot OX11 0QX, UK
[11]Centre de Recherches Nucléaires, F-67037 Strasbourg, France
[12]Universität Zürich, CH-8001 Zürich, Switzerland

ABSTRACT

The crystal barrel spectrometer used at LEAR, CERN to study the products of $\bar{p}p$ and $\bar{p}d$ annihilations is described. A 1380 element array of CsI crystals measures photons from the decay of π^0, η, η' and ω mesons. A segmented drift chamber in a 1.5 T magnetic field is used to identify and measure charged particles. A fast on-line trigger on charged and neutral multiplicities and on the invariant mass of secondary particles is available. The performance of the detector is discussed.

(a) Present address: Zöffelverfahrenstechnik GmbH, D-7500 Karlsruhe, Germany.
(b) Currently with the University of Mainz.
(c) Present address: Universität Bochum, D-4630 Bochum, Germany.

For Publication in Nuclear Instruments and Methods

1 INTRODUCTION

The study of $\bar{p}p$ annihilations began some thirty years ago with bubble chambers at LBL, CERN and BNL, and has since been pursued at these laboratories together with Serpukhov and KEK. The advent of the Low Energy Antiproton Ring (LEAR) facility at CERN, with its intense and extremely pure $\bar{p}$ beams, enables the quality of the data to be further improved. Several mesonic resonances were seen for the first time in $\bar{p}p$ interactions, and at least two candidates for exotic states ($\eta(1430)$, $f_2(1565)$) have been reported [1]. The final states consist mainly of charged pions and kaons, together with photons that have originated in most cases from the decay of short lived particles such as π^0, η and ω. However, all experiments to date have suffered from a lack of adequate detection facilities for γ's, so that only 40% of all annihilation channels (those with at most one π^0 or η) could be investigated in detail.

With this in mind the Crystal Barrel Spectrometer (CBAR) for the measurement of charged particles (pions, kaons) and photons has been constructed and installed at LEAR. The spectrometer covers almost the full 4π solid angle and is optimized to investigate $\bar{p}p$ and $\bar{p}n$ annihilation reactions at rest and in flight up to the maximum LEAR momentum of 2 GeV/c. The detector is the first to allow a kinematically complete reconstruction of complicated final states involving charged and neutral particles in $\bar{p}p$ annihilation reactions at low incident momenta. Typical processes are: $\bar{p}p \rightarrow \pi^+\pi^-\pi^0(\pi^0 \rightarrow \gamma\gamma)$; $\bar{p}p \rightarrow \eta\eta$ $(\eta \rightarrow \gamma\gamma)$; $\bar{p}p \rightarrow K^+K^-$; $\bar{p}p \rightarrow \omega\eta$ $(\omega \rightarrow \gamma\pi^0)$; $\bar{p}p \rightarrow f_2(1565)\pi^0$ $(f_2(1565) \rightarrow \pi^0\pi^0)$. Very crucial for the detector system is a fast on-line trigger on charged and neutral multiplicities and on invariant mass combinations of the secondary particles. This allows the suppression of well known channels and enhancement of rare channels of specific interest.

The interest in $\bar{p}p$ and $\bar{p}n$ reactions is twofold. Firstly, to measure branching ratios and cross sections for the primary reactions and to understand them in terms of theoretical descriptions, which can be either conventional (meson/baryon exchange) or in terms of a quark-gluon picture. The latter is of particular interest, as QCD is not well tested in this low energy domain [2]. Secondly, to study the spectroscopy of meson resonances. This includes the confirmation of well known meson resonances in decay modes which have not previously been explored, and a search for non-$\bar{q}q$ states (exotics), such as glue-balls, hybrids and multi-quark states, candidates for which have already appeared in earlier $\bar{p}p$ experiments or in other reactions [3]. Many of the exotics are expected to decay into neutral channels such as $\pi^0\pi^0$ or $\pi^0\eta$, so that a good capability for the detection of γ's and for their invariant mass reconstruction is vital for such investigations.

The detector has been operational at LEAR since the end of 1989 and has now produced its first results [4]. It is intended to stay at LEAR for several years in order to explore fully $\bar{p}$ annihilation reactions on liquid and gaseous hydrogen and deuterium targets both at rest and in

flight. A later use on other accelerators such as Super LEAR or a ϕ-, B- or τ-charm factory is also possible.

2 APPARATUS

2.1 Overall description

The overall layout of the apparatus is shown in fig. 1. Antiprotons from LEAR, in the momentum range from 0.1 to 2.0 GeV/c, enter the solenoidal magnetic field along its symmetry axis. The magnet provides a maximum field of 1.5 T for the momentum analysis of charged particles.

Antiprotons of 0.2 GeV/c stop in the 44 mm long liquid hydrogen target (6 in fig. 1). Antiprotons of higher momenta are used for in-flight measurements. In both cases the antiprotons leave the LEAR beam line and vacuum system through a thin beryllium window which is immediately followed by beam defining counters. A silicon counter in front of the liquid hydrogen target provides a first trigger for valid events.

Two concentric cylindrical multi-wire proportional chambers (PWC) (5 in fig. 1) are used to obtain the multiplicity of charged particles and provide a fast trigger on K^0_S decays by detecting a change in multiplicity between the inner and outer chambers.

A cylindrical jet drift chamber (JDC) (4 in fig. 1) surrounds the proportional chambers. The drift chamber has 30 sectors, each containing 23 sense wires which are staggered by $\pm$ 200 μm to resolve the left/right ambiguity. With a spatial resolution (σ) of 130 μm for each of the 23 measurements of track coordinates, a momentum resolution (σ) of between 2% and 12% is obtained for transverse momenta between 0.1 and 1.0 GeV/c. In addition, measurements of pulse-height can be used to distinguish between charged pions and kaons for momenta below 0.5 GeV/c. The z-coordinates of tracks are measured by charge division with a precision (σ) of 7 - 9 mm.

A barrel-shaped, modular electromagnetic calorimeter (3 in fig. 1) surrounds the drift chamber and has 1380 elements. The CsI crystals, 30 cm long corresponding to 16.1 radiation lengths, are each viewed by a single photodiode mounted on the edge of a wavelength shifter placed on the rear end of the crystal. This configuration improves the light collection between the output of the CsI crystal and the photodiode. Each crystal covers 6° in θ (polar angle) and 6° in ϕ (azimuthal angle) except for the two sets of three layers closest to the beam axis where the angular acceptance is increased to 12° in ϕ. The range of polar angles covered by the complete calorimeter is $12° \leq \theta \leq 168°$.

The top and bottom of the magnet yoke are covered by a scintillation counter hodoscope which is used to trigger on cosmic ray muons. These are used for testing the proportional and jet drift chambers and also the CsI detectors between running periods.

For experiments with stopping antiprotons the liquid hydrogen target and surrounding proportional chamber can be replaced by a hydrogen gas target. Whereas in liquid hydrogen the majority of stopped antiprotons annihilate from atomic S-states ($\mathbb{L} = 0$), in hydrogen gas at STP the number of annihilation events with $L = 0$ and $L = 1$ (atomic P-states) are roughly equal [5]. By comparing results obtained with liquid and gaseous targets the initial angular momentum state for particular classes of annihilation events from stopped antiprotons can be determined.

2.2 The magnet

The magnet is a conventional solenoid which produces a maximum field of 1.5 T at the centre of the cylindrical inner volume containing the electromagnetic calorimeter and wire chambers. This inner volume has a length of 157 cm and a diameter of 153 cm. The solenoid is encased in a box-shaped flux return yoke (fig. 1).

The inner part of the iron yoke, originating from the DM1 magnet once used at the DCI collider (Orsay) and later employed in the ASTERIX experiment [6] at LEAR, was surrounded by additional iron sheets of 4 and 3 cm thickness, separated by a 3 cm air gap, to provide sufficient magnetic shielding for the stronger field (maximum 1.5T) from the new aluminium coils. (The maximum field strength of the old magnet was 0.8 T). The yoke consists of three parts; the central yoke surrounding the solenoid and two endplates. Both endplates are subdivided into two halves and suspended on rails. The two halves can be moved apart to allow free access to the inner volume from both ends. All cables and cooling hoses for the detector and liquid hydrogen target are fed through circular openings of 48 cm diameter in the endplates.

The aluminium coil consists of 24 double pancakes each of 17 turns. The pancakes are connected hydraulically in parallel and electrically in series outside the magnet to give a total of 408 turns. Sets of six double pancakes of the coil are packed between 1 cm thick stainless steel plates which rest on the central yoke. Thus the coil is subdivided into four modules. This package of four coil modules and five steel plates is clamped together with eight longitudinal steel rods. The cross-section of the conductor is 29 x 31 mm^2 with a bore of 13.5 mm diameter for the cooling water. The ends of the 48 conductors pass through holes in the central yoke at one side. The operating conditions at the maximum field value of 1.5 T require a supply voltage of 500 V and current of 4848 A, to give a total power consumption of 2.42 MW. The cooling water flow is 70 m^3/h for pressures of 26 bar and 3 bar at the entrance and exit, respectively. At full field the temperature difference between the incoming and outgoing water is 30° C. A layer of 3 cm thick thermal insulation covering the inside of the coil reduces the heat

flow from the coil to the detector inside. Four flow sensors and a water temperature monitor are connected to an electrical interlock system. Local temperatures are monitored with 34 sensors placed at various positions on the coil.

The excitation curve was measured between 0.90 T and 1.54 T with a nuclear magnetic resonance probe and shows only a small saturation at the highest fields:

$$B[\text{Tesla}] = 0.31715\, I + 0.00437\, I^2 - 0.00123\, I^3 \qquad (1)$$

where I is the magnet current in kiloamps.

Field maps for all three components of the magnetic field $\vec{B}$ were measured over an inner central volume of 30 cm diameter and 160 cm length along the cylinder axis using Hall probes in order to verify the homogeneity of the field in the region where the JDC operates and to obtain a parametrization of the field. The homogeneity satisfied the design specification for the magnet; at 1.5 T the variations of the z component of the magnetic field within the JDC volume are less than $\pm$ 1.5%. The following parametrizations describe the field over this region. (The z axis coincides with the nominal cylinder axis and has its origin at the centre of the JDC, the r coordinate refers to the distance $r = \sqrt{x^2 + y^2}$ from the z axis; z and r are measured in cm):

$$B_z\,[\text{Tesla}] = (15003 - 0.28\, z^2 + 0.14\, r^2)/10^4$$

$$B_r\,[\text{Tesla}] = 0.28\, z\, r/10^4.$$

Embedded in the coil is the mechanical support for the crystal barrel. It consists of two high precision rails positioned parallel to the cylinder axis of the magnet and carrying the crystal barrel which weighs 4 tons. The rails rest on the five half-ring steel plates which support the four coil sections. The high precision rails are adjustable both in height and in the longitudinal direction. The corresponding rails of a support trolley outside the magnet can be attached so that the crystal barrel can be rolled in or out of the magnet. Transport and handling of the barrel, which can be split into two halves for repairs and for access to the PWC and JDC, is done by means of two trolleys which move on rails fastened to the floor.

2.3 Antiproton beam, counters and hydrogen target

The antiproton beam is extracted from LEAR at momenta in the range 0.1 to 2.0 GeV/c with spills that can last for up to about 3 hours, after which refilling from the Antiproton Accumulator (ACOL) is necessary. Typical beam intensities are in the range 10^4 to 10^6 $\bar{p}$/s depending on whether measurements for stopping antiprotons or interactions in flight are being made.

The beamline from LEAR leading to the Crystal Barrel experiment includes two splitters which allow sharing of the extracted beam with other experiments. The antiproton rate at the target required by the Crystal Barrel experiment for stopped $\bar{p}$ reactions does not exceed a few 10^4 $\bar{p}$/s. If the other experiment requires high $\bar{p}$ intensity the extracted beam from LEAR can easily supply 10^6 $\bar{p}$/s. With such sharing, the beam sent to the Crystal Barrel experiment consists mostly of the outer "fringe" of the extracted beam. Therefore, in spite of the fact that theoretically the splitting should reduce the emittance of the split beam, it is difficult to determine exactly the characteristics of the beam that enters the experiment. Nevertheless, more than 90% of this beam can be focussed on the counter S_1 located at the end of the LEAR vacuum tube. (See fig. 2).

The requirement that the PWC be as close as possible to the annihilation vertex requires a special design for the liquid hydrogen target vacuum chamber, with the separation between the LEAR and the target vacuum located 35 cm upstream with respect to the target centre (See fig. 2). In this region the beam passes successively through a 100 μm beryllium window at the end of the LEAR vacuum, a beam-defining counter S_1 and a 50 μm Mylar window at the entrance to the target vacuum. The volume between the two windows is filled with air at normal pressure. For stopping antiproton experiments where a 200 MeV/c beam is used, the counter S_1 is an 18 mm diameter disc of scintillator, 100 μm thick, surrounded by a 35 mm diameter annulus of 3 mm thick scintillator. The whole arrangement is viewed through 1 m long Plexiglass light guides by four 15 mm diameter photomultipliers located outside the magnetic field. Discrimination between the small pulses from the central thin scintillator and the larger pulses produced by the surrounding annular counter provides information for beam steering and focussing. For measurements of in-flight interactions in the momentum region 0.6 to 1.9 GeV/c, the counter S_1 can be replaced by a thicker (1-3 mm) scintillator. In a recent experiment at 1.2 GeV/c, a fast multi-wire proportional counter of compact geometry was used successfully in place of S_1. Intrinsic efficiencies close to 100% were reached with each of these counters; this was checked by means of coincidences with other beam counters.

A segmented silicon diode just before the liquid hydrogen target (fig. 2) operates as a $\bar{p}$ transmission counter and defines beam particles that produce events inside the target volume as well as enabling the position and focus of the beam to be optimised. The counter also gives the start signal for the drift time measurement in the JDC and opens the gate circuits for the CsI detectors and PWC. At a $\bar{p}$ momentum of 200 MeV/c, only about 40% of the antiprotons counted by scintillator S_1 hit the silicon counter due to multiple scattering in the vacuum windows and scintillator S_1. At higher momenta this geometrical efficiency increases to about 80%. The intrinsic efficiency of the counter is measured to be consistent with 100%.

In the first round of experiments at 200 MeV/c beam momentum, the Si counter ($Si_{2\text{-}5}$ in fig. 2) consisted either of four 3 x 3 mm^2 PIN diodes with implanted P and N layers [7] glued

onto a 12 μm aluminized Mylar foil, or an approximately circular (~ 9 mm diameter) surface-barrier detector of large area (50 mm^2), adapted to the size of the entrance window of the target. By etching the gold surface layer of the surface barrier detector, the anode was divided into four sectors which are read out separately [8]. Both silicon detectors were about 200 μm thick resulting, for antiprotons with 200 MeV/c momentum (21 MeV kinetic energy), in an average energy loss of 0.9 MeV and a multiple-scattering angular spread of 0.6° (planar rms width). In some runs an additional 200 μm thick, 3 x 3 mm^2 Si counter Si_1, placed 5 mm before the group of four counters Si_{2-5}, was used for beam focussing and, if required, as an additional trigger to define interactions occuring close to the beam axis.

The silicon counter (Si_{2-5}) is located 28mm in front of the liquid hydrogen target window and attached to the target frame by a thin Vespel holder. Heat conduction through the detector support and signal cables, results in an operational temperature of -100°C, whilst the leakage current and the noise of the detector are considerably reduced relative to the values at room temperature. The signals are fed through 1 m long cables to fast preamplifiers which are followed by timing filter amplifiers providing a signal height of 300 mV for a 1 MeV energy loss. An uncertainty in the trigger time of less than 0.5 ns arises from the signal to noise ratio and the rise time of the signals. The radiation damage accumulated in the first runs did not affect the performance of the Si counters. After a total of 50 days of bombardment with 10^3 to 10^4 $\bar{p}$/s on each PIN diode, it was found that the leakage current increased by less than 5 nA at the operational temperature. The performance of the surface-barrier detectors was also not affected after 20 days of beam time. In test experiments [9] with protons from the Munich Tandem accelerator, PIN diodes were found to be still operational below 0°C after exposure to doses above 100 kGy, corresponding to 3 x 10^{13} $\bar{p}/cm^2$ at 200 MeV/c.

For in-flight measurements the silicon detector can be replaced by a similar four-quadrant detector of thickness 1 mm. A 25 mm diameter scintillator (S2) or a 28 mm diameter silicon counter, located ~ 20 cm downstream from the target, provides a veto signal for antiprotons that do not interact in the target.

The liquid hydrogen target is 17 mm in diameter and 44 mm long with a 10 mm diameter entrance window. At a momentum of 200 MeV/c, the incident antiprotons stop in the region of the target centre with a longitudinal spread (σ) due to range straggling of 0.6 mm. For in-flight measurements the fraction of antiprotons that interact in the liquid hydrogen decreases from 1.4% at 0.6 GeV/c to 0.8% at 1.9 GeV/c.

It is also planned to use a hydrogen gas target in place of the liquid target. Antiprotons stopping in gas have a higher probability of annihilating from P-wave orbitals of the $\bar{p}$-p atom formed after the antiprotons have come to rest (see section 2.1). The target (fig. 3) is a cylinder of 420 mm length and an outer diameter of 81 mm made from 0.5 mm thin aluminium tube.

The entrance opening of 60 mm houses the antiproton entrance counter, a small gas chamber operated at 70 Torr (isobutane) in the avalanche mode [10]. The opposite end of the target is closed by a Mylar window (diameter 47 mm). At a beam momentum of 100 MeV/c, more than 90% of the antiprotons are expected to stop inside the target. The maximum pressure for the H_2 gas is restricted by the mylar foil to 1.5 bar.

When the gas target is used, the PWC is replaced by a scintillating fibre detector [11]. This detector consists of 3 layers, each of 252 scintillating fibres (total 756 fibres), glued on to the tube of the gas target and parallel to the beam axis. At the front of the target each fibre is connected to a simple light conducting fibre. The readout of these fibres is done outside the magnet by two position-sensitive photomultipliers (Valvo XP4702), each with a 64 channel, segmented dynode and a common anode.

The fibre counter is divided into 126 sectors. Each sector of 5 fibres is connected to one pixel of the photomultiplier and contains two fibres from each of the outer and inner layers and one from the middle layer. (In the middle layer only every second fibre is used). The efficiency for detecting a passing minimum ionizing particle is 82% and each sector covers an angle of 2.8° in the plane perpendicular to the beam axis. Multiple scattering by the aluminium cylinder and the scintillating fibres (for a typical particle of 450 MeV/c) contributes 250 μm to the uncertainty in the vertex reconstruction. Each channel from the photomultiplier is amplified and connected to a LeCroy PCOS III signal and data processing system. The common anode signal is used as a fast trigger for the start of data acquisition.

2.4 The proportional wire chambers

Two cylindrical proportional wire chambers, C_1 and C_2, provide additional (r,ϕ) coordinates close to the annihilation vertex and also the trigger for the final-state charged multiplicity. Figure 4 shows the mechanical construction of the inner chamber (C_1). The design for C_2 is similar. Because of a lack of space in which to accommodate preamplifiers, there is no cathode readout and hence no z information. The anode wires (15 μm diameter gold-plated tungsten) run parallel to the magnetic field axis at radii of 25.5 and 43 mm, respectively. The inner chamber has 90 anode wires and the outer chamber 150 wires, both with a wire pitch of 1.8 mm and a wire length of 35 cm. The wires are strung with a mechanical tension of 0.30 N. The cathode cylinders, 3.5 mm from the sense wires, are made of aluminium foils, 22 μm thick. The (negative) high voltage is applied to the cathode foils. The chamber walls are made of 1 mm Rohacell sandwiched between the cathodes; 50 μm thick aluminized Kapton foils (0.2 μm aluminium deposit) provide the external shield at ground voltage. The end flanges that hold the sense wire printed circuits and supply the high voltage and gas lines are made of fibreglass-reinforced epoxy (Stesalit AG). The outermost diameters of C_1 and C_2 correspond to solid angles of 99% and 97% of 4π respectively. The thickness of material in C_1 and C_2 traversed by a particle emerging at right angles to the beam is 2.2×10^{-3} radiation length.

The chambers run with a gas mixture of 69.5% argon, 30% ethane and 0.5% Freon, R13B1 ($C Br F_3$), and the gas flow is about 1 l/h. A smaller ethane fraction would lower the high voltage required for full efficiency but would increase the width of wire clusters. The detection efficiency was measured with a ^{106}Ru electron source. Full efficiency ($\geq 99\%$) for minimum ionizing particles is reached at 2450 V for a current threshold of 3.5 μA. C_1 and C_2 are operated at a nominal voltage of 2550 V. The average cluster width is typically 1.6 wires.

When the Crystal Barrel detector is moved into the magnet, a 17 mm diameter CCD camera (Panasonic WV-CD1E) is slid into the barrel cavity through the downstream pipe to monitor the insertion of the liquid hydrogen target into the inner proportional chamber. Light is provided by a light fibre system.

2.5 Drift chamber

Tracking information for charged particles is given by the cylindrical drift chamber (JDC) shown schematically in fig. 5. It also provides information on charged particles from photon conversions before, or in, the chamber and on backscattered charged particles from the barrel calorimeter. The JDC has a jet-chamber type of drift cell [12] and is divided into 30 azimuthal sectors and 23 radial layers with 8-mm spacing. This segmentation keeps drift times relatively short and allows sufficient ionization samples for good dE/dx resolution so as to give $\pi^{\pm}/K^{\pm}$ separation up to about 500 MeV/c. The inner (outer) sense wires are at a radius of 63 mm (239 mm), with a sensitive length of 399 mm, giving a detection solid angle equal to 95% of 4π. A track fit requires at least three layers, resulting in a 93% coverage for tracking.

The wires are positioned with 40 μm rms accuracy. They are crimped into gold-plated, brass pins; an impact-resistant cyanacrylate glue gives a gas seal. Delrin bushings, molded around the pins, are glued into holes in the aluminium endplates. The 20 μm diameter sense wires are made of a resistive, 29.7 Ω/cm, stainless steel (Elgiloy), which allows the determination of axial position through charge division, and are strung at a tension of 0.39 N; a ± 200 μm azimuthal staggering resolves the usual left/right ambiguity. The grounded sense wires are alternated on the sector midplane with guard wires, at -2318 V, which control the gas gain. The guard and field wires (2430 in all) are 152 μm diameter aluminium, coated with 0.64 μm of gold, and are strung at a 1.7 N tension. All wire tensions were verified with a (slightly modified) Metrimpex NE-660A tension meter, which measures the frequencies of the wires vibrating in a 0.15 Tesla transverse magnetic field.

Field wires on the sector boundaries are electrically paired radially to simplify voltage distribution; this has little effect on field homogeneity. Voltages on these pairs increase almost linearly with radius, so as to maintain (except for the area within about 4 mm of the sense wire) a fairly homogeneous drift field of 1000 V/cm; the voltages were chosen with the help of the

GARFIELD [13] drift chamber simulation program. Kapton printed circuit artwork on some inner chamber surfaces helps to define boundary conditions: equipotential lines at the endplates reduce the field distortion there, while strips on the outer shell are kept at a voltage which is low enough to collect most electrons from ionization beyond the outermost drift cell, while not distorting the field as much as would the grounded shell.

To minimize the volume of CsI(Tℓ) required for the calorimeter, the JDC is made compactly, fitting within a length x diameter of 535 mm x 535 mm. It is also a relatively low-mass device. The inner cylinder of the JDC is a 0.73 mm thick carbon fiber/epoxy composite. Thin aluminium foil fixed to its inner surface shields against electrical noise from high impedance or plane waves, while its outer surface is insulated with Kapton. The total thickness of the cylinder corresponds to 0.0025 radiation lengths (L_R) for radial trajectories, still dominating the 0.001 L_R thickness of the gas mixture or the 0.007L_R thickness (average) of the wires. The outer shell is 2.03 mm thick aluminium. Its thickness, including the cables, etc. beyond it, corresponds to 0.03L_R (average), while the mass at the JDC ends (endplates, electronics, etc.) corresponds to 0.20 L_R. The aluminium endplates are 5.7 mm thick over most of their area, though thicker at their inner and outer radii. The relative thinness required that they be pre-stressed before being strung with wire. The inner cylinder, although load bearing, is replaceable. Thus, at a later stage, a beryllium cylinder could replace the present one. Similarly, the outer shell can be removed to allow access for repairs, although replacement wires are normally threaded through the assembled chamber.

The "slow" gas used is a 90:10 mixture of CO_2/isobutane (C_4H_{10}) [14,15] at ambient pressure (~ 0.96 ± 0.02 standard atmospheres at CERN) and at a regulated temperature of 25°C. There are no additives (e.g., water or alcohol vapour) to the gas, since significant radiation damage is not expected under our operating conditions. For an 1000 V/cm electric field and 1.5 T magnetic field, the electron drift velocity is 8.4 μm/ns, and the Lorentz angle is 7.2°; calculated drift lines and isochrones are shown in fig. 6. The single-pass gas system continually flushes the 80.3 ℓ chamber volume with ~ 10 ℓ/h of gas. CO_2 and isobutane from the CERN gas system (with the CO_2 first filtered through an Oxysorb cartridge to remove oxygen impurities) are mixed in a ratio controlled with Edwards/Datametrics 825 mass flowmeters and a type 1605 controller. Absolute pressure is monitored by an Edwards/Datametrics 590A barocell sensor and a type 1450 readout. The oxygen contamination of the exhaust gas is monitored with a Teledyne 310 analyser.

Since the electron drift velocity under our conditions is inversely proportional to the gas density, as well as being sensitive to composition, it is necessary that the temperature, gas mixture and pressure be known to fair accuracy. For example, for a maximum position error of 30 μm from each factor, one must know the temperature to ± 0.36°C, the CO_2 content to ± 0.15% and the absolute pressure to ± 0.12%. The first two quantities are controlled and

monitored, while the pressure is recorded to allow later correction. In addition, a monitor chamber directly measures drift velocity and gas gain in the JDC exhaust gas.

2.5.1 Monitor drift chamber

A small monitor drift chamber (MDC) receives the exhaust gas of the JDC and directly measures the changes in drift velocity [16]. The MDC has also been used for a precision measurement of the dependence of drift velocity on pressure, temperature and gas mixture [17]. It operates at approximately the same drift field as the JDC. The MDC, however, is connected to the JDC exhaust gas via a 10 m long copper pipe and is outside the magnet. It therefore has a gas temperature which is in general different from that of the JDC and so the drift velocity changes as measured in the MDC cannot be directly applied to the JDC but have to be corrected for the temperature difference.

A schematic drawing of the MDC is shown in fig. 7. The chamber consists of a cylindrical drift volume of 3.5 cm length and 3 cm diameter, and a proportional chamber containing 9 signal wires. This set-up is contained in a steel chamber which can be evacuated for a quick exchange of the gas. The steel chamber has a quartz window on the top and a Mylar window at the bottom which are aligned with the axis of the drift volume. The beam of a pulsed N_2 laser (λ = 337 nm, pulselength about 3 ns), which is situated on top of the steel chamber, enters through the upper quartz window, hits an aluminized Mylar foil covering half the entrance aperture to the drift volume and then a second Mylar foil across the exit aperture of the drift volume.

Electrons released by the laser light pulse from these two locations drift down along the axis of the cylindrical drift volume, finally reaching the proportional chamber where they are amplified. The proportional chamber is electrostatically separated from the drift volume by a cathode grid. The distance between the upper Mylar foil and the lower foil is accurately known, hence the drift velocity can be determined from the time difference between the arrival of the two electron pulses in the PWC. The PWC output signal is fed through a discriminator into a common multihit TDC whose start signal is provided by a photodiode which detects the light reflected from a third quartz window mounted outside the steel chamber. The two PWC signals are measured by separate ADC's which are gated on during the corresponding arrival times of the two pulses.

Diffusion broadens the pulse with the longer drift time (upper foil) relative to the shorter drift time pulse; thus the measured time difference between the two pulses depends not only on the drift velocity but also on the discriminator threshold and pulse height. By correcting for the latter two, the absolute drift velocity can be measured to a precision better than 0.05%. For a maximum drift length of 2.7 cm, this corresponds to an uncertainty in position of 15 μm.

2.6 The electromagnetic calorimeter

The electromagnetic calorimeter is designed to provide high-efficiency photon detection with good energy and spatial resolution over an energy range from 20 MeV to 2000 MeV in order to enable the reconstruction of π^0, η, η' and ω from $\bar{p}p$ annihilations. This requires a modular detector system covering a solid angle of almost 4π (fig. 1). It consists of 1380 individual modules arranged in a vertex-pointing geometry over the range of polar angles from 12° to 168°. The modules have the shapes of truncated pyramids with dimensions determined by the polar angle of the module. Thus 13 different crystal shapes are needed. As the detector operates in a high magnetic field (1.5 T), readout of the scintillation light with photomultiplier tubes is excluded and silicon photodiodes are used.

We have chosen for the photon detector thallium doped CsI crystals which have similar scintillation properties to NaI, the standard scintillator for high-resolution photon detection, but a shorter radiation length. Table 1 summarizes the properties of CsI(Tℓ) scintillator. The long decay times of the scintillation light from CsI(Tℓ) are actually less serious than first appears. As silicon photodiodes do not have any internal amplification a charge integrating amplifier with integration times of order 1 μs must be used to minimize noise. Unlike NaI(Tℓ), the scintillator is only slightly hygroscopic and this together with the better mechanical properties of CsI(Tℓ) are important features that simplify the problems of mechanical support.

The shower containment and hence the energy and spatial resolutions depend on the crystal dimensions. As a compromise between good energy resolution at high energies and mechanical problems due to the weight of the crystals and available space, we have chosen a length of 300 mm (16.1 L_R) for the crystals. Thus most of the longitudinal shower energy of a 2 GeV photon is contained in the crystal and the degradation of the energy resolution due to fluctuations in leakage from the rear of the crystal is less than 1% [18].

The choice of transverse dimensions for the crystals is a trade off between physics aims and financial limitations. A smaller crystal size improves the spatial resolution and shower separation but increases the number of crystals and electronic readout channels. Furthermore, adding the signals from a large number of neighbouring crystals results in increased electronic noise, which degrades the energy resolution. As a compromise we have chosen a crystal size that covers 6° in both polar and azimuthal angles. For crystals at small and large polar angles ($\theta < 30°$ and $\theta > 150°$) the azimuthal angular range was increased to 12°. The specification of the crystal barrel calorimeter is summarised in Table 2.

The weight of the crystals is about 4 tons, and the requirement to minimize the reduction in solid angle due to the supporting elements puts serious constraints on the design of the support structure. In order to avoid substantial conversion of photons in front of the active detector volume, minimum amounts of preferably low-Z materials have to be used. As the JDC

is located in the center of the calorimeter the support structure is designed as two self-supporting halves enabling free access to the JDC.

On the basis of extensive static calculations, Monte Carlo studies, and financial considerations, several conceptual designs using carbon-fibres, beryllium, aluminium, or stainless steel as possible structural materials were investigated. The final design uses special aluminium alloys for all supporting components. To give a minimum load on the inner aluminium wall, which could be reduced to 10 mm (0.11 L_R) in thickness, each individual crystal was suspended from the outside support structure. For this purpose, the crystals and associated electronics are enclosed in titanium cans of 0.1 mm thickness (fig. 8). Another feature of the CsI detector design is a minimum amount of material (0.11 L_R of aluminium and 0.056 L_R of titanium) in front of the active detector. This mechanical design allows an easy exchange of units for repair and reduces to 4.4% the loss in solid angle due to the support structure elements. For handling and servicing purposes the detector is mounted on rails and can be rolled out of the magnet onto a moveable trolley. (See section 2.2).

The crystals were manufactured by BDH Ltd (UK) according to acceptance specifications which determined the geometrical dimensions, the absolute light output and the maximum variation of the light output along the length of the crystals. Following the specifications used for the CLEO II detector [19] we required a variation in the light output of less than 5% along the first 20 cm (starting from the thick end) and less than 2% for the rest. The light output measured with a ^{137}Cs source was specified to be larger than 22% with respect to a small CsI reference crystal of 2.5 cm diameter and 2.5 cm length. Measurements carried out at CERN after delivery showed a distribution peaking at about 30% with a spread of 10% (fwhm).

As mentioned, the calorimeter operates in a magnetic field of 1.5 T and so silicon photodiodes are used to read out the scintillation light. Since the spectral emission of CsI(Tℓ) peaks around 550 nm, it is already reasonably matched to the sensitivity of photodiodes (fig. 9). However, there exists an order of magnitude mismatch between the light emitting area of a crystal and the sensitive area of a photodiode. In order to improve this a wavelength shifter (WLS) is used as an efficient light collection system. It consists of a 3 mm thick Plexiglass tile doped with an optically active pigment which absorbs light around 520 nm and emits it at a longer wavelength. For the present purpose it is the tile's property of concentrating the emission light onto its narrow lateral faces that is important as the photodiode is glued onto one of these. The other lateral faces are painted with a white diffuser to increase the light collection efficiency. Thus the scintillation light is collected by the front face of the WLS, which is identical in size to the crystal face, absorbed in the tile and re-emitted to be efficiently collected by the photodiode glued to a lateral face.

Each detector module was assembled from a crystal and a readout element (photodiode, preamplifier) whose performance (noise and gain) was selected to match the light output of the crystal. Before installation into the support cradle each module was cross-checked with a (Pu-^{13}C) source which gives a 6.1 MeV photon. Due to careful matching, the overall distribution of preamplifier output signals for all crystals shows an rms width of only about 10%.

2.7 The cosmic-ray counters

The cosmic-ray trigger telescope is used to check the proper operation of the complete detector *in situ* during periods when the antiproton beam is not available and can in principle be used to monitor the long-term gain shifts of the CsI crystals by comparing data taken with the detector at any time to a set of reference spectra.

The telescope consists of two identical hodoscope units, covering a sensitive area of 131.1 cm x 183.0 cm, mounted above and below the magnet. Each hodoscope is divided into three sub-units of 14 mm thick plastic scintillator. The scintillation light is detected by 5 cm diameter photomultipliers through non-adiabatic light guides. The scintillators are embedded in styrofoam and covered by aluminium sheets, to protect against mechanical damage.

The lower hodoscope unit is mounted at y = -155.2 cm below the interaction point with the long side oriented along the z-axis (beam direction). The upper unit is moveable in a direction perpendicular to the z-axis at y = 197.5 cm. It can be moved, on aluminium rails, a few metres along the top of the magnet in the direction of the positive x axis. When positioned at the centre of the (x,z) plane, the sensitive area of the upper hodoscope covers a solid angle of 0.546 sr whilst the corresponding solid angle of the lower hodoscope is 0.816 sr (seen from the interaction point). The energy loss by ionization of relativistic particles passing through the whole magnet and crystals is between 1.5 and 1.9 GeV, depending on the particle direction. Thus only cosmic muons with an energy above 2 GeV are able to pass through the complete detector. The energy, angle and charge distributions of such cosmic muons are well known, and therefore it is possible to simulate cosmic-ray energy spectra in the crystals by Monte Carlo calculations. By a comparison of measured and simulated cosmic ray energy spectra the crystals can be pre-calibrated with a precision of about 2%.

The highest trigger rate is achieved by a logical OR connection of the three scintillator signals and with the upper and lower hodoscope units in coincidence. A mean rate of about 22 events/s is measured, in agreement with predicted values.

2.8 The light pulser system

The overall gain stability of the CsI calorimeter is monitored by two independent light pulser systems, one for each half barrel. The light is guided through glass fibres onto the

wavelength shifters (WLS) of each individual CsI crystal and read out by the normal calorimeter electronics. Figure 10 shows the optical arrangement of the light pulser system.

The light source is a Xenon flashlamp (Hamamatsu L2189) operating at a repetition rate of 4 Hz. After the first few flashes, the variation in intensity is about 0.25%. The drive electronics for the flash lamp is designed so that the pulse shape of the light is similar to that of the scintillation light from the CsI crystals. The optical spectrum of the light is similar to that from CsI in the sense that the major part of the intensity has a wavelength within or below the absorption band of the wavelength shifter (WLS). Since the emitted spectrum of the wavelength shifter used with the CsI crystals is independent of the wavelength of excitation, the optical spectrum of the light from the flash lamp is not critical.

A system of mixers and diffusers (fig. 10) approximately equalises the light intensities in all fibres and keeps the relative intensities of different fibres constant. A mechanical system moves six glass optical density filters into or out of the light path to give 64 different light intensities, covering almost three orders of magnitude. The size of the filters and the mechanical arrangement of the moving parts enables a chosen attenuation to be reproduced at least to within 0.1%.

A reference system is used to monitor the flashlamp output. It consists of a monitor (MON in fig. 10) and reference (REF) for each light pulser system. The monitor, placed before the optical filters, uses a wavelength shifter and photodiode (as used in the CsI readout) to measure the relative light intensity from flash to flash to within 0.1% accuracy during a light pulser run. As the filter combinations have been calibrated to an accuracy of 0.25% the relative light intensity after different filter combinations is known to 0.3% accuracy even when the intensity is attenuated with the filters by a factor of 600.

The reference intensity monitor was planned to provide an absolute calibration point for the intensity of light in the final light mixer and fibres. Again a wavelength shifter and photodiode are used to monitor the light intensity. A NaI crystal doped with an ^{241}Am source and a 6 cm x 6 cm x 3 cm CsI crystal, to detect cosmic rays, are also mounted on the wavelength shifter as reference light sources. Since this system does not fully match the accuracy of the rest of the light pulser system it is only used for monitoring purposes. As an absolute calibration point the sum of the light in each half of the barrel normalized to the π^0 invariant mass peak measured in physics events is now used.

The Xe flash lamps and filters are computer controlled by a VME system. This allows the electronics to be tested and the relative gain of the whole calorimeter electronics to be monitored in a 10 minute period during the pause between LEAR spills, which occurs every 1 - 3 hours.

The overall response function of the calorimeter electronics can be measured with the calibrated filters to an accuracy of about 0.3%.

The light pulser gives, within a few minutes, a fast diagnosis of the state of the crystals and their readout system. It reports on which crystals cannot be read out, have large noise, bad linearity or other problems. An off-line analysis program produces correction factors for each crystal to give gain corrections.

3 ELECTRONICS AND READOUT

3.1 PWC Electronics and readout

The chamber signals are fed in groups of eight to the PCOS III current preamplifiers (LeCroy 2735PC) through 3 m long, 75 Ω shielded flat cables, soldered on the anode printed circuit boards. Low-frequency noise signals are attenuated by a high-pass RC filter ($R = 10\ k\Omega$, $C = 330$ pF) at the readout end of the cable. The 10 kΩ resistor also prevents the signal wire from building up charge when the chambers are operated with a cable disconnected from the preamplifier.

Each 16-channel preamplifier card amplifies the input signals which are then fed into discriminators. The 16 ECL logical output signals are fed through 10 m long twisted-pair cables into the PCOS III receivers (LeCroy 2731A). The discriminator thresholds are set by a DC level from the receivers. The minimum (maximum) threshold corresponds to an input current of 2 μA (15 μA). A receiver can process up to 32 wire signals (two preamplifier cards).

The logical signals are delayed by a computer controlled delay (300-682 ns) and strobed by an external gate with a length of 300 ns supplied by the incident antiproton trigger. The signals are then sent through ECL lines to the crate readout controller (LeCroy 2738) and then through the CAMAC interface (LeCroy 4299) to the computer.

Fast OR signals from the receivers provide the charged multiplicity trigger. Channels are grouped into adjacent pairs by wire wrapping inside the receivers. Adjacent hits (including boundary hits in adjacent receivers) are grouped into clusters. The logic consists of ECL-based CAMAC majority logic units (LeCroy 4532) which give an analog signal corresponding to the number of clusters in each chamber. Fast ADC's (LeCroy 4504) digitize the information and provide the cluster multiplicity (0-15) for each chamber, which is then compared to a preset multiplicity by a programmable look-up unit (LeCroy 4508). To allow for detector inefficiencies and electronic noise, the logic for each chamber can be programmed to accept a multiplicity value within a preset range. An accept flag is set when the multiplicity conditions are fulfilled.

3.2 JDC electronics

Each sector of the JDC is instrumented with two 24-channel, surface-mounted preamplifier cards [20]; one preamplifer card on each endplate. Provision has been made for an inter-channel resistor network (not presently implemented) to cancel cross-talk. The AC-coupled input amplifier is based on the Fujitsu MB43468PF chip, which determines the 35 ns rise time. A Motorola MC10116 chip provides the differential output. The amplifier gain is trimmed, channel by channel, to 18 mV/μA; at this gain, the output signal is linear over the ± 100 mV range of the readout system. Noise is equivalent to 5500 input e^- when measured without output cables and 7500 input e^- when measured with 21 m cables.

Shielded, twisted-pair cables carry the output signals. Once outside the detector, the signal wires are regrouped from a sector to a layer orientation. This increases the readout parallelism, since it is likely that far fewer nearby channels will fire in a layer than they do in a sector, and so the readout processors share the load fairly evenly, event by event.

The signal cables connect to receiver cards which are plugged into the backplanes of the flash ADC crates. The receiver cards hold the pull-down resistors for the open-emitter preamplifier outputs. There are also 0.01 μF coupling capacitors serving as high-pass filters, transmitting the signal to the next stage. These capacitors determine the low-frequency cutoff of the system - about 270 kHz. The signals are finally terminated and amplified by Struck DL300V differential amplifier boards having a gain of 9.4 and a common-mode rejection of ~ 20 dB for the frequencies of interest.

Placing the preamplifier pull-down resistors near the flash ADC electronics keeps the total preamplifier power dissipation at the chamber to 122 W for the 1380 channels. Because of the need for constant, uniform gas temperature, the heat from the electronics must be isolated from the chamber: integrated circuit chips on the preamplifiers are in thermal contact with an aluminium plate which, in turn, is cooled by circulating dimethylpolysiloxane coolant (Syltherm XLT) at its inner and outer radii. The cooling plates are instrumented with platinum thermometers which control, through a Eurotherm 818S electronic controller, the coolant temperature. A number of other thermometers, both platinum and integrated circuit types, monitor the temperature of the JDC itself (section 4.6).

High voltage is supplied by two LeCroy HV 4032A power supplies (32 channels), with the endplate equipotential traces fed from a single channel through a resistive voltage divider. All lines are fitted with discrete RC filters a few meters from the JDC; the chamber is protected against the energy storage both in these filters and in the HV cable capacitance by 1 MΩ carbon resistors in series at the chamber. Current monitoring, in addition to the μA-scale readout of the LeCroy supply, is possible over a 10-2000 nA range through custom built units having a (roughly) logarithmic scale.

The unsaturated drift velocity in the "slow" gas used for the JDC is linearly dependent on the electric drift field, which implies that the field wire voltages must be reasonably stable. The regulation of the LeCroy supply is $\pm$ 1V $\pm$ .05%, which translates into a $\leq$ 20 μm effect on the resolution. Currents drawn by the chamber are sufficiently small that their variation has no significant effect on the chamber voltage and resolution.

3.3 The electronics for the CsI detectors

The signals from the individual CsI channels are used for the measurement of deposited energy as well as the determination of multiplicities for trigger information. The system for each channel consists of a preamplifier driver mounted on the CsI crystal assembly, a main shaper amplifier, a discriminator and two commercial ADC systems used in parallel to obtain sufficient dynamic range and sensitivity. The output from the discriminator in each channel is used together with the Fast Cluster Encoder (section 5.3.3) to calculate the multiplicity of each event.

The processing of the CsI signals from the photodiode has to be a reasonable compromise between the effects of noise and limitation of the signal rate due to pulse pile up. Good noise performance is necessary since the outputs of many calorimeter channels are added together in the analysis of a particular event. The signals from CsI are rather slow, with a main component of about 0.9 μs decay time and a further component of 7 μs. (See table 1). The slower component affects the tails of the pulses and so some additional shaping has been introduced to reduce this effect.

The charge sensitive preamplifier for signals from the Hamamatsu S2575 PIN silicon photodiodes was developed at MPI Munich. The present version, modified for our purposes, uses a 2SK 300-2 FET manufactured by SONY at the front end and has a time constant of 240 μs. Output signals of 0.3 mV/MeV on average (corresponding to about 2000 photoelectrons per MeV) are then amplified in a differential driver stage with a gain of 6.8 per branch, driving a 20 m long twisted-pair line which is back terminated.

The input to the shaper amplifier unit is a quasi-differential receiver stage followed by a variable gain stage. Here the output for the discriminator branches off. The main shaping is done in the next two stages by differentiation with two pole-zero cancellation circuits (PZC) having time constants of 10 μs and 1 μs respectively. Slight additional differentiation is done with a circuit adjacent to the second PZC. The three stages also include integration with a 1 μs time constant. When the PZC's are properly adjusted, the effect of the longer time constants in the CsI decay can be effectively suppressed. The output pulses in this case are quasi-gaussian in shape corresponding to a 1 μs time constant. It was observed that the preamplifer output pulses for different channels are slightly different in shape, indicating differences in the decay time of individual CsI crystals. For optimum performance the PZC's were individually adjusted for

each channel using pulses obtained under realistic running conditions. A 500 ns delay line in front of both output stages enables proper timing between the ADC signal and the ADC gate given by the main trigger. The shaper amplifier has variable gain in order to allow individual adjustment of each channel to the same sensitivity, so that a single threshold bias can be used for all discriminator channels.

The output stages of the shaper amplifier for both ADC's are designed for a 50 Ω load and provide variable DC bias for the control of ADC pedestals. The connections to the ADC's are made by 7 m long, 50 Ω cables with a 2 kΩ series resistance on the ADC input and a 50 Ω series resistance at the shaper amplifier output. These resistances, together with the 50 Ω ADC input resistance, provide proper attenuation and back termination of the cables.

Since we use long ADC gate lengths of 6 μs, low frequency noise from 50 Hz pick-up and harmonics due to ground-loops can be a serious problem. Originally 50 Ω π-type attenuators were used in front of the ADC's, but the noise level was found to be unacceptably high. A change to the 50 Ω and 2 kΩ series resistance attenuators described above, which present to each ADC a high source impedance, reduced the noise by roughly a factor of 10. This noise seems to be a many channel effect and cannot be explained on the basis of a one-channel ground-loop. Another source of noise was the inductive pick-up of stray magnetic fields in the crate by the 500 ns delay lines. This was reduced by shielding the most affected modules (depending on their position in the crate) with ARMCO sheet. The noise performance is discussed in more detail in section 8.2. AC-coupling is used in the photodiode ADC signal chain: i.e., for the photodiode signal connection, the connection between preamplifier and driver, and for the connection in front of the output stage of the shaper amplifier.

For the discriminators the leading-edge type was chosen for simplicity and to give small input-output delay. They are connected to the shaper amplifiers by 7 m long, 50 Ω cables. The input stage is a quasi-differential receiver intended to isolate the ground of the shaper amplifier from the discriminator ground at low frequencies. The pulses are then differentiated, using pole-zero cancellation with a time constant of 400 ns, and amplified. At the comparator input they have a rise time of 600 ns. This rise time could be reduced slightly by using shorter differentiation time constants, but only at the expense of a considerable increase in noise. The threshold at 10 MeV had a width (due to noise) of roughly 2 MeV when the cosmic-ray spectrum was observed in coincidence with the discriminator output. The noise rates above threshold seem to be acceptable down to a threshold of 7 MeV.

Both the shapers and discriminators are based on the NE5534 operational amplifier, which was found to exhibit very good noise performance for our purposes. Hybrid and surface mount technologies are used nearly throughout. The shaper modules each contain 8 channels with separate gain and pedestal controls on the front panel. The discriminator modules also

contain 8 channels each. Except for the preamplifier-drivers, the system is located in the electronics hut where the bulk of the electronic hardware resides.

Two ADC systems are used in parallel because there is no single system available with both fast readout and sufficient dynamic range; we would need a 15-bit ADC to cover the full energy range with good sensitivity. A range of 0-2000 MeV is required for in-flight running with 0.1 MeV/channel sensitivity for reasonable accuracy on signals corresponding to an energy deposition of 1 MeV. A LeCroy 4300-B FERA system gives fast readout for the software trigger. Its 2048 channels cover the full energy range, but with low sensitivity (~ 1 MeV/channel). A LeCroy 2282 system with 4096 channels and limited range (0-400 MeV) gives high sensitivity (0.1 MeV/channel). LeCroy selected matching ADC hybrids for each FERA module so that, even with a 6 μs wide gate, all pedestals lie within the required range.

4 DATA ACQUISITION AND MONITORING

4.1 Overall description

Once the signals from the various detectors have been digitized, and the trigger has selected the event for recording, the data have to be read out, assembled and written to tape. Checks must be made on the data. These are the tasks of the data acquisition system. The same hardware is also used for the trigger (section 5), starting and stopping runs, and setting up the digitizing electronics. Figure 11 shows a simplified diagram of the data acquisition system and fig. 12 shows the overall layout of the hardware. Most of the software was written in the C language and is completely new.

The data acquisition system is designed to maximize the recording rate of high quality data. Firstly, this requires the reduction of raw data by zero suppression and data packing, which is done by the digitization electronics. Table 3 shows the number of channels and how much compressed data each subdetector produces. Parallel readout by separate Central Processing Units (CPU's) for each subdetector, referred to as Local Event Builders (LEVB), into VME-based memory quickly prepares the data for the Global Event Builder. (See fig. 11). The Global Event Builder (section 4.5) synchronizes the other LEVB's. When an event is accepted, it assembles the data from the sub-detectors into a Zebra format record [21] and sends the data to a micro-VAX3600 for on-line event analysis (sampling) and writing to tape.

We chose the IEEE-standard VMEbus for the readout because it is very flexible and, being an industry standard, is cost effective and a large choice of modules is available. It can also easily be extended. Several different computer types, all based on the Motorola 68K series CPU's, have been used. These were selected according to the needs of their specific tasks; for example the crystal readout needs a fast CPU for the software trigger and the FORCE

CPU21-B microprocessor using a MC68020 running at a clock frequency of 25 MHz without insertion of "wait-states" was the fastest available at the time.

The VME computers do not have local hard disks (except for the FORCE). Instead, they use the micro-VAX as a host computer to provide remote disk space. This provides more disk space at lower cost, and also allows all VME computers to access all files, simplifying software development and distribution of data. Access to the remote disks is over a thin-wire Ethernet local area network using a low level protocol [22]. This network also assists in fault finding and software development by allowing remote access to the VME-based computers. To achieve maximum throughput on the CAMAC branch, a set of fast CAMAC routines was implemented conforming to the ESONE syntactical form. This package is coded in 68020 assembly language and is accessible with C calling conventions.

The VME-based computers run an industrial version of the OS-9/68K operating system [23]. This is a flexible and powerful UNIX-like system tailored to real-time applications. Interprocessor communication via "pipelines" and "data modules" allows synchronization of the many applications in the multiprocessor system. The programming languages used are C [24] and Real-Time Fortran [25], with assembly code for time-critical functions.

Rapid movement of data from one VME crate to another requires a crate-interconnect bus. The data acquisition system uses two types: the VME Subsystem Bus (VSB) and the VME Vertical bus (VMV) from CES. VSB was originally intended as a sub-bus within a VME crate, to avoid overloading the main system bus. However it can also be used to transfer data between crates over short distances (~ 3m). The Global Event Builder accesses the CsI event builder (Software Trigger) and the JDC data via VSB.

The VMV bus (fig. 12) allows rapid transfer of data over large distances (up to 4 Mbytes/s over 50 m). A long range bus is needed because the electronics hut, where front end digitization takes place, is roughly 45 m from the run control hut, which houses the micro-VAX and tape drives. VMV provides a common address, data and control bus to all the computers connected to it. This allows transparent access from one component to another, which eases synchronisation and control of the many concurrent processes. Each connection to a VME crate uses a CES VBR 8212 (slave) module as an interface. The Global Event Builder sends data via a VBE 8213 (master) module. A Macintosh IIx microcomputer for experiment control and monitoring (section 4.2) is connected via a CES MAC 7212 (master/slave) module, allowing it to send and receive data over a distance of some 72 m.

A model 10089 buffered VME bus DR11-W emulator from Ikon Corporation is used to transfer event data from VME via Direct Memory Access (DMA) to a micro-VAX 3600 which

monitors the data and writes the data to tape. Round 2400 ft, 6250 bpi, magnetic tapes or IBM 3480 compatible cassette drives are used for standard data taking, with Exabyte videotape drives for some special purpose data such as that taken with the cosmics trigger.

The program on the micro-VAX which controls the DMA transfer, also controls the tape drives and tape writing. Furthermore, it writes the events into a region of shared memory for monitoring purposes. A software package called the Model Buffer Manager [26] manages this shared memory. Several monitor tasks access the events in the shared memory, analyse the data and check that the various subdetectors are working correctly.

Each subdetector (PWC, JDC and CsI) has its own monitor task which provides information in two ways; by error messages when faults are detected and by histograms of the accumulated data. The tasks use the CERN HBOOK histogram package [27] with the histograms stored in further shared memory regions. A histogram display program, "Presenter", accesses these memory regions and so can display up-to-date plots without interrupting the monitor tasks. The "Presenter" program can be run in several places simultaneously, without the users interfering with each other. "Presenter" uses the CERN HPLOT [28] histogram display package.

Another monitor task, the event display, analyses whole events. It does complete event reconstruction and then graphically displays the event in various formats. CPU limitations prevent reconstruction of many events, and so this task cannot produce histograms of physics interest on-line. It does, however, give the experimentalist confidence in the quality of data being accumulated and provides crude, but quick, feedback on important questions such as whether the trigger conditions are filtering out the required data.

4.2 Experiment control and monitoring

The experiment control is performed by use of a Macintosh IIx personal computer which offers a user-friendly way of communication and presentation of data with mouse-based input and high resolution colour graphics windows. Moreover, excellent programming tools exist to allow for rapid program development and testing. The run control and monitoring program is a new development and was written entirely in the C language using the "Think C" development system. It acts as a supervisor task to the processors located on the VME system. The software was designed to avoid modal dialogues according to [29], i.e. all actions that are possible can be performed interactively at almost any point of operation without waiting periods. The Macintosh is used to set the experiment status, (e.g. lightpulser run, pedestal run, data taking etc) and to start and stop the data acquisition. It sets flags which define the parts of the detector to be read out, defines which software and hardware triggers are to be used and can be used to edit trigger definition files.

The status of the most critical parts of the experiment (magnetic field, target, JDC temperature etc.) as well as the settings for a run and information on the data acquisition (event rate, DMA rate, number of blocks transferred etc.) are presented in one status window along with information on the number and size of the ZEBRA blocks that have been assembled. Moreover, the Macintosh allows the monitoring of more than 3900 crystal related histograms which are filled online in the FORCE CPU. All histograms can be printed out or stored on disk for later use with fitting or presentation programs.

The status of VME and CAMAC crates is shown in a symbolic map of the experimental layout, and the status of voltages, currents, temperatures, gas mixtures and pressures is shown using colour bar charts. In a colour real-time event display the decisions of the various trigger levels are presented, PWC hits are drawn in a 3D projection of the chambers and crystal energy depositions are entered in a map of the crystals. Online help information is also available.

All information concerning runs is stored on disk as an 'Electronic Run Book' using "Hypercard" [30]. The run book is a complete object oriented database application which allows searching and sorting of run information on the basis of specific criteria.

4.3 JDC data acquisition system

4.3.1 The readout process

The readout chain is logically structured into three levels, allowing highly parallel data reduction and readout. The first level carries out digitization of the 1380 JDC analogue signals and zero suppression; the second reads out the zero suppressed data and the third level collects the data, ready for the Global Event Builder. The associated readout system is physically split into two halves, for the inner and outer regions of the JDC. Figure 13 shows a simplified layout. A further description is given elsewhere [31].

Level 1 consists of 16 crates, each with 24 flash ADC (FADC) modules, a hardware scanner as central system controller and an interface module which communicates with level 2. Since the structure of the global trigger system causes the trigger signals to arrive after the analogue signals, common stop mode is used where the incoming signal is continuously digitized and stored in a cyclical buffer until the stop signal arrives. If the hardware trigger indicates a valid event the interface module passes an interrupt to level 2 which thereupon initializes the scanner to search the FADC memories (a fast scan) for valid hit information. A valid hit is defined by data above a given threshold. Upon completing this process the addresses of all hit start and hit end locations are passed to level 2. So, at the end of level 1, the level 2 microprocessors store addresses describing the FADC memories which are to be read out.

Level 2 consists of two VME crates, each housing eight microprocessor boards (MicroSys CPU07). Each CPU07 is connected to one FADC crate. When level 1 is complete,

the CPU07 reads the FADC data from the addresses found by the scanner. The CPU07 also does error checking and recovery on its FADC crate. At the end of level 2, the zero suppressed data are stored in the 16 CPU07 microprocessors.

Level three consists of a JDC "Local Event Builder" 68020 microprocessor housed in each of the level 2 crates. These assemble the data from the CPU07 microprocessors into a memory buffer accessible by the Global Event Builder via VSB bus. They also synchronise the readout process with the Global Event Builder.

An on-line processing system to reduce the JDC data to (q,t) information for each hit is currently being developed and would reduce the amount of chamber data to be transmitted from 10,000 to about 800 bytes for a four track event. For this the ADC data has to be linearized and integrated to find the charge (q) deposited, and the hit time (t) has to be calculated.

4.3.2 Hardware details

The FADC's are Dr B Struck DL305 and DL310 modules, housed in DL300 crates. The DL305 and DL310 modules are fast (100 MHz), four-channel analog-to-digital converters based on a monolithic 6-bit flash ADC (Siemens SDA 5010). After digitization the incoming signal is cyclically buffered in a 256 (DL305) or 1024 (DL310) word high speed memory, covering maximum drift times of 2.56 μs or 10.24 μs respectively. The DL310 modules digitize the outer four JDC layers, which have the longest drift times. To enhance the dynamic range and to improve the amplitude resolution, the ADCs are operated with a nonlinear response curve (~ 7.9 mV/bin in the lower range to ~ 119.4 mV/bin in the upper range). This results in an effective resolution of 8 bits. Every board carries a four-channel DAC, which can be set by software for baseline offset correction. Up to 24 FADC modules (instrumenting 48 JDC sense wires) reside in one DL300 crate.

The DL302 scanner is a programmable controller module which can be operated in two basic modes. In sampling mode it addresses the 256 or 1024 memory locations of all FADC modules in parallel at a frequency of 100 MHz for the digitization. In fastscan mode all modules are addressed sequentially with a clock frequency of 25 MHz to search for data above threshold. To increase accuracy and reliability of operation, the timing behaviour of the scanners has been improved by applying an external, stabilized, 100 MHz common clock to all scanners.

The interface to the level 2 microprocessor is a DL307 module that communicates with a DL307V adapter board plugging into the I/O extension slot of the CPU07. The physical connection is made by a 64-line flat ribbon cable. Different DL300 crate signal lines are available to generate interrupts on the associated CPU07.

The CPU07's from MicroSys are based on the MC68000 CPU operating at a clock frequency of 12 MHz. They each have 256 kBytes of dual-ported, on-board RAM and 128 kBytes EPROM. For speed, they boot from RAM disks, for which FORCE RR2 memory boards with 512 kBytes of write-protectable, non-volatile (battery backup) CMOS RAM are used. The EPROM stores a basic OS-9/68K operating system and an OS-9/NET emulation implemented over the VMEbus. Communication between the CPU07's and the JDC Local Event Builder is via pipes within OS-9 and shared memory locations using predefined signal codes. An OS-9 device driver handles synchronization with the FADC system.

Currently the JDC Local Event Builders use Eltec Eurocom 5 processor boards each with a 68020 CPU, 1 Mbyte of dual-ported, on-board RAM, 20 MHz clock and an Ethernet interface. An upgrade to Motorola MVME 165 CPU's which use an MC 68040 is being tested.

4.4 CsI calorimeter data acquisition system

The CsI signals are digitized by two ADC systems, namely LeCroy FERA and LeCroy 2282, as described in section 3.3. The FERA data are transferred via ECLbus to a memory module in the CsI event builder VME crate which also provides the software trigger that reconstructs on-line the invariant masses of the detected final state particles. If the software trigger accepts the event, the program then reads out the 2282 data via a CAMAC branch driver. The Global Event Builder then reads both sets of data via VSB bus (see section 4.5). Figure 14 shows a simplified layout.

The FERA ADC's are divided into two identical systems. (Only one system is shown in fig. 14). Each has one CAMAC crate with 23 LeCroy FERA 4300B ADC's and a second CAMAC crate with 22 FERA ADC's and a LeCroy FERA 4301 driver. The two crates have their ECL, command and read enable busses connected in "daisy-chain". LeCroy recommends that one driver module be used for each crate, but to read 90 ADC's this would require an extra CAMAC crate and a more complicated readout system. The present solution, however, works well.

FERA digitization commences at the end of the 6 μs input signal gate, and takes 8.5 μs. Pedestal subtraction and data compression take a further 2.5 μs, and then the data is read out by ECLbus to the driver which relays the data to a CES HSM 8170 memory module in the software trigger VME crate. This readout proceeds at almost 10 Megawords/s, typically taking less than 10 μs for an event. About 25 μs after the start of the analogue signals, the data for all crystals are available to the software trigger for processing.

The LeCroy 2282 ADC's are also divided into two identical systems. Each has one CAMAC crate with fifteen LeCroy 2282 ADC's and a LeCroy 2280 system controller. After a 1 ms conversion time, the data are stored in the controller. If the software trigger accepts the event, the trigger program reads the 2282 data via a CAMAC branch driver. Although this takes a long time (about 3 ms), it is acceptable since readout only takes place for good events. When readout is complete, a semaphore is set to indicate that readout of the calorimeter information has terminated and the system is ready to transfer the data.

The readout system and software trigger are implemented on a FORCE CPU21-B microprocessor which uses an MC68020 running at a clock frequency of 25 MHz. To avoid CPU wait-cycles the board is equipped with 512 kBytes of fast (30 nsec) static onboard memory. The trigger software also sets up the readout for both ADC systems with pedestal subtraction and zero suppression. It writes a unique station identifier to each FERA module so as to identify from which module the data comes. It also writes the pedestal value, increased by one for the FERA and by five for the 2282 ADC's, to the pedestal memory for each channel so that only crystals with significant energy deposits ($\gtrsim$ 1 MeV) are read out.

4.5 The global event builder

The Global Event Builder (GEVB) synchronises and collects data from the Local Event Builders (LEVB), the PWC digitization electronics and the FACE Latches (see section 4.1 and fig. 11). It sends the data to the micro-VAX for monitoring and recording on magnetic tape. It uses an ELTEC Eurocom 5 VME microprocessor, equipped with a 20 MHz 68020 CPU, 1 MByte dual-ported memory, and an Ethernet interface. It has a CAMAC branch driver for reading the PWC data from the PCOS III modules; a VSB bus interface to read from and synchronise with the JDC and CsI LEVB's; and a VMV Bus interface for data-module communication, FACE-latch readout (section 5.3.3), slow control readout and to send data to the micro-VAX.

The global event builder uses a shared memory region, known as a "data module" in OS-9/68K, for communication with the LEVB's and with the MacIntosh II run-control computer. This "data module" contains information on the run status (start, stop, pause, resume), which subdetectors are to be read out, the slow control data and the hardware trigger set-up information. The MacIntosh II writes to this "data module", and the GEVB reads from it and distributes the information to the LEVB's.

The global event builder program "EVB" concatenates the data into ZEBRA format. ZEBRA is the standard CERN data-structure management system [21] which defines a format suitable for transferring data between computers. Data from each subdetector is stored in one or more ZEBRA banks. The EVB program collects the banks for an event into a linear structure, a ZEBRA logical record, and packs these into physical records using a special C implementation

of ZEBRA. When a physical record is too full for the next event, the program sends it to the micro-VAX.

Upon startup, the GEVB performs a number of initialisation tasks and then waits for the "start of run" signal in the "data module". Once this occurs, it proceeds with run initialisation, sending a "start-of-run" header and some run specific and trigger information to the micro-Vax for writing to tape; it initialises the hardware trigger and also the hardware for the PWC and FACE-latch readout. It then waits for an "accept event" signal from the software trigger. Once this occurs, it collects the CsI, FACE-Latch and PWC data. It then waits for the JDC LEVB's to signal that their data is ready. Once this occurs, it collects the JDC, scaler and hardware trigger data to complete the ZEBRA logical record. It then signals to the LEVB's that event readout is complete, so that they can prepare for the next event. This process repeats until a "stop run" signal occurs in the "data module". The EVB program also reads "slow control events" from the slow control LEVB and interleaves these into the main event stream.

4.6 Slow controls and monitoring

The slow controls and hardware monitoring of the Crystal Barrel detector are performed by a VME-based system, as shown in fig. 15. The control and monitoring functions run on a dedicated microprocessor (VIP module), which can operate independently of the main data acquisition. It shares a VME crate with memory modules and with interfaces to CAMAC, GPIB (IEEE-488) and RS232, together with a Motorola I/O system that makes use of the VME P2 backplane. The VME-GPIB interface communicates with the power supply for the CsI preamplifiers, while the VME-RS232 interface is used to take data from the gas analyser used with the JDC.

The VME CAMAC branch driver connects with two CAMAC crates, one in the electronics hut and one in the experimental area. The crate in the hut contains the following: a multichannel differential scanning ADC for monitoring a variety of analogue signals, for example from the magnet power supply and the JDC gas mixing and flow control system; an interface for the LeCroy HV4032A high voltage supplies for the JDC and an input register (IGOR unit) for reading high voltage supply current digitizations from the JDC. The CAMAC crate in the experimental area contains two ADC channels and a TDC channel which receive signals from the test chamber that monitors the drift velocity in the JDC gas. (section 2.5.1).

The VME crate also contains an 8-channel differential ADC and a dual parallel port that is used as an I/O register. Communication with these units is via the Motorola I/O channel interface. The ADC and I/O register are used to read analogue signals from solid-state temperature sensors via a multiplexor module. The I/O register selects the channel to be multiplexed for reading by the ADC. At present 90 sensors monitor the temperature of the JDC, the crystals and the magnet to a relative accuracy of $\pm$ 0.2°C.

The I/O register serves also to monitor some 30 crate power supplies. To avoid ground loops and electrical pick-up, an optical signal is produced at the crate to indicate that a crate power supply is working correctly. This is done either by internal monitoring circuits (if any) in conjunction with an interface which converts the electrical signal into an optical one, or by external voltage control boxes which turn a LED 'on' if the whole set of applied voltages from the crate are within the specified range. The optical signal travels via plastic optical fibre to a multiplexed receiver module. This converts the optical signals to TTL signals, and allows the I/O register to read out the status of 8 crates as a single byte. In the future, voltage control boxes may also be used to monitor other fixed low voltages such as those of the power supplies for the JDC preamplifiers or the crystal preamplifiers.

The slow control and monitoring software (fig. 16) runs on the VIP processor in the VME crate. All the programs are written in C using the OS9 operating system as for the other CPU's used in the data acquisition system. At present the monitoring task scans over the various sub-components of the equipment every 15 seconds, making appropriate checks and writing the data and status for each component to a data module in the memory of the VIP. The possibility of eventually running separate processes to monitor each sub-system at differing time intervals is forseen.

The interface to the human operator consists principally of a display of the actual data and the status information stored in the data module. Each time the monitoring task has finished its loop it sends a signal to the display programs which are currently running to refresh the screen of a dedicated VDU with the latest data. The user may switch from a main "page" containing general information and the status of each sub-system, to any of several detailed data presentations for the various subdetectors.

The user may further interact with the monitoring task through the "action" program. This feature provides facilities for switching on or off the monitoring of any sub-component, changing defaults and limits, and stopping the monitoring program whenever necessary. Another possible action is the setting up of the high voltages for the JDC. Any action is recorded in a log file, together with date, time and name of the operator.

Whenever the monitoring task finds a fault condition such as a tripped voltage on the PWC or a high temperature it provides warning and alarm messages which can be read by the run control (Macintosh) computer.

The data written to the data module are read by the global event builder via a VMV receiver module in the VME crate and then transferred to tape, in special "slow control events" interspersed at a rate of 1 per 100 among the standard data events. As the Event-Builder is only

active when data taking is in progress it is intended to independently provide, once per minute, a copy of the data module to the VAX via TCP/IP. These data will be stored in the VAX slow control data base and some of the most critical quantities will be recorded in histograms which the user may inspect using the Crystal Barrel "Presenter" program described in section 4.1.

5 TRIGGER SYSTEM

5.1 General description

At an event rate N, a measuring device with dead time t is able to sample only the fraction R of Poisson-distributed events:

$$R = \frac{1}{1 + tN}$$

For this reason, the trigger system for the Crystal Barrel experiment is built in three consecutive stages of increasing complexity and dead time. Each stage reduces the rate of accepted events by about one order of magnitude, thus minimising the effects of dead time on the rate of those events finally selected for measurement. The overall layout of the trigger system, with the relevant dead times and typical event rates is shown in fig. 17.

Level 0 gives the start signal for the electronics and is defined by the incoming antiproton or by different test trigger conditions, e.g. cosmic counters, test pulser, light pulser etc. As this level is built in programmable ECL technology, trigger sources can be changed in a few seconds by the operator at the experimental control console (section 4.2) without making any hardware modifications.

Level 1 is a hardware stage and combines the start signal of level 0 with the information on charged multiplicity, which is calculated independently for both the PWC and JDC. The total multiplicity in the crystals is determined by a fast cluster encoder (FACE). This uses the output of the discriminators in the amplifier chain for each CsI crystal, to determine the number of crystal clusters recorded in the barrel calorimeter. At this level any combination of charged and total multiplicity can be required to select special event topologies.

Level 2 is a software trigger using the CsI crystal readout microprocessor to identify photon clusters and to calculate invariant masses of all possible $\gamma\gamma$ combinations. The software trigger can then be used to select particular combinations of final state particles which decay to photons; typically π^0 and η.

5.2 Level 0 hardware

The different trigger sources such as the signals from the beam entrance counters (S_1 and $Si_{1\text{-}5}$), the signal from the veto scintillator (S_2) behind the target, the cosmic ray counter triggers

and the light- and test pulsers are fed into CAMAC discriminators. The discriminator thresholds can be adjusted by CAMAC commands to adapt to the different input signal levels whilst a programmable delay line allows the adjustment of timing for the following coincidence unit. LeCroy 4508 Programmable Lookup Units (PLU 1 and 2) in overlap mode serve as computer controlled coincidence units (fig. 18). A programmable output of this unit is connected to the next PLU (3 and 4) as a strobe to produce fixed output pulse lengths. Some of the output lines from this second set of units are used as a code for the different trigger conditions. These signals are fed into a CAMAC trigger register which is gated by the DAQ computer. An output from the PLU 3 and 4 is used for the start of the timing units used to generate the strobe signals for the detector components. A signal from PLU 1 is used as the input for a retriggerable monoflop to produce a logical output in the case where there are two antiproton entrance signals inside a pileup window. This pileup flag is also stored in the trigger register for further trigger decisions. Several CAMAC scalers connected to different outputs (programmable or fixed) allow monitoring of the incoming rates. All trigger conditions are set by writing the appropriate memory contents into the PLU's via CAMAC.

5.3 Level 1 hardware

The information from the trigger register is sent to PLU 5 for coding purposes and then enters the level 1 decision PLU 6, where the information from the charged multiplicity triggers for the PWC and JDC is also collected. The output flag from the Fast Cluster Encoder is also recorded in this unit. At this level any combination of charged and total multiplicity can be chosen for selecting special event topologies. The typical processing time up to this point is about 20 μs due to the cluster search procedure in the FACE and the maximum drift time measured in the outer layer of the JDC (4 μs). If the chosen trigger conditions are fulfilled, the output of PLU 6 is sent to the next level (PLU 7) to make the final decision. If not, then a fast clear signal is forwarded to PLU 7 to generate a fast system reset.

5.3.1 PWC multiplicity logic

The logic to detect the number of charged annihilation products in the PWC is based on an analogue sum of the hits in each chamber which is then digitized by a flash ADC (fig. 18). The digital values from the two chambers are compared in a PLU with a predefined multiplicity. This procedure allows any combination of multiplicities in the two chambers and gives the possibility to correct for inefficiencies by setting a range of multiplicities which are valid. Asking for an increase in multiplicity of one or two in the outer layer of the PWC also allows events with a K_S decay in the volume between the two chambers to be selected.

In the hardware the signals from the fast output of the PWC readout system PCOS III (grouped in pairs) are fed into LeCroy 4532 majority logic units, which produce an analogue output proportional to the number of hits fired in the unit. The 4532 is used in cluster mode so as to get the correct number of tracks from the chamber. The analogue outputs from the 4532

for each layer of the PWC are summed and connected to the input of a LeCroy 4504 fast ADC. The digital output (4 bit) of this unit is then connected to a LeCroy 4508 PLU for the final decision. An output flag is generated if the conditions in both layers are satisfied.

5.3.2 JDC multiplicity logic

The detection of the number of charged tracks in the JDC uses the analogue buffer output signal of the FADC's for the 6 sense wire layers 2, 3, 4, 5, 20 and 21 [32]. The signals from each end of the sense wires are amplified and added in discriminators specially designed for this experiment. The digital outputs are connected to six LeCroy 4532 majority logic units, which are open only during the actual drift time. The analogue signals from these units are digitized by two LeCroy 4504 flash ADC's and the results compared by four PLU's which are preset with the ranges of multiplicities for each layer (fig. 18). An output of the last PLU is used as a flag for trigger level 1 to show that the trigger condition has been met. A special program allows either ranges of multiplicities for each layer to be selected or the number of tracks inside the JDC to be chosen. In the latter case the algorithm combines the information from the six layers in such a way as to select events with the correct number of tracks even in the presence of inefficiencies or noise hits. The program prepares the appropriate contents for the different PLU's and stores this information in files for downloading during trigger setup.

5.3.3 The FACE

The FACE (FAst Cluster Encoder) is a hardware processor to calculate the multiplicity of clusters in the crystal matrix. The algorithm used in the FACE is briefly described as follows. The crystals are mapped onto a plane. The result is a rectangular matrix with 26 θ-rows and 60 ϕ-columns. The matrix is filled with *"ones"* and *"zeros"* according to whether the energy deposited in a crystal is above or below threshold. The logical OR of all elements in each row is formed. This process is the same as projecting the matrix onto the θ-axis. Thus a data word of 26 bits length with groups of *ones* is obtained. In the following this word is called the "mask word" and the number of sets of consecutive *ones* in the mask word is n. The matrix is cut into "slices" using the groups of *ones* in the mask word. The resulting slices still have 60 columns, but there are now only as many rows as the number of *ones* in each connected group of *ones* in the mask word. This gives n slices. For each slice the projection of each column onto the ϕ-axis is taken. This yields n times 60-bit data words again with groups of *ones*. Next all the groups of consecutive *ones* in each 60-bit data word are counted and summed. Except for very special and rather unlikely cluster topologies the result gives the multiplicity of clusters in the matrix.

The signals from the CsI crystals go from the shaper amplifiers into discriminators to avoid spurious contributions to the cluster multiplicity due to noise (section 3.3). The optimum discriminator threshold was estimated from Monte Carlo studies to be about 25 MeV. The ECL logic signal from the discriminators is then stored in VME latch modules. These latch modules are hardware storage devices with a gate which, when set, allows one to store logical signals

(ECL) from the external input. The gate is set externally and is open for about 400 ns in run conditions. The latches can also be read from and written to via VMV bus for test purposes. Each latch module has 32 channels and the stored signal (after the gate) is present at the backplane of the module. These signals can be constantly accessed until an external reset is applied to the latches.

After the latches have been filled and the gate closed the FACE reads the latch data from the backplane of the latch modules. It takes the FACE about 25 μs to calculate the multiplicity of clusters. After that the 5 bits containing the multiplicity are sent to the programmable lookup unit (6 in fig. 18) where the trigger decision is made.

5.4 The software trigger.

The software trigger [33] is an integral part of the CsI calorimeter read-out system (section 4.4 and fig. 14) which uses a Motorola 68020 VME-based microcomputer at a clock frequency of 25 MHz. The event information from the FERA system is transferred into VME so that about 25μs after the start of the analogue signals from the barrel calorimeter, the data from the crystals is available for processing. The trigger processor decodes the zero-suppressed, packed FERA data and gets the positions and calibrated energies of the crystals which have fired from lookup tables. These tables occupy about 4 MByte of memory. The energies are entered into a $(\theta\text{-}\phi)$ projection of the calorimeter. At this point, a first decision on the total energy deposited in the calorimeter can be made after about 100 μs.

With knowledge of the energy signal in each crystal, it is possible to perform a search for local maxima in energy deposition (clusters) and to separate overlapping electromagnetic showers using the following procedure. The positions of crystals which have fired are sorted into a linear list according to their energy deposition using a hash procedure. Here, the crystal with the maximum energy corresponds to the center of an electromagnetic shower. The energy of the corresponding photon is calculated by summing up the neighbouring crystals and at the same time the neighbours are removed from the list. By going through the ordered list in this way, one gets all local maxima of energy deposition. Furthermore, charged clusters can be separated from those due to neutrals by applying a cut on the cluster size which depends on the cluster energy.

In order to determine the number of radiatively decaying mesons (e.g. $\pi^0 \rightarrow \gamma\gamma, \eta \rightarrow \gamma\gamma$), the invariant mass m_{ij} of all possible pair combinations P_{ij} is calculated from the measured energies E_i and E_j.

$$m_{ij} = \sqrt{2\, E_i E_j (1 - \cos \xi)}$$

where ξ denotes the opening angle between the photons. ξ is calculated from the measured polar coordinates (θ,ϕ) of the two photons with

$$\xi = \text{acos}\ (\sin\theta_i\cos\phi_i\sin\theta_j\cos\phi_j + \sin\theta_i\sin\phi_i\sin\theta_j\sin\phi_j + \cos\theta_i\cos\theta_j)$$

For reasons of speed, the calculation for the various combinations is performed using a 6-dimensional lookup table, which contains for each possible pair P_{ij} the invariant mass for the angles (θ_i, ϕ_i), (θ_j, ϕ_j) (4 MByte) and the energies E_i and E_j (8 MByte). By counting the number of mass combinations that fall into a 50 MeV window around the meson masses, a trigger decision on radiatively decaying mesons is possible in a time which is of the order of a millisecond. To gain the maximum execution speed possible, the algorithm is coded in C with assembly language functions for the time critical parts.

6 CALIBRATION

6.1 Calibration of the JDC

The calibration procedure for the JDC consists of several steps. Initially, simple cuts and offsets need to be determined so that the measured data can be transformed into a meaningful range of values. Following this, a z calibration is performed to obtain the charge division to z conversion. Next an r-ϕ calibration is made for the conversion of drift times into r and ϕ positions in the chamber. Finally, a dE/dx calibration is performed to convert measured pulse height information and reconstructed momenta into particle likelihoods.

6.1.1 Scaling of the raw data

The data which come from the JDC consist of four pieces of information for each recorded hit.

1. The wire number of the hit.
2. A measured drift time for the hit.
3. A measured amplitude from the preamplifier at the +z end of the JDC.
4. A measured amplitude from the preamplifier at the -z end of the JDC.

Before these data can be converted into position information, it is necessary to make sure that the drift times lie within the expected range and that the measured amplitudes are larger than some noise threshold which also has to be determined. The time correction is simply an offset which arises from the fact that the time-zero from the flash ADC's is several hundred nanoseconds earlier than the event time-zero. This offset is obtained by histogramming the fit times of many hits, and then fitting the sharp edge at time-zero of this spectrum. In principle, this could be done for every wire in the chamber; however, in practice it is only necessary to do this for each of the sixteen flash ADC crates. The time offsets from these crates usually differ by less than 5 to 10 ns. After these time-zero's have been fitted, an amplitude cutoff is determined

by looking at the pulse height distributions on every wire. A very clean cut between signal and noise can then be made.

6.1.2 Z-calibration of the JDC

The z coordinate of a hit is obtained from the two measured amplitudes by using charge division.

$$z = z_0 + z_L \cdot \frac{A_+ - \alpha A_-}{A_+ + \alpha A_-}$$

where z_0 is the location of the centre of the wire, z_L is the electrical length of the wire, α is the relative gain between the two electronics chains at either end of the wire, and A_+, A_- are the two measured amplitudes. Each of the 690 sense wires in the JDC have their own z_0, z_L and α, leading to 2070 calibration constants which need to be determined. Typically z_0 is 0 cm, z_L is 23.68 cm and α is between 0.90 and 1.10.

In order to obtain these constants, data are taken with the magnetic field off and requiring at least four tracks in the JDC. On an event by event basis, these data are taken to be a series of lines all emanating from the same vertex point. Events in which the software finds at least three tracks each containing no fewer than 10 out of 23 possible hits are then fitted using an initial set of calibration constants with the constraints that they are straight lines and that all lines intersect at a common point in the target region. This yields a set of measured amplitudes and fitted z coordinates which are written to an external file. This procedure is repeated for over 50,000 events. The measured amplitudes and derived z coordinates are then fitted using a MINUIT [34] based procedure to give an improved set of the 2070 calibration constants. The whole procedure is iterated three or four times until a stable set of calibration constants has been found. The calibration procedure yields a z-resolution (σ) of between 7 mm and 9 mm, depending on the wire.

6.1.3 r-ϕ calibration of the JDC

The r-ϕ calibration uses the two-body final states $\pi^+\pi^-$ and K^+K^- which produce monoenergetic pions and kaons at 927.8 MeV/c and 797.9 MeV/c respectively. This allows the two charged tracks to be treated as one single helix spanning the full detector, and provides a strong constraint on the reconstructed hit positions. In addition, this calibration method has the advantage of providing an absolute reference and a cross check on the magnetic field [35].

An electrostatic simulation program Garfield [13] is used to create a set of drift time tables for several different drift velocities (arising from variations in atmospheric pressure, gas temperature, etc). Each table maps the drift time to a given wire into a pair of hit coordinates

with a time granularity of 25 ns. During processing of the data, linear interpolation between the table values is used to determine the coordinates of each hit.

Collinear events are selected by requiring exactly two long tracks in the JDC with an opening angle greater than 164°. No more than two clusters may be seen in the crystals, and the tracks are required to point to these. Events passing these cuts are fitted by a helix in (x,y,z) which treats both tracks as part of one long track. Events which pass the helix fit with greater than 1% probability are accepted.

The calibration procedure consists of repeatedly processing a set of approximately 500 collinear events, using a drift time table obtained by interpolation between the pre-calculated tables, and varying the interpolation factor. The width of the peaks in the momentum distribution of the reconstructed monoenergetic collinear final states (fig. 19) as a function of the interpolation factor exhibits a minimum corresponding to the optimal drift time table. The width of the $\pi\pi$ peak is 19.0 MeV/c, corresponding to σ_p/p of 2.0% at p = 928 MeV/c.

During processing of the data, variations in atmospheric pressure are followed on a run-by-run basis by correcting the interpolation factor with respect to the atmospheric pressure of the calibration data-set. The resulting r-ϕ resolution as a function of drift distance for one layer in the JDC is shown in fig. 20.

6.1.4 dE/dx calibration

The energy loss of charged particles is measured in the JDC using the truncated mean technique; for each track the lowest 10% and the highest 30% of a dE/dx sample of ≤ 23 wire measurements are rejected. Each wire is calibrated individually. Using the mean energy loss of high momentum pions, different run periods can be compared. Figure 21 shows, for pions, the measured dE/dx values normalized to the Bethe-Bloch energy loss function. The projection for $\beta = 0.9$ (see inset in fig. 21) determines the dE/dx resolution to be $\pm$ 18% [36]. An example of the observed π/K separation is given later (section 8.1) in fig. 26(a).

6.2 Electromagnetic calorimeter calibration

The signal from each crystal, after amplification and shaping, is digitised in the FERA and 2282 ADC's. It is this digital information which is recorded and conversion factors are then required to obtain the amount of energy, in MeV, deposited in the crystal. Determining the calibration factors for each crystal, involves several stages which are described below. The calorimeter is calibrated *in situ* using antiproton-proton annihilation data.

6.2.1 Hardware adjustments

During assembly, crystals with low light output were fitted with preamplifiers with high output etc., so that all crystals gave approximately the same size signal for the same energy

deposited. Soon after completion of the detector, a minimum ionising particle calibration (see section 6.2.3) was carried out. Using these results, the amplification of each receiver channel was adjusted so that the minimum ionising peak appeared in the same place (within ± 3%) for all crystals.

The FERA and 2282 pedestals (ie. the ADC values corresponding to zero energy deposited) were adjusted to be roughly at 80 and 400 channels respectively. This was achieved by varying the DC levels on the outputs from the receivers. When taking data the pedestal positions are measured frequently (~ every 4 hours) since they can drift with temperature changes etc. The results are stored in the FERA and 2282 data acquisition systems for pedestal subtraction before readout.

6.2.2 FERA to 2282 gain ratio

The FERA and 2282 ADC systems overlap up to energies of about 400 MeV. This allows the FERA ADC's to be calibrated in terms of the 2282 system, whether or not the 2282 system has already been calibrated. For each crystal a straight line is fitted to a plot of FERA vs. 2282 ADC values. The data for this plot can be either from the lightpulser or from antiproton annihilations. The slope of the fit gives the "FERA gain ratio" for each channel. The intercept is usually non-zero due to non-linearities in the FERA at low energies and is used to correct the FERA pedestal and hence reduce the effects of this non-linearity. The FERA system is used to extend the range of measured energies beyond 400 MeV.

6.2.3 Energy calibration using minimum ionising peak method

High-energy charged particles can traverse the whole length of a crystal with only electromagnetic energy losses. For pions this corresponds to an energy loss of 170 MeV, providing a calibration point for each crystal. For this method, antiproton-proton annihilation events were recorded with the magnet off, so that charged particles (mostly pions) travel along the crystal.

Figure 22 shows a typical minimum ionising peak. It was produced by histogramming the energy deposited in a crystal when no energy was recorded in any of the eight neighbouring crystals. This reduces the background from photons and from charged particles which interact hadronically in the CsI. This method does not need a pre-calibration and so was suitable for initial adjustment of receiver amplifications and provided a pre-calibration for the π^0 invariant mass method described below. It gives high statistical accuracy for roughly 10^6 minimum bias events. However, the calibration has some systematic deviations arising from its dependence on charged particles as these give a different pattern for the energy deposited than do the photons in which we are primarily interested.

6.2.4 Energy calibration using π^0 invariant mass method

The most prominent feature of a histogram of invariant masses of pairs of photons detected in the electromagnetic calorimeter is a peak at 135 MeV from the decay $\pi^0 \rightarrow \gamma\gamma$. This peak can be used to calibrate all crystals, using data from antiproton-proton annihilations taken with an all-neutral trigger. Since these data can also be used for physics analysis, the method requires no extra beam time.

Figure 23 shows a typical histogram of $\gamma\gamma$ invariant mass-squared values for a particular crystal. It was produced by first selecting events in which the total energy recorded in the barrel calorimeter was close to twice the proton mass, so as to avoid events with large missing energy, and with 8 or less photons, so as to reduce the combinatoric background. For these events, whenever a crystal recorded a photon the histogram for that crystal was filled with all mass-squared values for that photon paired in sequence with all other photons recorded in the event. Usually one of these pairs is from a π^0, giving an entry in the π^0 peak. The other entries form the combinatoric background seen in fig. 23. In order to calculate the mass-squared values a pre-calibration is required.

The 1380 histograms obtained in this way are fitted using a Chebyshev polynomial for the combinatoric background and a Gaussian for the π^0 peak. The peak position for a given crystal is determined largely by the pre-calibration factor of that crystal, since this factor is present in every entry in the histogram. The position is hardly affected by the pre-calibration factors of other crystals since these are averaged out and only contribute to the width of the peak. Hence a new set of calibration factors can be calculated which will shift the π^0 peaks closer to the correct values. The method is then iterated until all the π^0 peaks are in the correct positions.

This method is based on the photon energy deposited in the crystals and the derived π^0 invariant masses, the measurement of which is the main function of the electromagnetic calorimeter. The method does not suffer from the systematic effects of the minimum ionizing peak method and gives high statistical accuracy ($\pm \frac{1}{2}\%$ per channel) for 1.2×10^6 all neutral events. However, it needs a pre-calibration of $\pm 20\%$ accuracy for the π^0 peaks to appear clearly. In the early stages of the experiment, the pre-calibration was provided by the minimum ionising peak method described above. Later on it was possible to use the calibration obtained for the previous run period as a pre-calibration. The calibration factors from the π^0 invariant mass method are those which are used in the data analysis.

6.2.5 Monitoring of gain stability

The CsI crystals are normally calibrated once each run period, of typically between 1 and 3 weeks. Changes in the crystal calibration factors during the run are monitored using the lightpulser (section 2.8). The calibrations can change, either by small drifts due to electronics gain changes, or by large steps if electronics components fail and have to be replaced. The

lightpulser allows new calibration factors to be determined without requiring a new set of antiproton annihilation data to be taken.

7 OFF-LINE RECONSTRUCTION, DATA ANALYSIS AND MONTE CARLO

The aim of the Crystal Barrel experiment is to study particles produced in $\bar{p}p$ annihilations. To this end the raw data from the detector have to be processed into a set of measurements for the particles in each event; this is the purpose of the off-line reconstruction system. Several additional software tools are provided to help in the analysis of the data. Finally, to fully understand the properties of the observed events a Monte Carlo simulation of the detector is available.

The computer code necessary to handle these tasks is written in Fortran 77, and maintained using the CMZ code management system [37]. The code has been prepared so that it can run on a variety of different computers (VAX, IBM, Alliant, SUN, DEC Stations). The data for each event are stored in the form of ZEBRA data banks [21], and the results of the off-line processing are added to the event as extra banks. The data is stored on IBM cartridges or Exabyte 8 mm video cartridges.

7.1 Off-line reconstruction

This is divided into several distinct tasks, each handled by a separate computer program. The reading and writing of tapes, initialization and loading of constants, and calling of the appropriate reconstruction/analysis code is handled in a single program. This program is thus always run when looking at data. It contains various dummy routines so that a user can insert his/her own specific code for various tasks (e.g., for analysis). The other code that can be called from this main job is described in the following sub-sections.

7.1.1 Database

All calibration constants are stored in one file, the database. This file has a directory structure based on the ZEBRA direct access software [21]. In the reconstruction many sets of constants are needed. For each run period one type of constants is kept in one directory, e.g., the calibration constants for the CsI crystals form one such directory. Within a particular directory the different sets of constants are identified by the range of runs for which they are valid and optionally by the calibration method. Thus each type of constants may vary from run to run independently, but typically a set is valid for several days.

7.1.2 Crystal reconstruction

The signals in the barrel calorimeter are used to measure the energy deposition and direction of particles entering the barrel. The reconstruction is optimized for analyzing the electromagnetic showers from photons. A search is made for clusters of neighbouring crystals

with energy depositions above 1 MeV. The energy sum of the crystals (the cluster energy) is required to be at least 20 MeV. If more than one local energy maximum is found inside a cluster, then the cluster is considered to consist of more than one photon (or charged particle). In this case the cluster energy is shared between the photons (or charged particles) according to the relative magnitude of the energy sum of each local maximum crystal and its eight neighbours. Statistical fluctuations can generate secondary maxima. In order to get rid of these misidentifications the centre crystal of a local maximum must have at least 20 MeV energy deposited.

To correct for the 1 MeV energy cut for neighbouring crystals and the different radiation lengths of material in front of the crystals, a cluster energy dependent function derived from Monte Carlo calculations is applied to the reconstructed energies. The direction of the photons is calculated using the centre of gravity of the crystals in the cluster weighted by the energy.

7.1.3 JDC

Information from the JDC is used to measure a charged particle's trajectory and momentum. Raw signals on the JDC wires are converted to positions in space using the time relative to the start of the event, the magnitude of the signal on both ends of the wires and a knowledge of the gas, pressure, temperature and electric and magnetic fields inside the JDC. These hits are then processed by the pattern recognition algorithms which try to associate them into track segments. Initially, very loose roads are built in the r-z projection by assuming that all tracks pass near the assumed vertex position (0, 0, 0). After this, the algorithms concentrate on the r-ϕ projection. In this projection, one needs not only to associate the hits into tracks, but also to decide on which side of the JDC sector the track has passed (the left-right ambiguity). Initially, one looks for r-z roads in adjacent JDC sectors which nearly match. If this condition is satisfied, then an r-ϕ segment start can be made at the sector boundary. For those tracks which are contained in exactly one sector, an alternative algorithm taking advantage of the 200 μm stagger of the sense wires is used. Because of this stagger, the correct left-right solution will be smoother than the wrong one.

Once a segment start has been found, a projection algorithm is used to pick up additional hits by looking only at information in the r-ϕ plane. Once this has been completed, all track segments are passed to a simple circle fitter. The circle fit parameters are then used to match broken segments, and to pick up hits along the tracks which were missed by the pattern recognition. These final tracks are then passed to a helix fitting algorithm which does a full three dimensional fit for each track. This fit gives the particle's charge, its momentum, the distance of closest approach to the z-axis and its direction and z-coordinate at this point.

For events with more than one track, the helicies are given to a global vertex fitter which forces all tracks through a common point, the vertex. The fit initially includes all tracks whose

first hit is in one of the inner layers of the JDC. However, if this fit fails, tracks are dropped to produce a better fit. The vertex is generally found with an x-y resolution (σ) of about 1 mm, and a z resolution (σ) of about 5 mm.

Particle identification is made using the dE/dx information from the JDC. For each track in the JDC the χ^2 for each of the particles (electron, muon, pion, kaon, proton (and antiparticle)) are calculated. These χ^2 can then be used in the analysis, for example combined with information from kinematic fitting testing for a specific event topology.

7.1.4 Particle data banks

The information on charged tracks and the signals seen in the crystals is used to construct a bank of data on all the observed photons and charged particles in an event. Since charged tracks give signals not only in the JDC but also in the crystals, the latter signals have to be identified before the particle banks are created. This is done by extrapolating the trajectory of all reconstructed charged tracks to the surface of the crystals. If a signal in the crystals is found associated in space with this projection, it is considered to be the signal of the charged particle and not that of a photon. Using pions which have been clearly identified in the JDC, it is found that 98% of charged pions are associated with signals in the crystals. A data bank is created for every charged track and unassociated signal in the crystals; it contains the measured energy or momentum, and its direction of motion. These banks are used in subsequent event analysis.

A complication in this procedure is that extra signals are found in the crystals. These occur for two distinct reasons. When photons and electrons shower in the crystals, the showering does not always proceed in a geometrically regular fashion. A separate part of the shower, split off from the main shower direction, can appear. The result can thus be an apparent second maximum of energy in the final shower cluster in the crystals. It is found that 5% of photon showers suffer from this problem; the second shower is characterized by occuring close to the first shower (within 10° as seen from the event vertex), and by containing approximately 10% of the energy of the photon. The observation of such split-offs is a consequence of the excellent spatial and energy resolution of the detector. The split-off showers can be identified and added back to the main shower energy for the photon. A second effect is that only some 40% of charged particles give minimum ionizing signals when they pass through the crystals (measured for tracks with momentum over 750 MeV/c). The remainder interact, giving larger energy depositions along their extrapolated paths through the crystals, and in the process generate secondary particles which travel through the detector giving a second signal isolated in space from the first. These secondary signals cannot be easily identified as arising from charged tracks and thus they appear as distinct particles in the final particle data banks. On average there are 0.56 secondary signals per charged pion and 0.69 per charged kaon. For pions 66% of these signals have energies greater than 50 MeV, 43% have energy greater than 100 MeV, and the presence of such signals has to be allowed for in the subsequent analysis.

7.1.5 Analysis procedures

After reconstruction, the data on the particles in an event is stored on a data summary tape. To help in their analysis several packages are provided, including, for example, a combinatorial solving package searching permutations of photons to find π^0 (or η, η') decays, a kinematic fit package and an event display package. Analyses based upon finding resonances and/or specified topologies in events are already well advanced.

The data summary tapes are split into categories for users to search through for particular types of events. The categories are determined by event topology (e.g., number of charged tracks, number of photons in all-neutral events, etc).

7.2 Monte Carlo simulation

The Monte Carlo (MC) simulation of the detector is carried out in the framework provided by the CERN GEANT software [38]. The distinct physical volumes of the detector are modelled, and particles produced by simulations of $\bar{p}N$ annihilations are tracked through the detector. Energy losses, particle decays and interactions producing secondary particles are all modelled. The hadronic interactions of particles are modelled using GEISHA [39], and the electromagnetic showering by GEANT. The signal produced in each detector element is simulated and written out in a data format identical to that of the real data. A bank of data describing the generated event topology is also saved. The event can then be reconstructed and analysed using the same software as for real data.

7.3 Overall performance

The computer time (CERN IBM units) required to fully reconstruct a typical event is 300 ms and to generate a MC event is 2.5 seconds. About 25% of the present reconstruction time is spent processing the raw flash-ADC data from the JDC. This task will eventually be moved into the online system leading to a speed-up in the off-line data processing. It is anticipated that all events recorded by the experiment will be reconstructed (of the order of 50 million events so far), and that the number of generated MC events will be of a similar magnitude. To provide the necessary computer time a farm of six DEC Station 5000's is now used.

The offline reconstruction package has already processed over 20 million data events, and several million MC events have also been generated. Various data analyses are already well advanced or completed (see [4]). This indicates the robustness of the reconstruction code and analysis tools.

8 PERFORMANCE

8.1 Performance of the JDC

To study the performance of the JDC, proton-antiproton annihilations into all charged final states have been studied. The two body final states $\bar{p}p \rightarrow \pi^+\pi^-$ and $\bar{p}p \rightarrow K^+K^-$ used for calibration of the JDC (section 6.1.3) give two absolute points for the momentum resolution close to the upper end of the range of measured momenta. The final state consisting of four charged pions, in conjunction with a 4-C kinematic fit to energy and momentum balance is then used to measure the momentum resolution over the full range of detected momenta. Finally, the process $\bar{p}p \rightarrow \pi^+\pi^-K^+K^-$ is used to study the K - π separation of the detector.

The data for $\bar{p}p \rightarrow \pi^+\pi^-\pi^+\pi^-$ were selected by requiring exactly four tracks in the JDC. These tracks must start no later than layer 3, and end no sooner than layer 15. Also, in a 2-dimensional plot of total momentum versus total energy for the charged pions (fig. 24), these events must fall within a box 200 MeV wide and 200 MeV/c high. A 4-C kinematic fit to energy and momentum balance of the charged particles was made for the selected events. The deviations between the measured and fitted momentum give a measure of the momentum resolution of the JDC over most of the range of momentum acceptance. These data can be combined with the data from the two body final states to yield a plot of σ_p/p versus p (fig. 25). Because the momentum resolution is inversely proportional to the track length squared, and the tracks vary in length from 8 cm to 18 cm, these resolutions only give a measure of the overall performance for physics events.

Finally, the dE/dx performance of the JDC was examined by looking at data from $\bar{p}p \rightarrow \pi^+\pi^-K^+K^-$. These data were again selected by taking all events with exactly four tracks satisfying the length requirements for the previous final state. These events were then used in a 3-C kinematic fit to momentum balance, and those selected used in a 4-C kinematic fit to the $\pi^+\pi^-K^+K^-$hypothesis, (four combinations per event). Those events passing the hypothesis at the 10% level were then assumed to be $\pi^+\pi^-K^+K^-$ events. The dE/dx as a function of momentum for these events is shown in fig. 26(a). There is very clean K-π separation up to 500 MeV/c. Finally, fig. 26(b) shows the $\pi^{\pm}K^{\mp}$ invariant mass for these events. The $K^*(892) \rightarrow K\pi$ is clearly seen.

8.2 Performance of the CsI Barrel

The performance of the CsI Barrel is affected by electronic noise and by the failure of hardware such as the photodiode or electronics associated with the analog processing. Electronic noise, together with the amount of inactive material in front of or between the detector modules, degrades both the energy and spatial resolution. Breakdowns, on the other hand, would limit the availability of the detector.

The noise performance is determined by the capacitance of the photodiode and by the input capacitance of the preamplifier FET. A careful selection of low-noise components (dark current less than 5 nA) and a well matched amplifier and pulse shaping system results in an overall electronic noise (σ) of 420 photo-electrons, corresponding to an equivalent noise of 220 keV photon energy. In addition a coherent noise (σ) of about 60 keV per channel exists, which may contribute up to 6 MeV noise for an event where typically 100 channels have to be summed. This represents an uncertainty in the total energy measured by the calorimeter for the event of much less than 1%.

A reasonably low occurrence of breakdowns is found in a failure analysis. Due to the mechanical design, downtimes of less than three days for repair are required and are accepted as tolerable. Experience over two years of operation indicates that the preamplifier is the most likely component to fail. We found a mean time before failure (MTBF) of 660 years for the photodiode and 140 years MTBF for the preamplifier.

The light output of the crystal setup has been measured to correspond to an average of 1900 photoelectrons per MeV using a shaping time of 1 μs (peaking time 3 μs). This corresponds to 70% of the number of photoelectrons which are produced. Figure 27 shows the energy resolution (σ) as a function of energy as predicted by Monte Carlo simulations (see section 7.2) using EGS [40]. In addition two experimental results from annihilation reactions are included. The reaction $\bar{p}p \rightarrow \pi^0\gamma$ provides a mono-energetic gamma with an energy of 933.4 MeV. Here we find an energy resolution (σ) of 2.5%. Using photons originating from the decay of the mono-energetic η in the annihilation channel $\bar{p}p \rightarrow \pi^0\eta$ we derive an energy resolution (σ) of 5% at 95 MeV. Both values are consistent with the assumption of an $1/\sqrt[4]{E}$ dependence for the energy resolution. For energies greater than 50 MeV the angular resolution (σ) is better than 1.5° for non-overlapping showers if one uses the centre of gravity of a shower to reconstruct the impact point of a photon. The long term stability is monitored by means of the light pulser system and is better than 0.5% over a typical run period of two weeks.

The best way to demonstrate the performance of the detector is to show experimental results. Figure 28 displays as an example the reconstructed invariant $\gamma\gamma$-mass of selected annihilation reactions with six γ's in the final state. The radiative decays of π^0, η and η' are clearly seen. A mass resolution of $\sigma(m_{\pi^0}) = 9.9$ MeV and $\sigma(m_\eta) = 16.6$ MeV is obtained.

8.3 Performance of the trigger system

8.3.1 Level 0 hardware

The general quality of the recorded data depends on the level 0 hardware trigger, since this trigger gives the "time zero" for the drift chamber and opens the gates of the crystal ADC's with an accuracy of ± 300 ps. At 200 MeV/c, where the incoming antiprotons stop in the hydrogen target, every antiproton produces a valid event and pileup must be avoided. Pileup rejection

occurs for events in a window of ± 10 μs around time zero. With an antiproton flux of 20 k/s, the probability for undetected pileup is 0.08%. These events can be rejected offline by imposing energy, momentum and charge conservation.

8.3.2 Level 1 hardware

This trigger uses information from most subdetectors; the PWC, JDC and CsI crystals. Within 500 ns the multiplicity of charged particles is known from the PWC with an efficiency of 99%. At this stage an "all neutral" trigger can be selected by demanding zero charged particles in the event. This trigger gives maximal data acquisition at a rate which is currently about 30/s. Furthermore, the purity of this all neutral sample is over 90%. A negative trigger decision causes a fast system reset and prepares the detector for the next event within 30 μs. The JDC multiplicity logic gives additional information about charged tracks after 4 μs. This allows the selection of particles which traverse the whole chamber and produce hits in the outer layers. For such tracks the momentum determination is the best possible. The total multiplicity is finally known from the FACE after 25 μs. The JDC multiplicity trigger has an efficiency of 99%. The overall FACE efficiency for a specific multiplicity varies between 50% and 70% depending on the total multiplicity in the final state.

In the level one hardware trigger we can select events with a defined number of charged particles and photons with a probability of roughly 60%. If we relax the trigger requirements slightly and allow a window of ± 1 on the total multiplicity, then the probability to select the wanted events becomes > 90% at this trigger level.

8.3.3 Software trigger

The first stage decision on the total energy seen in the crystals can be made within 100 μs. This provides an efficient trigger on events with K_L particles, where only events with missing energy in a window around the K_L mass are accepted in addition to the already mentioned all neutral trigger. About 15% of these events have a good missing K_L which can be used in further analysis. In principle the software trigger can, within 1 to 3 ms, select any combination of final state particles which decay to photons.

8.3.4 Combined trigger performance

The application of all the hardware trigger levels, together with the software trigger, allows specific final states to be selected. Two representative examples are discussed below. In the trigger for collinear tracks, a charged multiplicity of two is selected in the PWC, two long tracks are selected in the JDC, two clusters of crystals are selected in the FACE and the software trigger restricts the two clusters to have a total energy below 500 MeV and an invariant mass of 325 ± 175 MeV/c^2. This selects back-to-back minimum ionising charged tracks, and the events are of the type $\bar{p}p \rightarrow \pi^+\pi^-$ or K^+K^-, which are used for the calibration of the JDC

(section 6.1.3). The data acquisition rate is 1 to 2 events/s, and roughly 20% of these events pass all off-line cuts to qualify as genuine $\pi^+\pi^-$ and K^+K^- events.

Another more complex example is the final state $\pi^+\pi^-\pi^0\pi^0\eta$. The PWC and JDC are used to define the charged multiplicity, the FACE determines the total multiplicity whilst the software trigger is used to identify π^0's and η's. This trigger gives a data acquisition rate of 8/sec and an enhancement factor of 50 as compared to a minimum bias trigger. We conclude that the multi-level Crystal Barrel trigger system is able to select rare final states with good efficiency.

8.4 Overall performance

The Crystal Barrel detector has been successfully constructed and has already recorded many millions of events. The overall reliability of the detector is indicated by an accumulated total of approximately 50 million events in 11 run periods, each typically lasting 10 days, in the first 2 years of data taking (1989-1991). The performance and high efficiency of detector components, readout electronics and the data acquisition system have been described above. The ability to trigger on observed energies, particle multiplicities and specific final state topologies has also been shown. The quality of the data obtained is indicated by the measured charged track momentum and photon energy resolutions (see figures 25 and 27). The observed particles in an event can be combined together to yield information on intermediate resonances in the data, as shown in figures 26 and 28 (note that no kinematic fitting is used in preparing these distributions, they rely on measured quantities only). Detailed analyses of data are already underway. For example [4], we have already published the results of an analysis of the reaction $\bar{p}p \rightarrow \pi^0\pi^0\pi^0$, where we confirm the existence of the recently observed f_2 (1515).

This ability to take large amounts of data under well controlled conditions, plus the large acceptance and ability to clearly resolve intermediate resonances, allows the collaboration to concentrate on the fulfilment of its physics program as outlined in section 1.

9 SUMMARY AND OUTLOOK

The Crystal Barrel spectrometer at LEAR, which is used to measure the products of antiproton-proton and antiproton-deuteron annihilations, has been described. The spectrometer uses a jet drift chamber, with 30 sectors each containing 23 wires, together with a 1.5 T magnetic field to measure the momentum of outgoing charged particles. A surrounding, barrel-shaped, CsI calorimeter with 1380 elements, is used to measure the photons from the decay of π^0, η, η' and ω mesons. Two concentric cylindrical multi-wire proportional chambers immediately surrounding the hydrogen target give the multiplicity of charged particles; they can also be used to select "all neutral" events and to provide a fast trigger on K^0_S decays. Used together with a fast encoder for clusters recorded in the photon calorimeter and a software trigger

allowing specific total energy and/or invariant masses to be selected, it is possible to trigger on well defined event topologies.

After installation of the equipment, a first data taking run took place in December 1989 with a 200 MeV/c antiproton beam using both minimum bias (i.e. open) and zero-prong ("all neutral") triggers to study antiproton-proton annihilations at rest. By the end of 1991 some 46 million events using the 200 MeV/c beam had been recorded, including 10 M minimum bias and 18 M zero prong events in liquid hydrogen. More specific hardware triggers included 4 M two-prong and 3 M four-prong events. The software trigger was used to take data on specific event topologies; 0.4 M $\pi^+\pi^-\eta$ triggers and 2.8 M $\pi^+\pi^-\ 2\pi^0\eta$ events. The apparatus has also been used to take 4.5 M zero–prong and 2.5 M single-prong events in liquid deuterium.

In order to allow simultaneous sharing of the LEAR beam with other experiments, almost all of the running in the period 1990-91 was at an antiproton beam momentum of 200 MeV/c. However, a short test run at 600 MeV/c was made in 1990, and a first data taking run at 1.2 GeV/c took place at the end of 1991. It is anticipated that the emphasis will now move to beam momenta in the range 0.6 to 2.0 GeV/c to allow higher mass states to be investigated. To use the hydrogen gas target (section 2.3), which will give increased P-state capture in $\bar{p}$ p annihilations at rest, a low momentum 100 MeV/c antiproton beam will be required.

Analysis of the very large body of data is now in progress and preliminary reports of results have been given at a number of conferences. A study of the reaction $\bar{p}p \rightarrow \pi^0\pi^0\pi^0$ with 55 k events from a sample of 1.2 M zero-prong triggers has been published [4]. A J^{PC} 2^{++} resonance at a mass of 1515 MeV with a width of 120 ± 10 MeV is required to explain the data. This resonance is identified as the f_2 (1515) previously seen [41] by the ASTERIX collaboration and which, it has been suggested, could be either a 4-quark or quasi-nuclear bound state. The reaction $\bar{p}p \rightarrow \pi^0\eta\eta$ has been studied with a total of 22.5 k events from a total of 11.3 M zero prong triggers. The results show that this final state is dominated by the production of the scalar f_0 (1560) meson which is observed in its $\eta\eta$ decay node. The f_0 (1560) is a possible candidate for a gluonium or glueball.

ACKNOWLEDGEMENTS

We would like to thank the technical staff of the LEAR machine group and all the participating institutions for their invaluable contributions to the success of the experiment. In particular from Karlsruhe we would like to thank F Kröner, H J Plotzizka and D Engel for their very efficient help in the mechanical engineering and set up of the support structure and the servicing devices for the electromagnetic calorimeter; the central workshop of the Kernforschungszentrum Karlsruhe for associated mechanical work and K Kärcher for valuable help in wiring up the crystal preamplifiers and setting up the JDC gas system. At CERN we particularly wish to thank R Volck for much work on the day to day maintenance of the

apparatus. From the University of Mainz we wish to thank Klaus Fuchs for development and construction of various electronic units. From the University of Munich we thank H Schumann for the design of the magnet, calorimeter support and the inner detector arrangement; M Haase, H Herbert, G Miller and H Willaredt for their help in building the detector as well as their constant assistance in maintenance and repair; also the electronic and mechanical workshops (led by Dr S Hegewisch and H Rauch) for designing and constructing many special parts of the apparatus. At the University of Zurich we wish to thank K Esslinger for the design and production of the crystal amplifiers. We also wish to thank Mrs P M Richens of the Rutherford Appleton Laboratory for her skilful wordprocessing of this manuscript.

We acknowledge financial support from the German Bundesministerium für Forschung and Technologie, the Schweizerischer Nationalfonds, the British Science and Engineering Research Council and the US Department of Energy (contract No. DE-FG03-87ER40323 and DE-AC03-76SF00098). K Königsmann acknowledges support from the Heisenberg Foundation.

Table 1
Properties of CsI(T1) scintillator

Parameter	CsI(T1)
Density	4.53 g/cm^3
Radiation length L_R	1.86 cm
Moliere radius	3.8 cm
Light output	0.85 relative to NaI
Maximum emission at	550 nm
Decay times	0.9 μs and 7 μs
Photon yield/MeV	4.5 x 10^4

Table 2
Specifications of the Crystal Barrel calorimeter

General layout	Barrel configuration
Polar angle range	12° - 168°
Solid angle	95% of 4π
Free inner length	540 mm
Free inner radius	270 mm
Number of elements	1380
Scintillator	CsI(Tℓ)
Active length	300 mm (16.1 L_R)
Readout	WLS and photodiode
Total mass	3.8 x 10^3 kg

Table 3

Number of channels and amount of data produced by the main detector components and by the slow control system for a typical annihilation event.

Detector	Number of channels	Raw data (bytes)	Zero suppressed data (bytes)
PWC	240	500	50
Jet chamber	1380	460000	10000
Calorimeter	2 x 1380	5800	500
Slow control	100	1000	1000
Trigger scalers	50	200	200
TOTAL			~12000

REFERENCES

[1] P Baillon et al., Nuovo. Cim. **50A** (1967) 393.
L Gray et al., Phys. Rev. **D27** (1983) 307.
B May et al. Phys. Lett. **B225** (1989) 450.

[2] C Amsler. Nucl. Phys. **A508** (1990) 501c.
A M Green and J A Niskanen, Prog. Part. Nucl. Phys. **18** (1987) 93.

[3] F Close, Rep. Prog. Phys. **51** (1988) 833.
T H Burnett and S R Sharpe, Ann. Rev. Nucl. Part. Sci. **40** (1990) 327.
C Amsler and F Myhrer, Ann. Rev. Nucl. Part. Sci. **41** (1991) 219.
L Montanet, Light quark mesons and exotics, p. 669, 3rd International Conference on Hadron Spectroscopy "Hadron 89", Ajaccio (France), September 1989 (ed. Ed. Frontières).
L G Landsberg, Exotic Hadrons, p. 535, XXIVth Rencontre de Moriond, New Results in Hadronic Interactions, Les Arcs (France), March 1989 (ed. Ed. Frontières).

[4] E Aker et al., (Crystal Barrel Collaboration), Phys. Lett. **B260** (1991) 249.

[5] M Doser et al., (ASTERIX collaboration). Nucl. Phys. **A486** (1988) 493.

[6] S Ahmad et al., (ASTERIX collaboration). Nucl. Instr. and Meth. **A286** (1990) 76.

[7] Photocell type F165 B, manufactured by Siemens Munich.

[8] Manufactured by Q-Par Angus, Leominster, UK.

[9] T Beha, W Dünnweber et al., IEEE Trans. Nucl. Sci (to be published).

[10] J.Lüdemann, Aufbau einer Niederdruckproportionalkammer zum Nachweis niederenergetischer Antiprotonen, Diploma thesis, Mainz University (1991).

[11] H.Hammer, Aufbau eines ortsauflösenden Szintillationsfaserdetektors, Diploma thesis, Mainz University (1991).

[12] H Drumm et al., Nucl. Instr. Meth. **176** (1980) 333.

[13] R Veenhof. Program GARFIELD user guide, CERN program library W5050 (1989).

[14] U Becker et al., Nucl. Instr. and Meth. **214** (1983) 525.

[15] V Commichau et al., Nucl. Instr. and Meth. **A235** (1985) 267.

[16] H Emerich, Eine Monitordriftkammer für das Crystal Barrel Experiment am CERN in Genf. Diploma Thesis, University of Munich (1989).

[17] C Kolo, Inbetriebnahme einer Monitordriftkammer am Crystal Barrel Experiment. Diploma Thesis, University of Munich (1990).

[18] E Blucher et al. Nucl. Instr. and Meth. **A249** (1986) 201.

[19] Cleo II Proposal. Report CLNS 85/634 (1985).
C Bebek, Nucl. Instr. and Meth. **A265** (1988) 258.

[20] C C Lo, S Olson, J Bistirlich. IEEE Trans. Nucl. Sci. **36** (1989) 462.

[21] R Brun, J.Zoll, ZEBRA user guide, CERN Program Library Q100, (1987).

[22] T Charity. OS-9 Network Disk Server, User Guide and Reference Manual. CERN report ALEPH 89-184 (1989).

[23] OS-9/68K. Microware Systems Corporation, 1984, 1987.

[24] Kernigham and Ritchie, The C programming language 2nd Ed. Prentice Hall 1988.

[25] H v d Schmitt, Physikalisches Institut Universität Heidelberg. RTF/68K Real-Time Fortran 77 for 68K Processors, Manual of Compiler and Run-Time Library (Version 3.4).

[26] A Vascotto, "Modular architectures for on-line systems". Proc. CERN School of Computing, Renesse, 1986, Geneva; CERN 87-04 (1987) p. 147.
C Boissat, R Jones, G Mornachi, Model Human Interface, CERN Report DD/89-11 (1989).

[27] R Brun, D Lienart. HBOOK user guide, CERN Program Library Y250 (1987).

[28] R Brun, N Cremel-Somon. HPLOT user guide, CERN Program Library Y251 (1988).

[29] Inside Macintosh, Vol I - V, Addison-Wesley (1985).

[30] M Kunze. The PS197 electronic runbook. To be published in the Proceedings of the Second International Workshop on Artificial Intelligence and Software Engineering for Nuclear and Particle Physics, L' Agelande, Ed. D Perret-Gallix, World Scientific Publishing, 1992.

[31] M Merkel. IEEE Trans. Nucl. Sci. **39** (1992) 159.
M.Merkel, Aufbau und Test des Datenerfassungssystems für den Zentraldetektor des Crystal Barrel Experimentes, Diploma thesis, Mainz University (1988).

[32] S.Walther, Entwicklung, Aufbau, Herstellung und Test eines Multiplizitätentriggers für das Crystal Barrel Experiment, Diploma thesis, Mainz University (1990).

[33] M Kunze, Aufbau und Test eines Triggersystems für das Crystal-Barrel Experiment, Thesis, Karlsruhe University (1990).

[34] F James, M Roos. MINUIT long write up, CERN Program Library D506 (1989).

[35] S.Spanier, Die Kalibration der Jetdriftkammer des Crystal Barrel Experimentes, Diploma thesis, Mainz University (1991).

[36] C.Strassburger, Nachweis von Vektormesonen im Crystal Barrel Detektor, Diploma thesis, Mainz University (1990).

[37] CMZ User Guide and Reference Manual, CERN Program Library (1990).
CMZ is a product of CodeME SARL, 10, Rue de l'Eglise, F-01630 St. Genis-Pouilly, France.

[38] R Brun, F Bruyant, M Maire, A C McPherson, P Zanarini GEANT3, CERN Report DD/EE/84-1 (1987).

[39] H C Fesefeldt, GHEISHA, PITHA Report, 85-02, RWTH Aachen (1985).

[40] R L Ford and W R Nelson. The EGS code system. Report SLAC-210 (1978).
W R Nelson, H Hirayama, D Rogers, EGS4 long write-up. CERN Program Library W5042 (1985).

[41] B May et al., (ASTERIX collaboration), Phys. Lett. **B225** (1989) 450; Z. Phys. **C46** (1990) 191, 203.

FIGURE CAPTION

1 Overall layout of Crystal Barrel detector showing (1) magnet yoke, (2) magnet coils, (3) CsI barrel, (4) jet drift chamber, (5) proportional chamber, (6) liquid hydrogen target, (7) one half of the endplate, (a) Longitudinal cross-section (b) Transverse view.

2 Overall layout of beam counters and liquid hydrogen target. Upper part: horizontal cut along the beam direction. Lower part (enlarged scale): vertical cut along the silicon counters Si_{2-5}.

3 Overall layout of (a) hydrogen gas target, (b) scintillating fibre detector, (c) antiproton entrance counter.

4 Drawing of the upstream (readout) end of the inner proportional wire chamber (C1). A-HV plug, B-ground plug, C-outer shield, D-cathode foil, E-signal wire, F-print, G-signal cable, H-O ring. The Rohacell walls are sandwiched between C and D. All dimensions are in mm.

5 Schematic drawing of the Jet Drift Chamber (JDC). Staggering of the sense wire positions, shown as thin lines in the expanded drawing, has been exaggerated for clarity.

6 Drift lines in a JDC sector for layers 11 to 14 (B = 1.5 Tesla). The drift isochrones (dashed lines) are equally spaced at time intervals of 0.2 μs.

7 Schematic drawing of the monitor drift chamber: (1) aluminized mylar foils, (2) cathode grid, (3) signal wires (small dots), field shaping wires (big dots), (4) high voltage supply, (5) quartz window, (6) tower of nine epoxy resin plates, (7) drift volume with eight Cu/Be ring electrodes, (8) proportional chamber, (9) Mylar window.

8 Cross-section of a CsI(T1) module: (1) 0.1 mm titanium can, (2) printed circuit board, (3) filters for bias and power supplies, (4) preamplifier, (5) light fibre, (6) brass cover, (7) wavelength shifter (WLS), (8) photodiode.

9 Optical matching of CsI (Tℓ) scintillator to the wavelength shifter. Dashed curve: spectral emission of CsI (schematic). Full line: measured transmission of wavelength shifter. Dotted line: measured spectral emission of wavelength shifter.

10 Overall layout of Xe light pulser system. LM: Light mixer (bar of Plexiglass), D: Diffusor, WLS: Wavelength shifter, PD: Photodiode, MON: Lamp intensity monitor, REF: Reference light source, CC: Crystal in calorimeter.

11 Simplified structure of the data acquisition system.

12 Overall schematic of the Crystal Barrel data acquisition system.

13 Simplified layout of JDC readout system.

14 Simplified layout of CsI calorimeter data acquisition system.

15 Slow control and monitoring hardware.

16 Software for monitoring the Crystal Barrel detector

17 Overall layout of the trigger system.

18 Schematic arrangement of hardware trigger electronics.

19 The measured momentum of charged particles in the two-body final states $\pi^+\pi^-$ (peak at 927 MeV/c) and K^+K^- (peak at 797 MeV/c). The $\pi\pi$ peak has a width (σ) of 19 MeV/c.

20 (a) The r-ϕ resolution of the JDC as a function of drift distance. (b) A projection of the uniform drift region showing ~ 125 μm resolution in these areas.

21 Measured dE/dx values after normalisation to the Bethe-Bloch energy loss function in the minimum ionising region.

22 Histogram from the 2282 ADC for a single crystal, for events in which no energy was recorded in the neighbouring crystals. The minimum ionizing peak is clearly visible.

23 Histogram of two-photon invariant mass squared values, where one photon entered a particular crystal. The π^0 peak is clearly visible. The fit is a Gaussian with fourth order Chebyshev polynomial, as used to determine the software gain correction for that crystal.

24 Total momentum versus total energy for the $\pi^+\pi^-\pi^+\pi^-$ ($n\pi^0$) final state. The momentum and energy are computed from the charged particles only.

25 The momentum resolution (σ) as a function of momentum. The points are the momentum resolution σ_p/p; data are obtained by fitting the four-prong final state $\pi^+\pi^-\pi^+\pi^-$. The solid curve is the momentum spectrum of the charged particles in this same final state.

26 (a) dE/dx as a function of measured momentum for the $\pi^+\pi^-K^+K^-$ final state. (b) The $\pi^\pm K^\mp$ invariant mass for the same final state. The peak is from the K*(892).

27 Energy resolution (σ) of the CsI calorimeter. Dashed curve displays EGS [40] simulations. The values marked $\pi^0\gamma$ and $\pi^0\eta$ are experimental results.

28 The invariant two-photon effective mass spectrum extracted from a six-photon event sample (15 combinations per event): one clearly sees π^0 and η peaks. The upper inset shows the $\gamma\gamma$ invariant mass distribution of those $\gamma\gamma$ pairs which do not contribute to the π^0 mass window; the combinatorial background is reduced and the η signal becomes more apparent. If the η mass window is also excluded, the $\eta' \rightarrow \gamma\gamma$ decay can be seen (lower inset). The peak at 770 MeV is due to $\pi^0\pi^0\omega$ events with $\omega^0 \rightarrow \pi^0\gamma$ where one very low energy γ was unobserved.

TABLES

1 Properties of CsI(Tℓ) scintillator.

2 Specifications of the Crystal Barrel calorimeter.

3 Number of channels and amount of data produced by the main detector components and by the slow control system for a typical annihilation event.

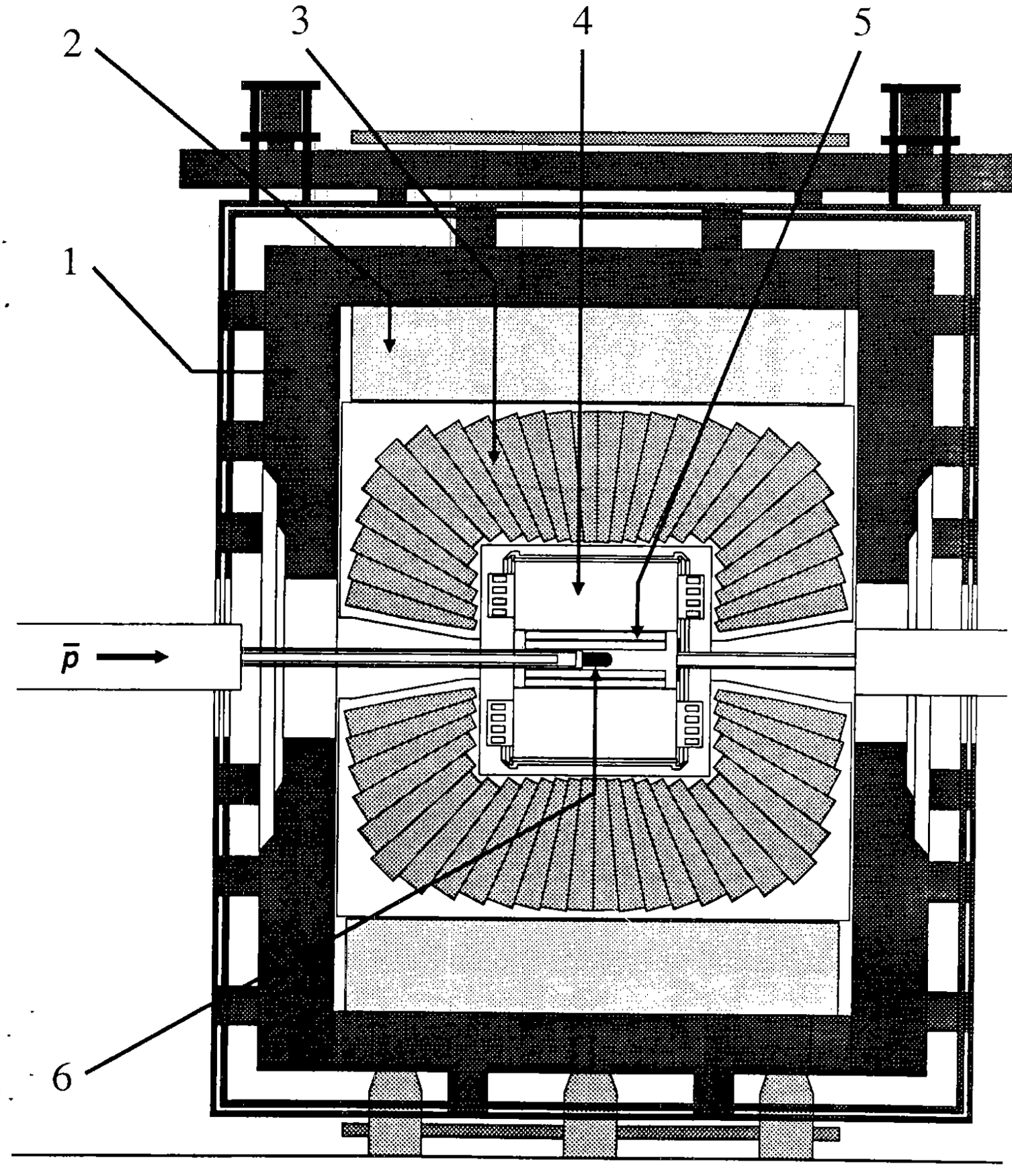

Figure 1(a)

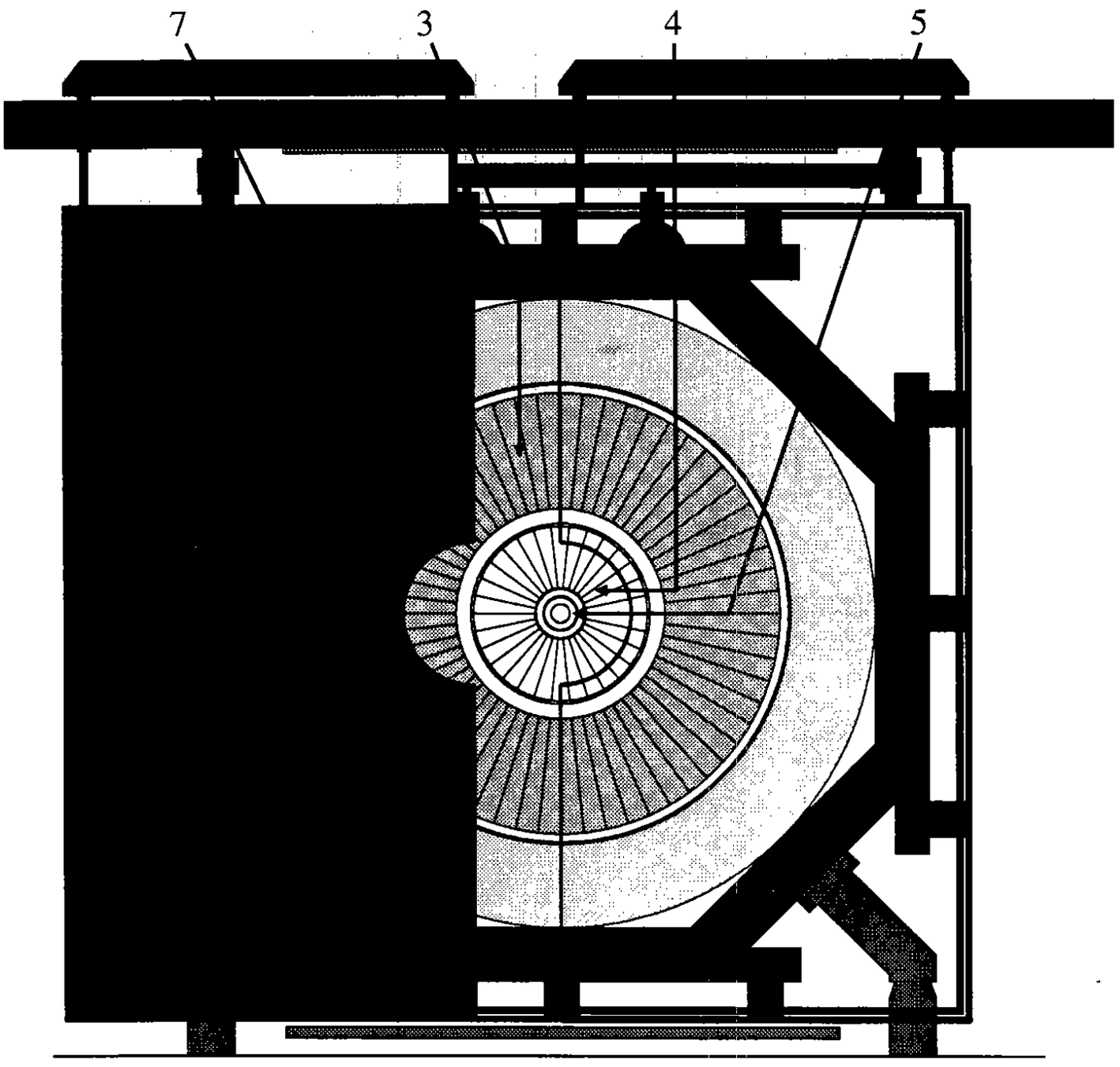

Figure 1(b)

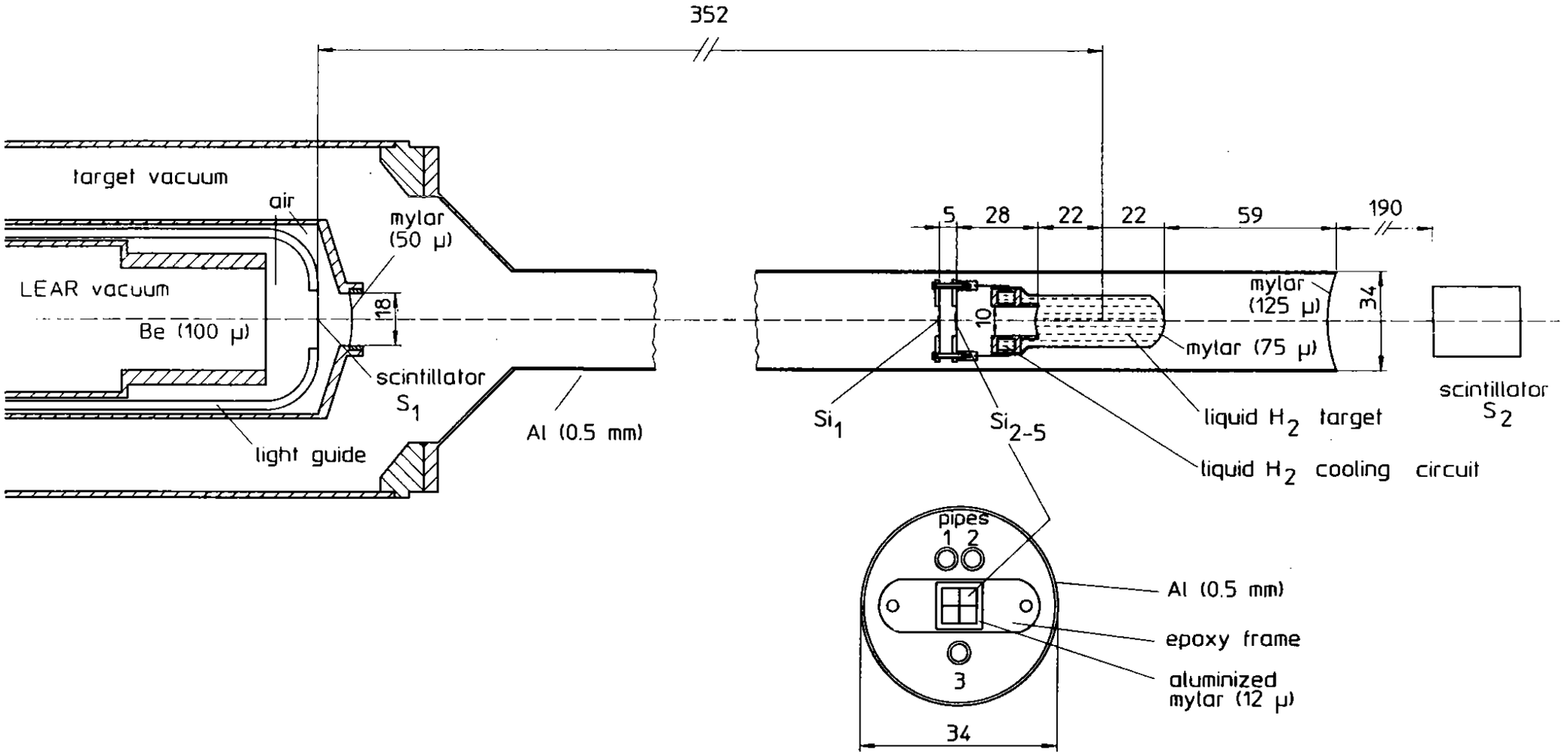
352
target vacuum
air
mylar
(50 μ)
LEAR vacuum
Be (100 μ)
18
scintillator
S1
light guide
Al (0.5 mm)
5
28
22
22
59
190
mylar
(125 μ)
34
10
mylar (75 μ)
scintillator
S2
Si1
Si2-5
liquid H2 target
liquid H2 cooling circuit
pipes
1 2
3
Al (0.5 mm)
epoxy frame
aluminized
mylar (12 μ)
34

Figure 2

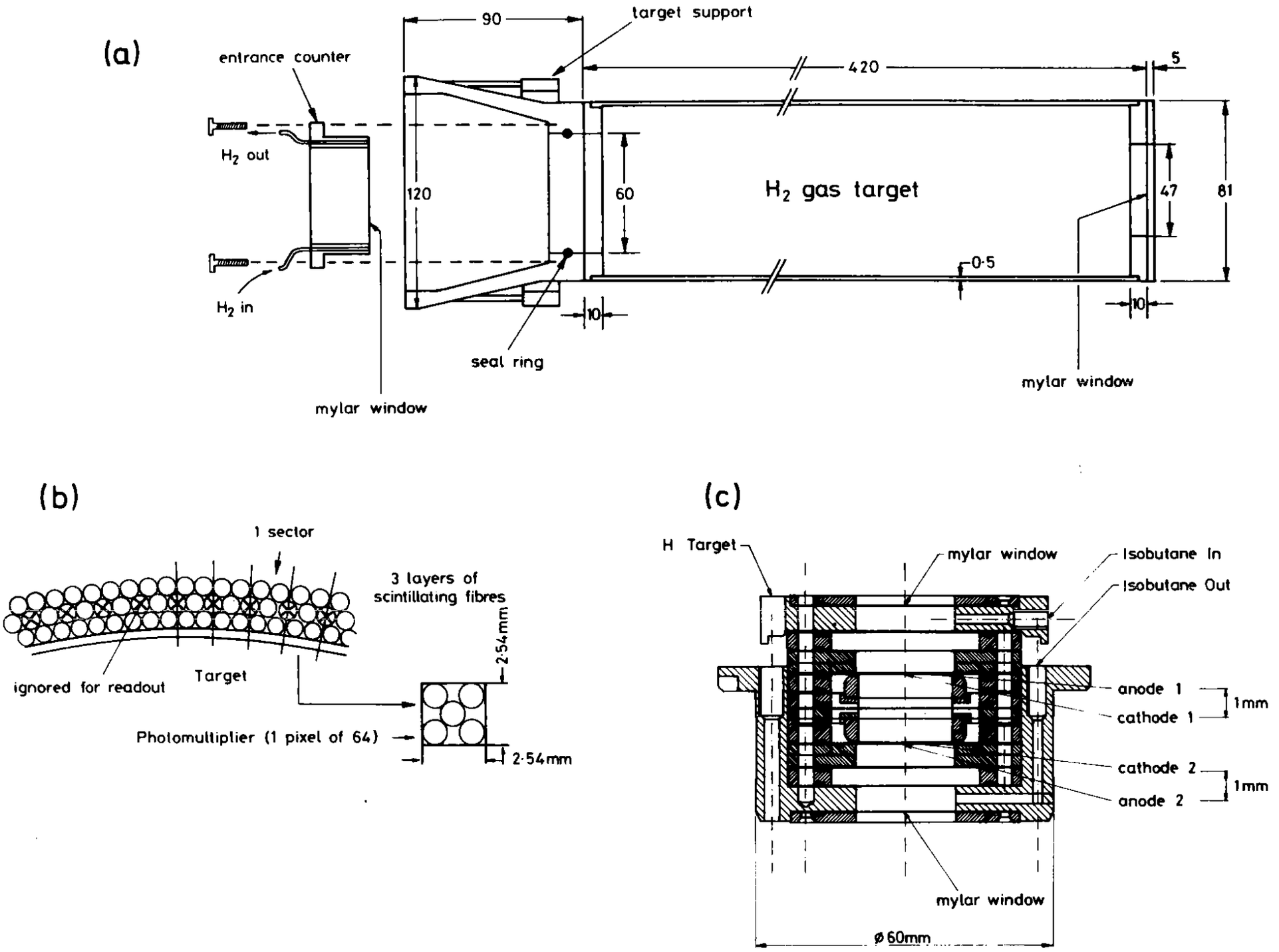
(a)
entrance counter
target support
90
420
5
H_2 out
H_2 in
120
60
H_2 gas target
47
81
0·5
10
10
seal ring
mylar window
mylar window
(b)
1 sector
3 layers of scintillating fibres
2·54mm
ignored for readout
Target
Photomultiplier (1 pixel of 64)
2·54mm
(c)
H Target
mylar window
Isobutane In
Isobutane Out
anode 1
cathode 1
1mm
cathode 2
anode 2
1mm
mylar window
ø 60mm

Figure 3

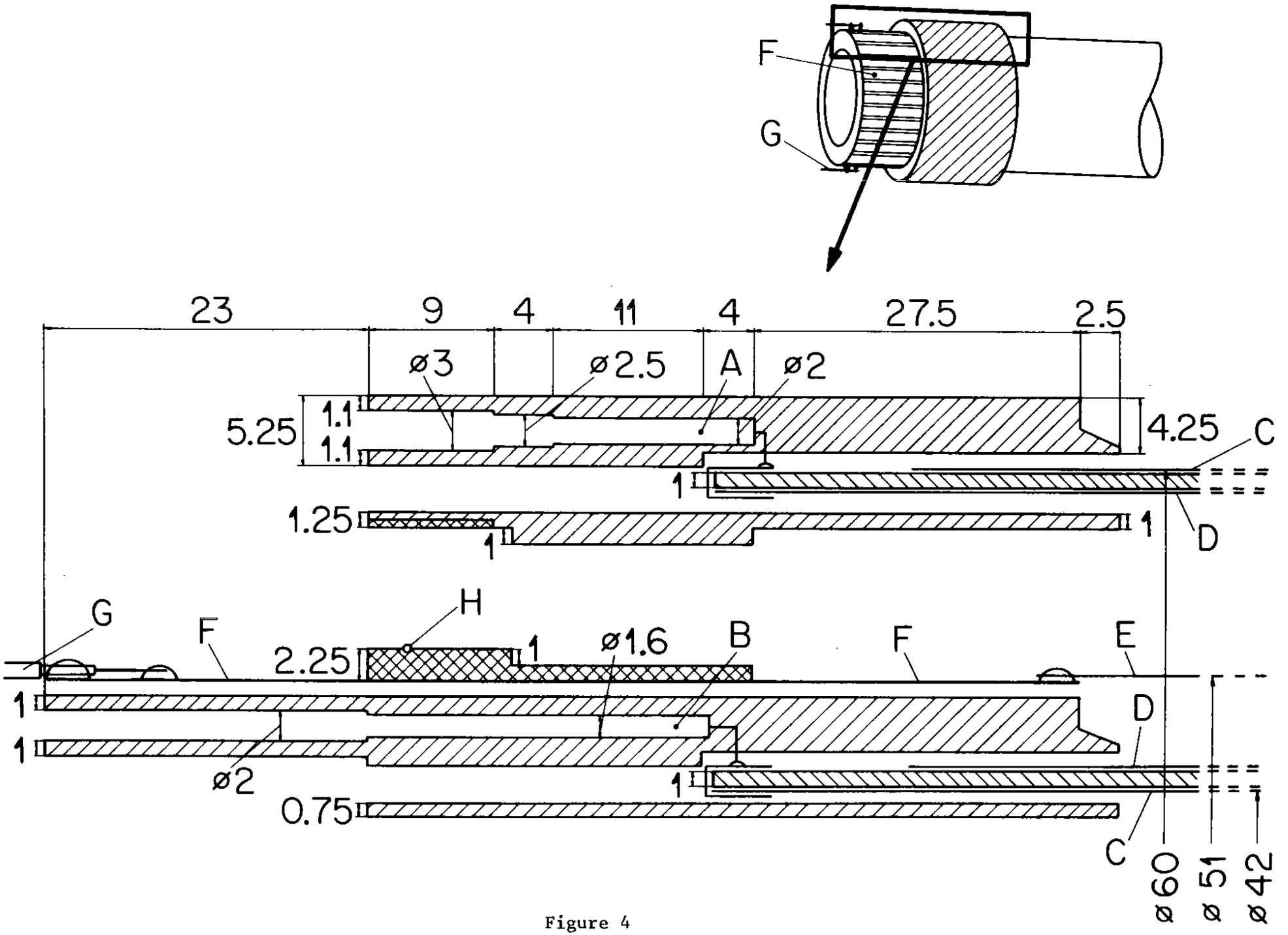
F
G
23
9
4
11
4
27.5
2.5
ø3
ø2.5
A
ø2
5.25
1.1
1.1
4.25
C
1
1.25
1
1
D
G
F
H
2.25
1
ø1.6
B
F
E
1
1
D
ø2
1
0.75
C
ø60
ø51
ø42

Figure 4

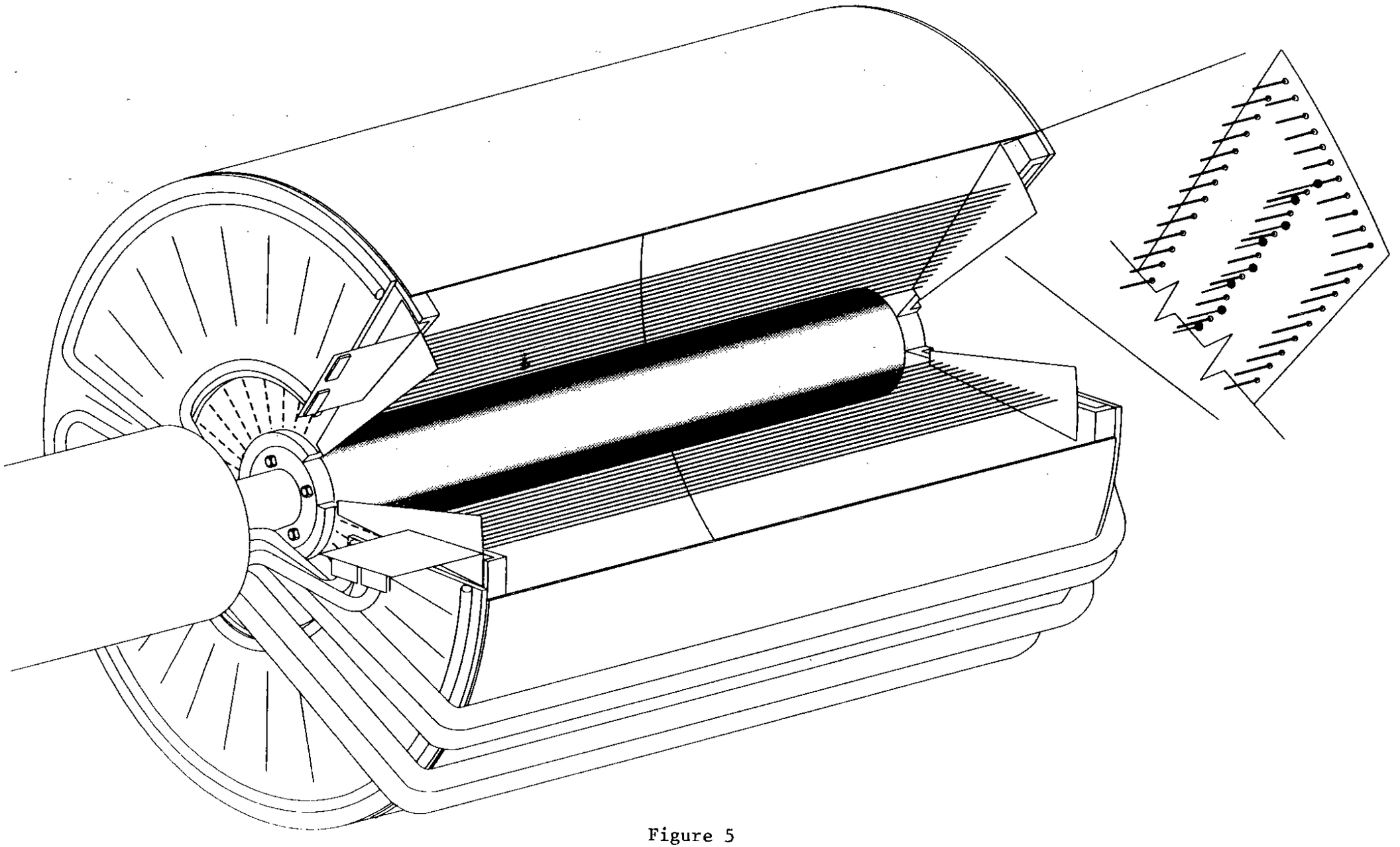

Figure 5

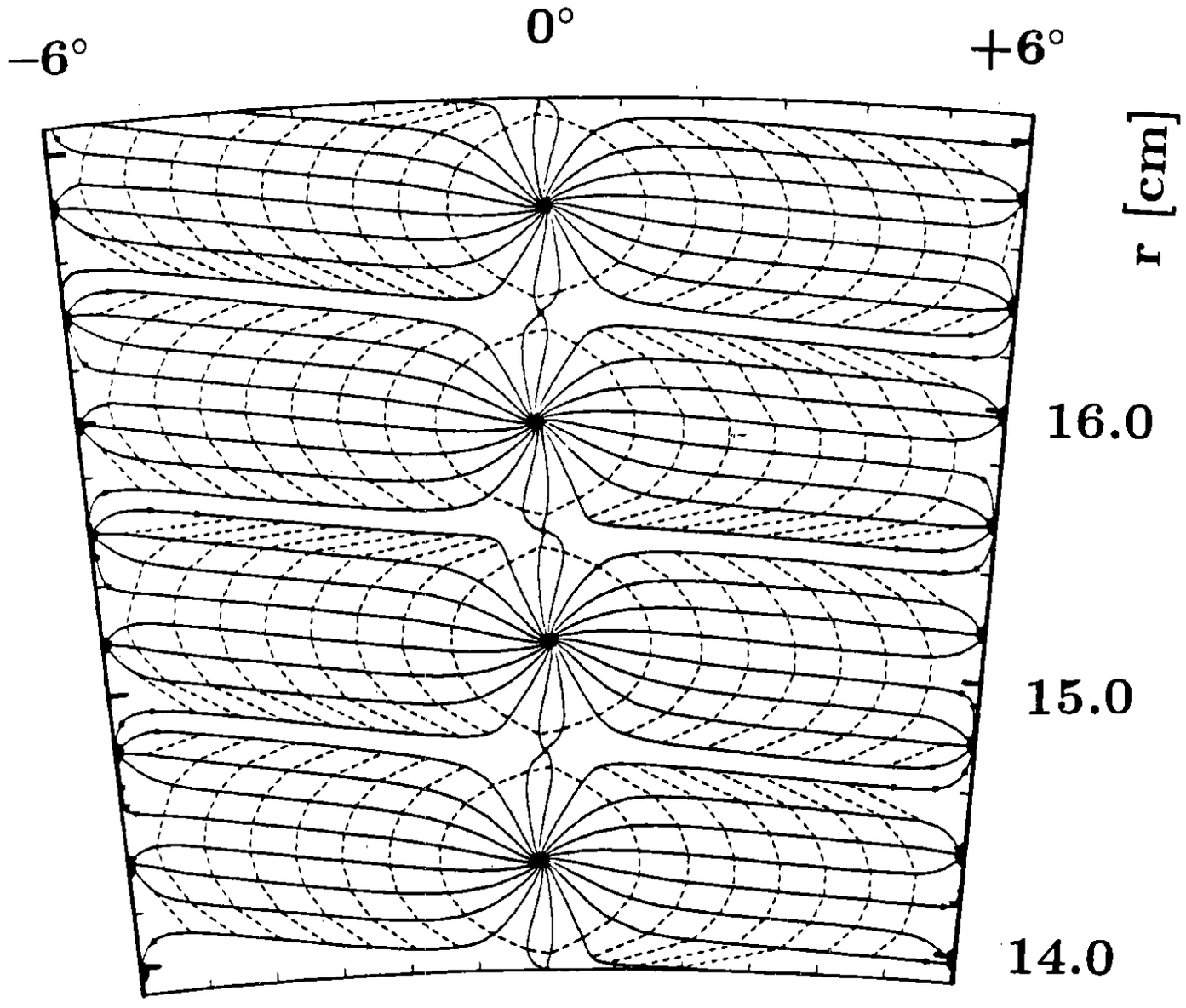

Figure 6

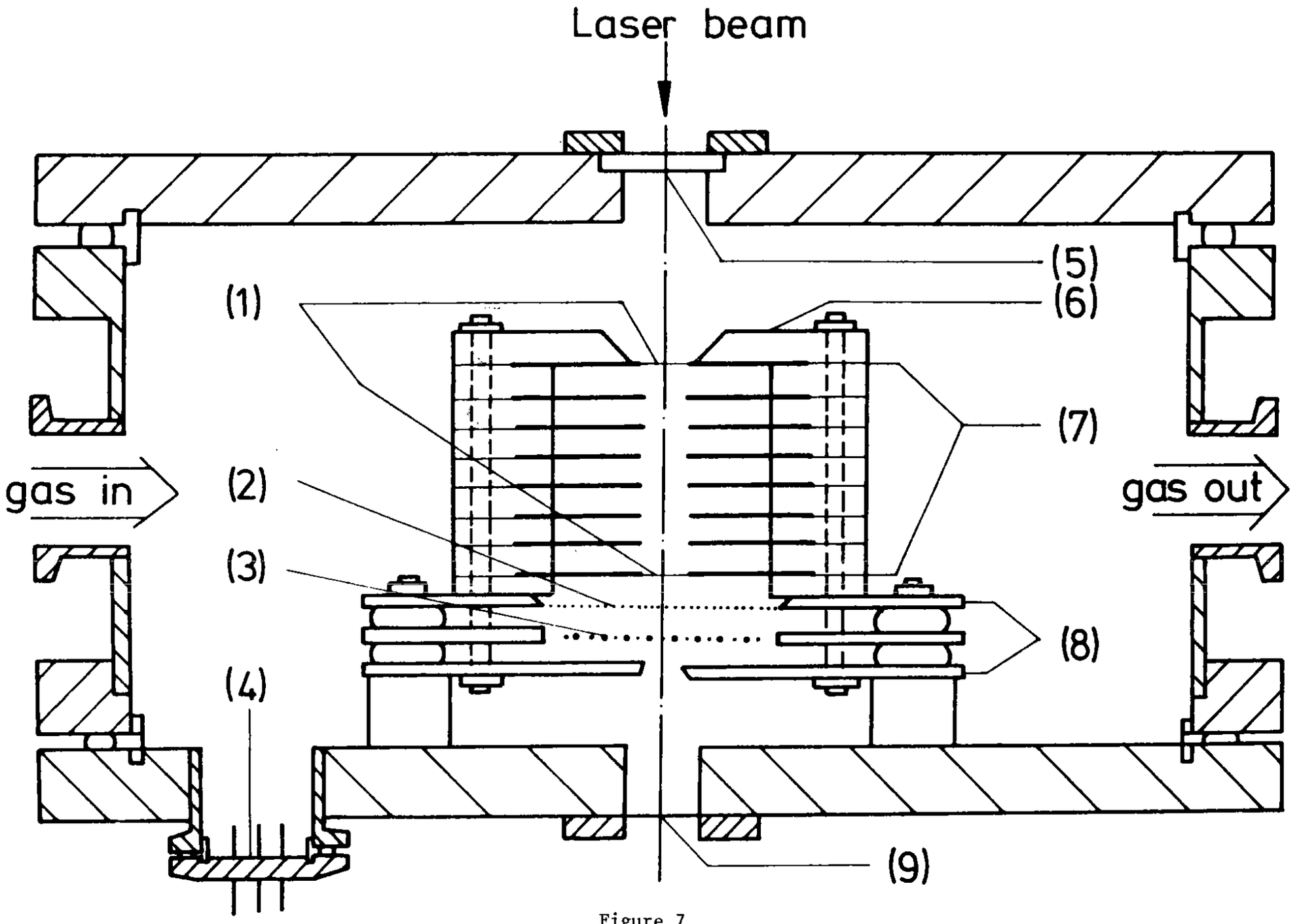

Figure 7

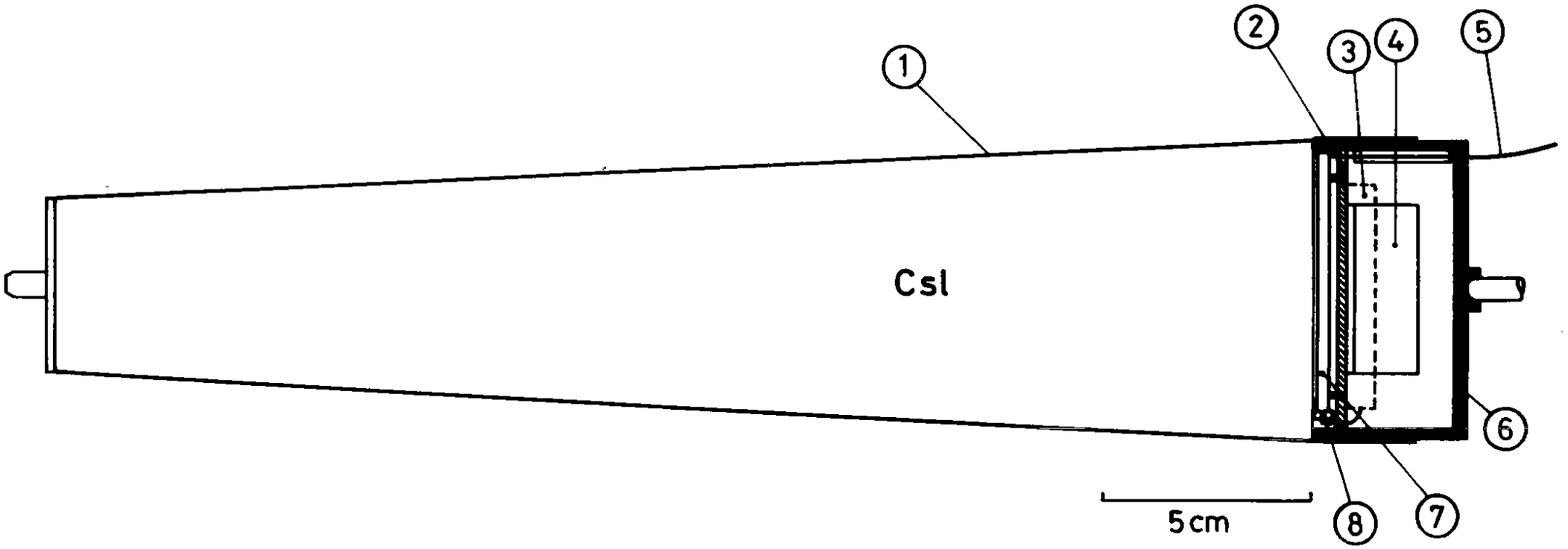

Figure 8

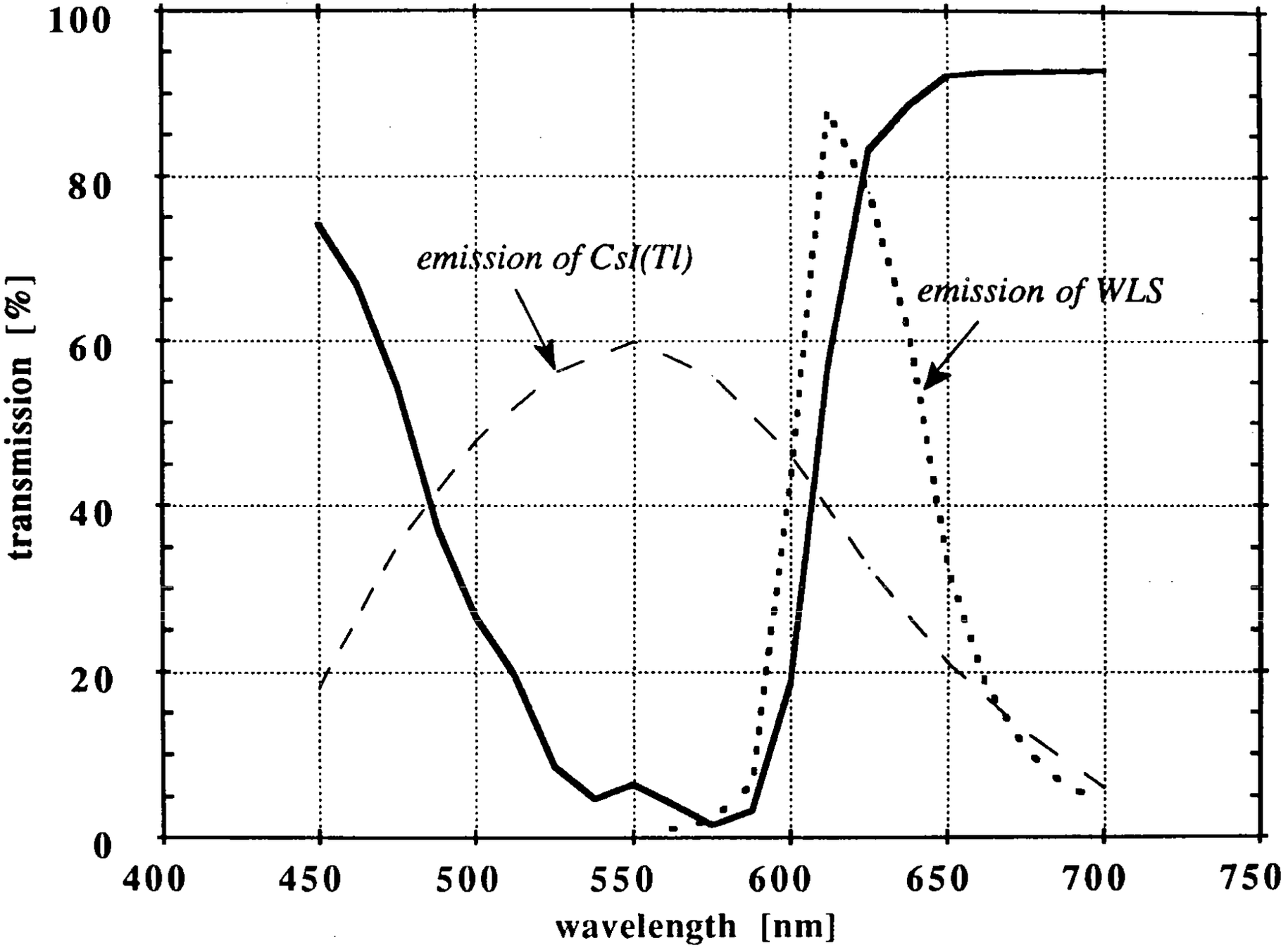
100
80
60
40
20
0
transmission [%]
400
450
500
550
600
650
700
750
wavelength [nm]
emission of CsI(Tl)
emission of WLS

Figure 9

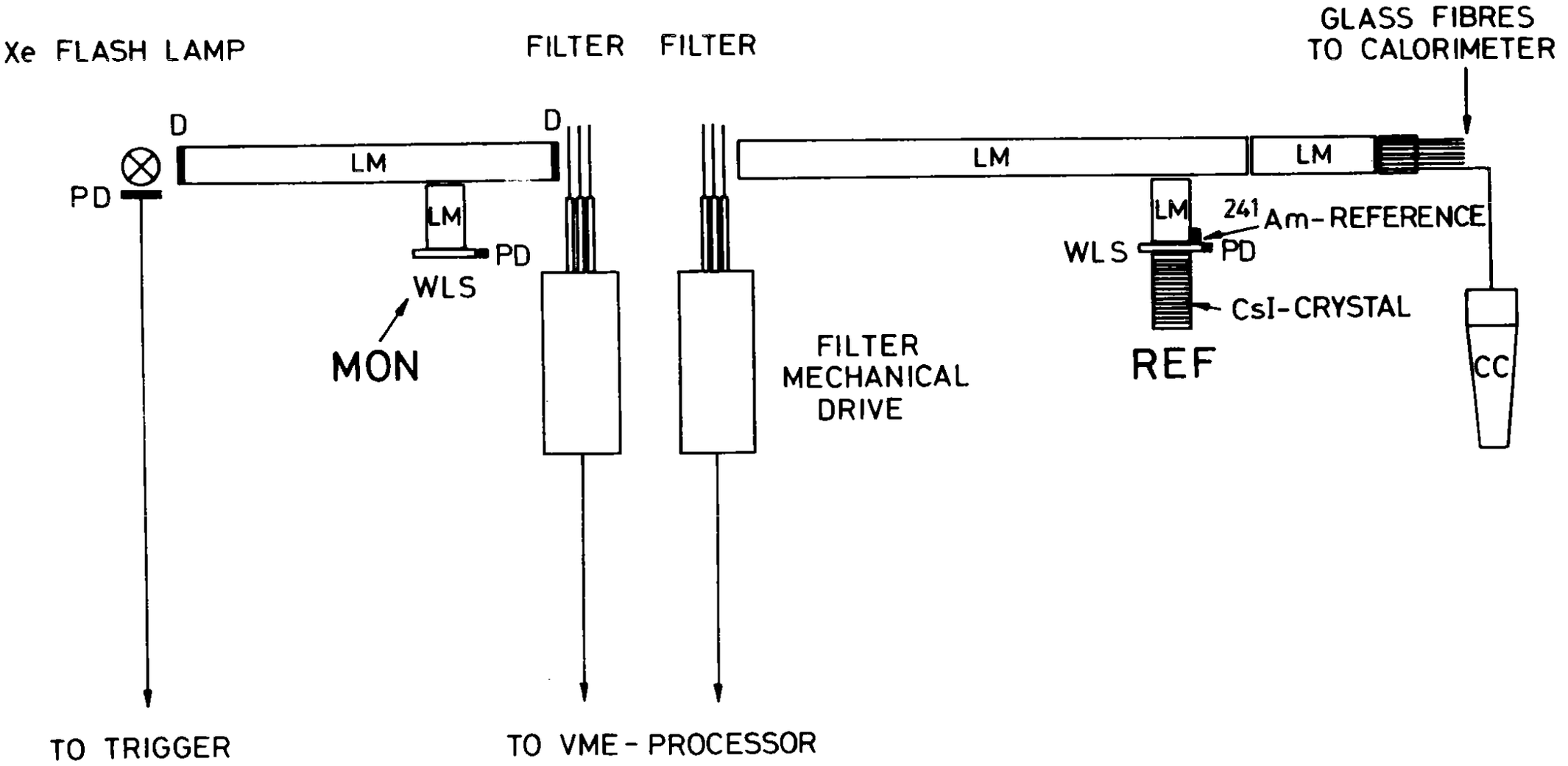
Xe FLASH LAMP
FILTER
FILTER
GLASS FIBRES
TO CALORIMETER
D
D
PD
LM
LM
PD
WLS
MON
LM
LM
LM
241
Am-REFERENCE
WLS
PD
CsI-CRYSTAL
REF
CC
FILTER
MECHANICAL
DRIVE
TO TRIGGER
TO VME-PROCESSOR

Figure 10

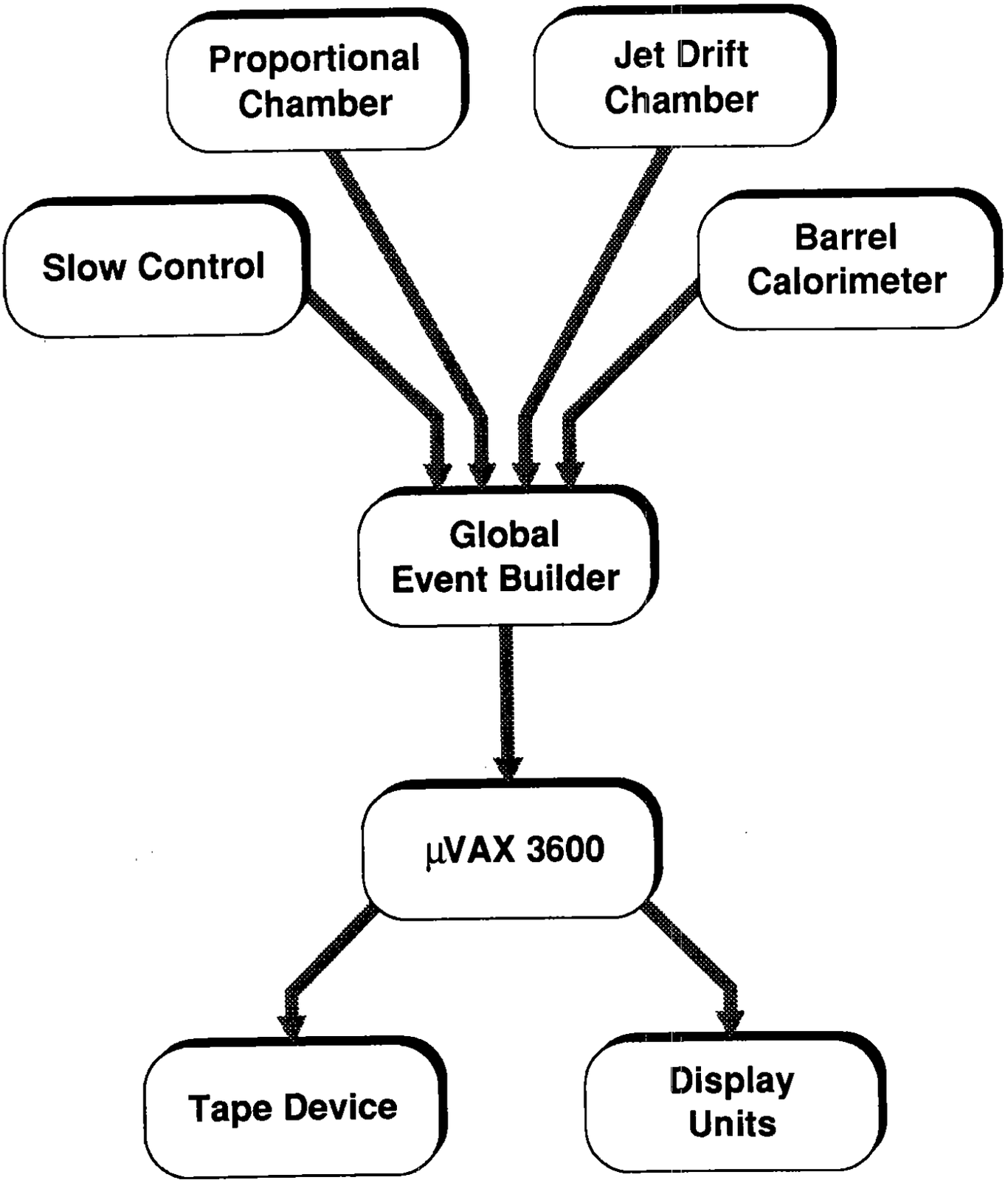
Proportional Chamber
Jet Drift Chamber
Slow Control
Barrel Calorimeter
Global Event Builder
μVAX 3600
Tape Device
Display Units

Figure 11

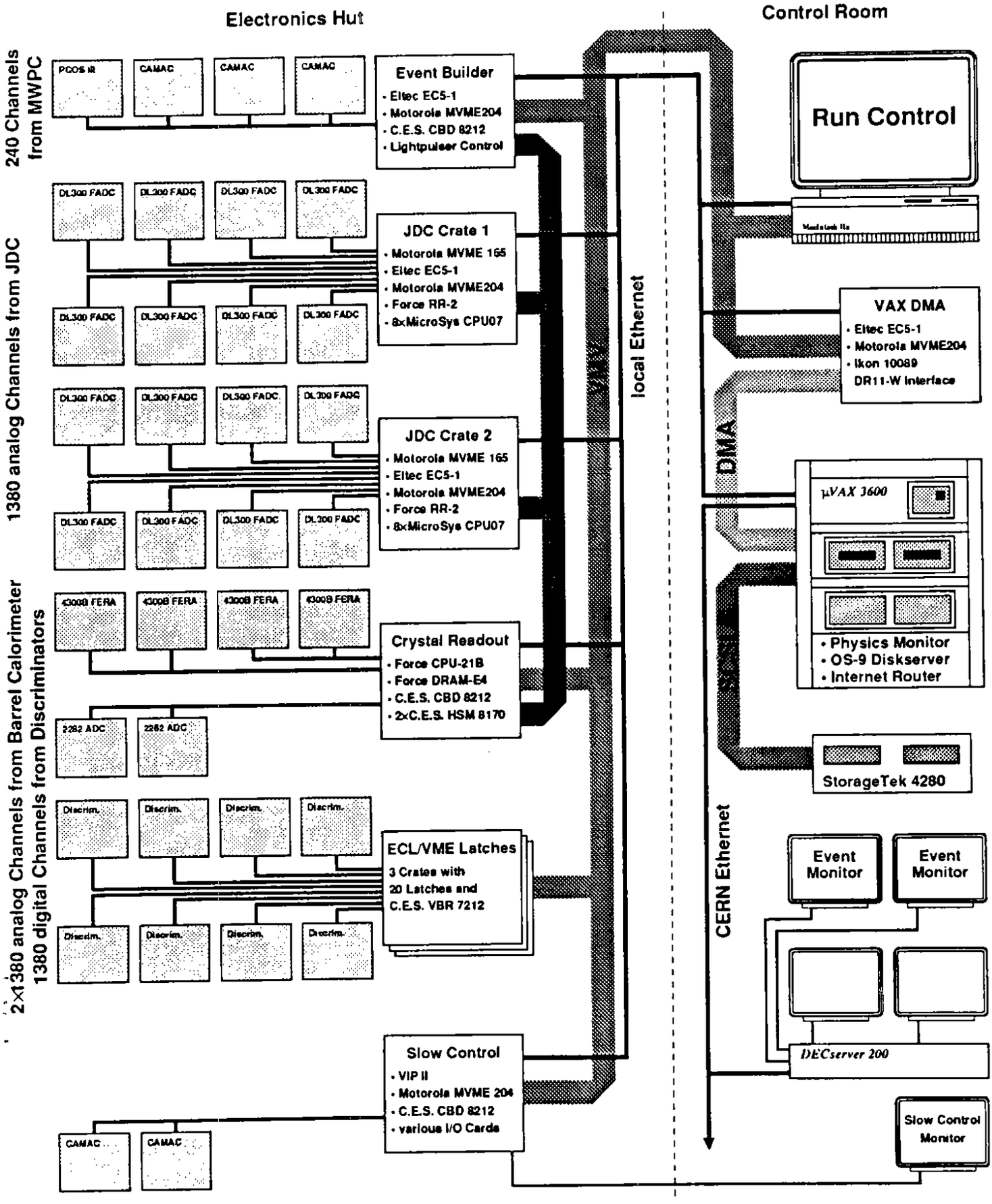
Electronics Hut
Control Room
240 Channels from MWPC
1380 analog Channels from JDC
2×1380 analog Channels from Barrel Calorimeter
1380 digital Channels from Discriminators
PCOS III
CAMAC
CAMAC
CAMAC
Event Builder
• Eltec EC5-1
• Motorola MVME204
• C.E.S. CBD 8212
• Lightpulser Control
DL300 FADC
JDC Crate 1
• Motorola MVME 165
• Eltec EC5-1
• Motorola MVME204
• Force RR-2
• 8xMicroSys CPU07
JDC Crate 2
• Motorola MVME 165
• Eltec EC5-1
• Motorola MVME204
• Force RR-2
• 8xMicroSys CPU07
4300B FERA
Crystal Readout
• Force CPU-21B
• Force DRAM-E4
• C.E.S. CBD 8212
• 2xC.E.S. HSM 8170
2282 ADC
Discrim.
ECL/VME Latches
3 Crates with
20 Latches and
C.E.S. VBR 7212
Slow Control
• VIP II
• Motorola MVME 204
• C.E.S. CBD 8212
• various I/O Cards
VME
local Ethernet
Run Control
VAX DMA
• Eltec EC5-1
• Motorola MVME204
• Ikon 10089
DR11-W Interface
DMA
μVAX 3600
• Physics Monitor
• OS-9 Diskserver
• Internet Router
SCSI
StorageTek 4280
CERN Ethernet
Event Monitor
Event Monitor
DECserver 200
Slow Control Monitor

Figure 12

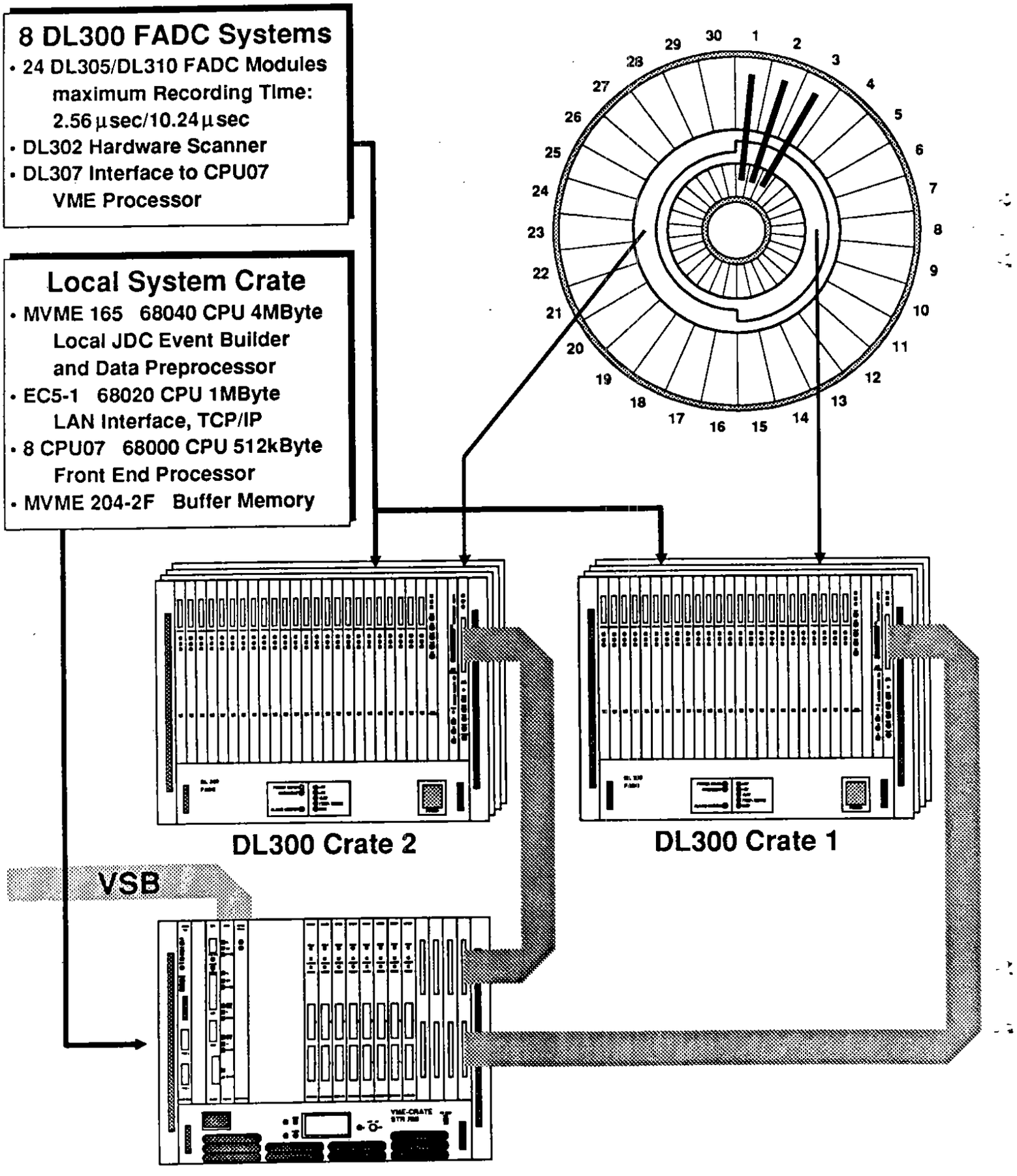
8 DL300 FADC Systems
• 24 DL305/DL310 FADC Modules
maximum Recording Time:
2.56 µsec/10.24 µsec
• DL302 Hardware Scanner
• DL307 Interface to CPU07
VME Processor
Local System Crate
• MVME 165 68040 CPU 4MByte
Local JDC Event Builder
and Data Preprocessor
• EC5-1 68020 CPU 1MByte
LAN Interface, TCP/IP
• 8 CPU07 68000 CPU 512kByte
Front End Processor
• MVME 204-2F Buffer Memory
1
2
3
4
5
6
7
8
9
10
11
12
13
14
15
16
17
18
19
20
21
22
23
24
25
26
27
28
29
30
DL300 Crate 2
DL300 Crate 1
VSB

Figure 13

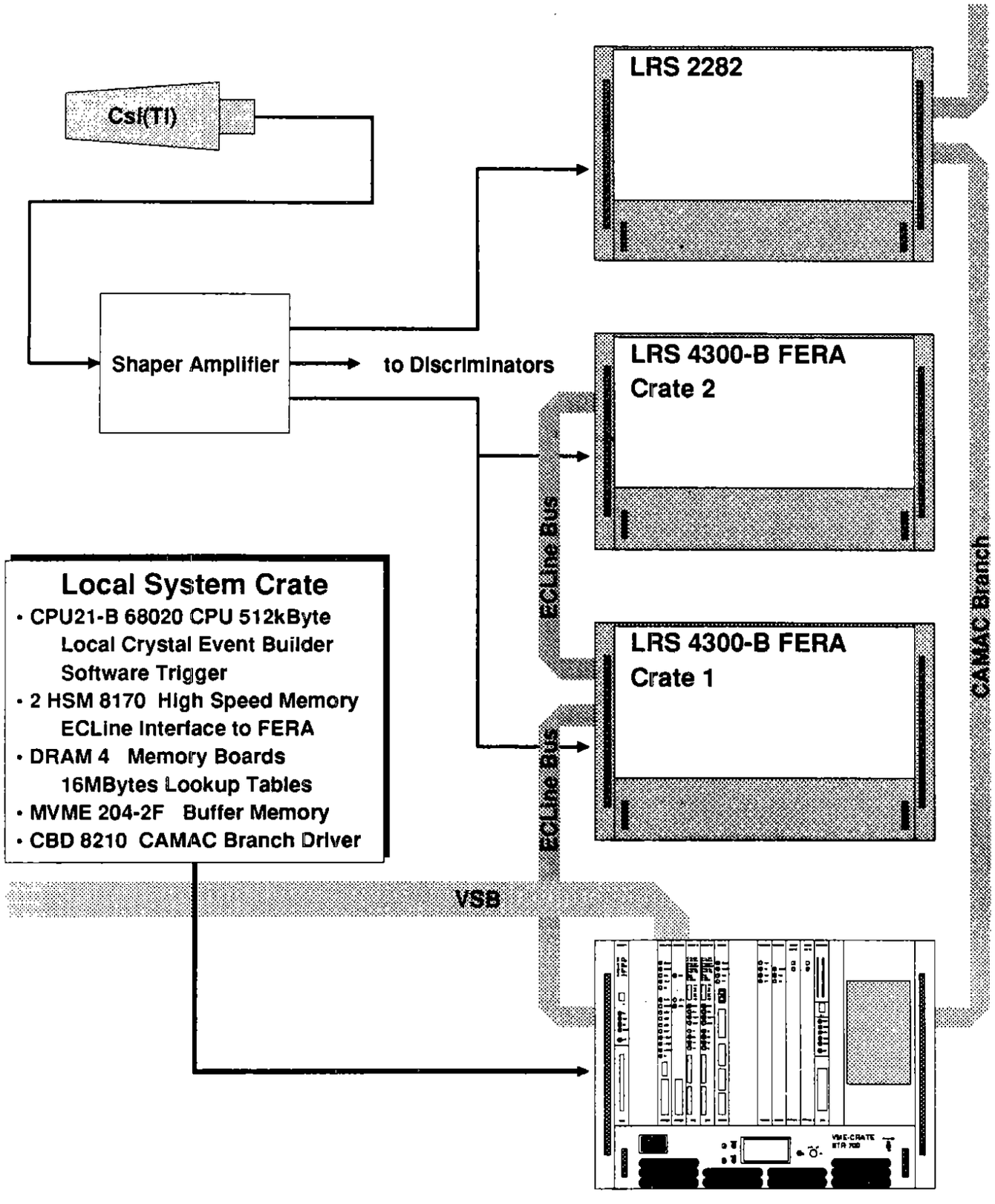
CsI(Tl)
LRS 2282
Shaper Amplifier
to Discriminators
LRS 4300-B FERA
Crate 2
LRS 4300-B FERA
Crate 1
ECLine Bus
ECLine Bus
CAMAC Branch
Local System Crate
• CPU21-B 68020 CPU 512kByte
Local Crystal Event Builder
Software Trigger
• 2 HSM 8170 High Speed Memory
ECLine Interface to FERA
• DRAM 4 Memory Boards
16MBytes Lookup Tables
• MVME 204-2F Buffer Memory
• CBD 8210 CAMAC Branch Driver
VSB

Figure 14

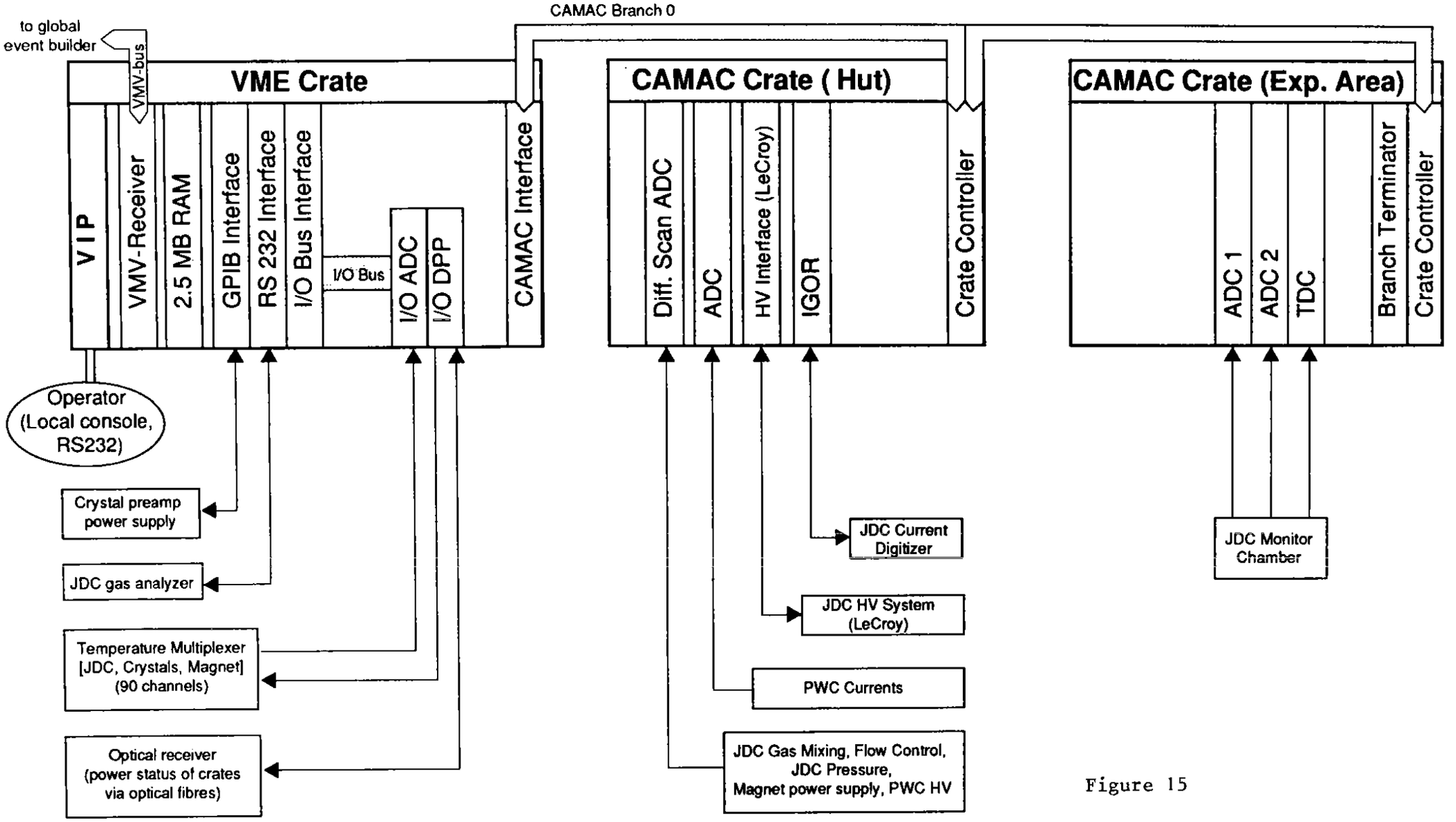
CAMAC Branch 0
to global event builder
VMV-bus
VME Crate
VIP
VMV-Receiver
2.5 MB RAM
GPIB Interface
RS 232 Interface
I/O Bus Interface
I/O Bus
I/O ADC
I/O DPP
CAMAC Interface
CAMAC Crate (Hut)
Diff. Scan ADC
ADC
HV Interface (LeCroy)
IGOR
Crate Controller
CAMAC Crate (Exp. Area)
ADC 1
ADC 2
TDC
Branch Terminator
Crate Controller
Operator (Local console, RS232)
Crystal preamp power supply
JDC gas analyzer
Temperature Multiplexer [JDC, Crystals, Magnet] (90 channels)
Optical receiver (power status of crates via optical fibres)
JDC Current Digitizer
JDC HV System (LeCroy)
PWC Currents
JDC Gas Mixing, Flow Control, JDC Pressure, Magnet power supply, PWC HV
JDC Monitor Chamber

Figure 15

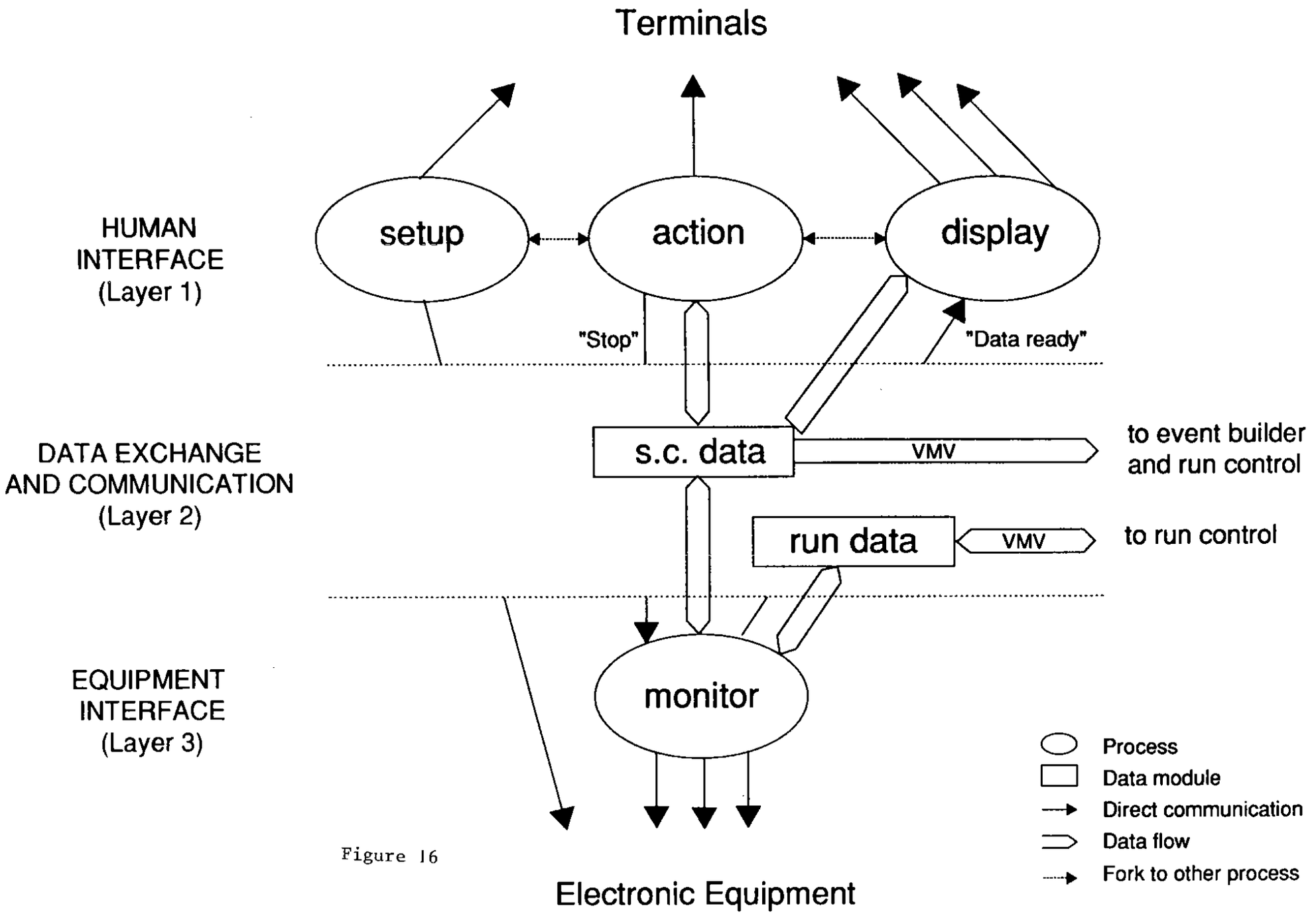
Terminals
HUMAN INTERFACE (Layer 1)
setup
action
display
"Stop"
"Data ready"
DATA EXCHANGE AND COMMUNICATION (Layer 2)
s.c. data
VMV
to event builder and run control
run data
VMV
to run control
EQUIPMENT INTERFACE (Layer 3)
monitor
Process
Data module
Direct communication
Data flow
Fork to other process
Electronic Equipment

Figure 16

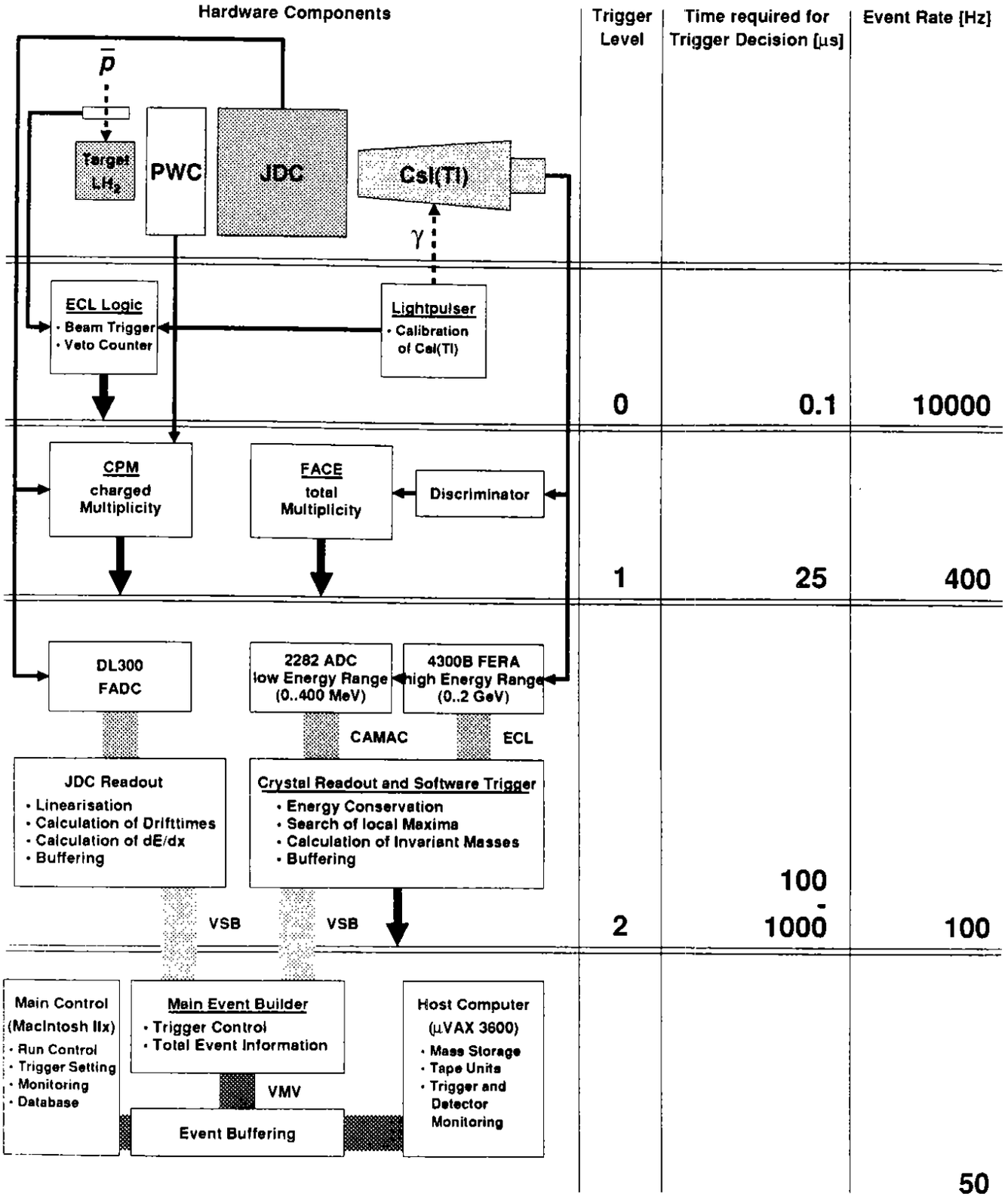
Hardware Components
Trigger Level
Time required for Trigger Decision [μs]
Event Rate [Hz]
$\bar{p}$
Target LH_2
PWC
JDC
CsI(Tl)
γ
ECL Logic
• Beam Trigger
• Veto Counter
Lightpulser
• Calibration of CsI(Tl)
0
0.1
10000
CPM
charged Multiplicity
FACE
total Multiplicity
Discriminator
1
25
400
DL300
FADC
2282 ADC
low Energy Range
(0..400 MeV)
4300B FERA
high Energy Range
(0..2 GeV)
CAMAC
ECL
JDC Readout
• Linearisation
• Calculation of Drifttimes
• Calculation of dE/dx
• Buffering
Crystal Readout and Software Trigger
• Energy Conservation
• Search of local Maxima
• Calculation of Invariant Masses
• Buffering
100
1000
VSB
VSB
2
100
Main Control
(MacIntosh IIx)
• Run Control
• Trigger Setting
• Monitoring
• Database
Main Event Builder
• Trigger Control
• Total Event Information
VMV
Event Buffering
Host Computer
(μVAX 3600)
• Mass Storage
• Tape Units
• Trigger and Detector Monitoring
50

Figure 17

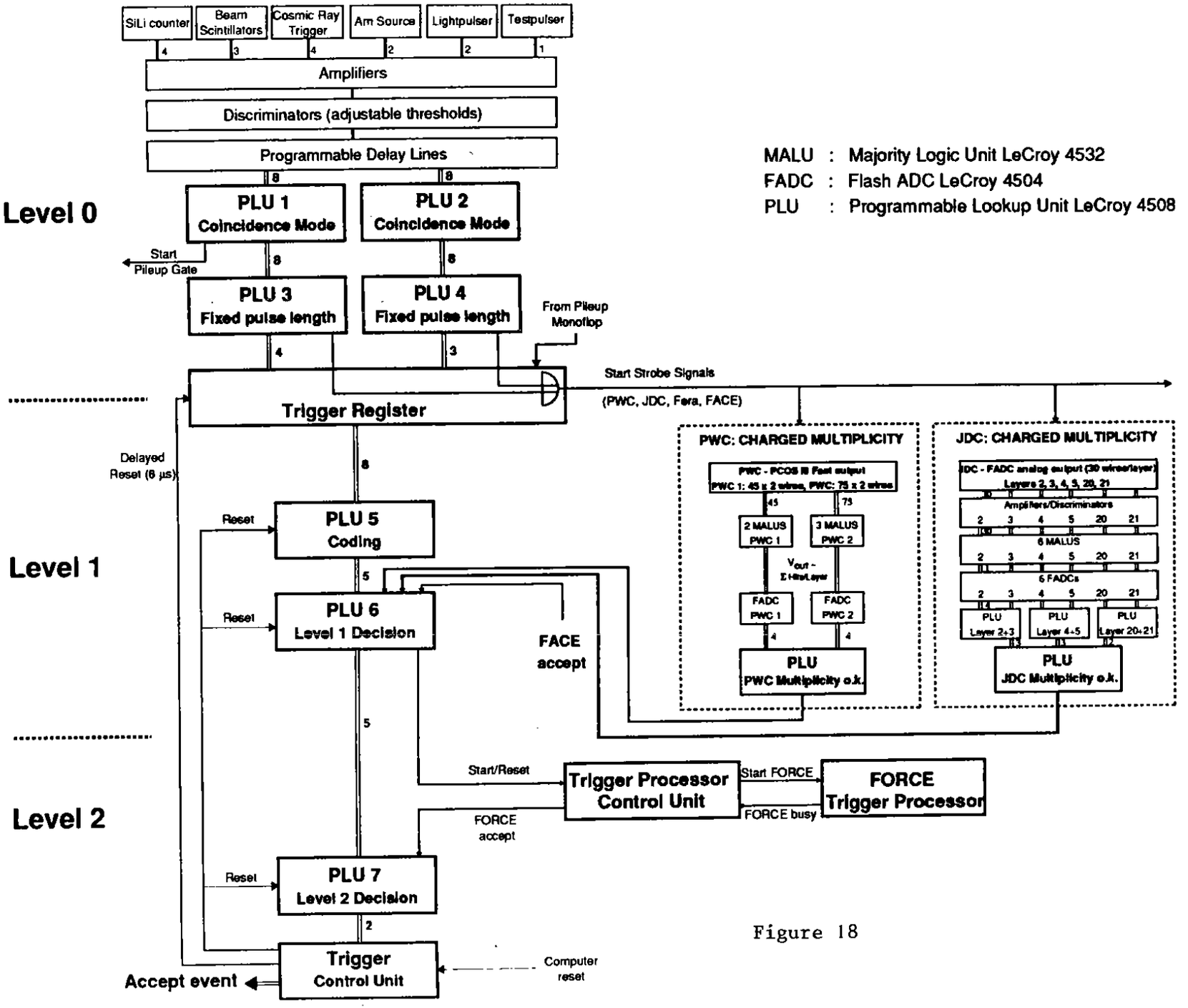

MALU : Majority Logic Unit LeCroy 4532
FADC : Flash ADC LeCroy 4504
PLU : Programmable Lookup Unit LeCroy 4508

Figure 18

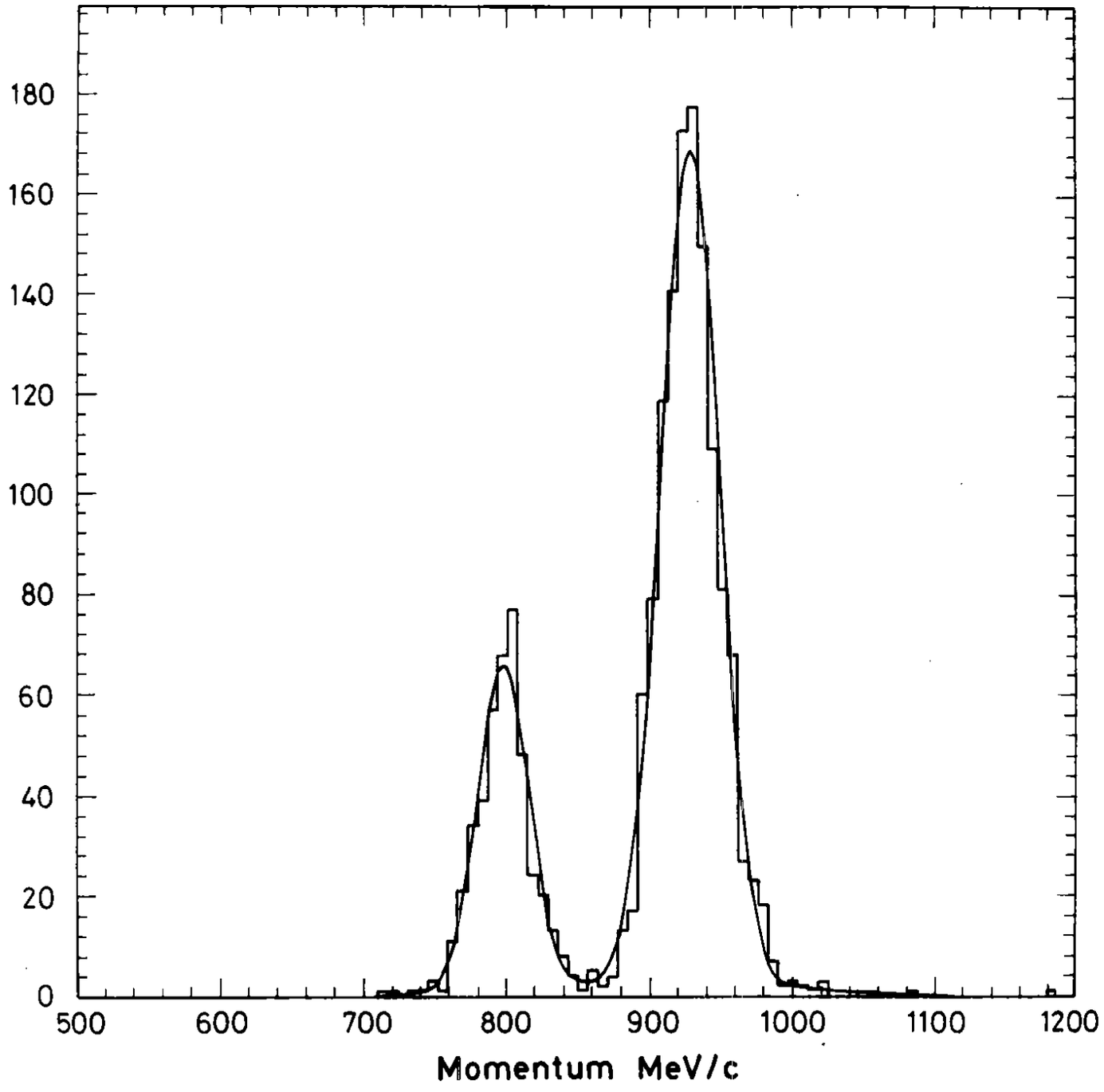
180
160
140
120
100
80
60
40
20
0
500
600
700
800
900
1000
1100
1200
Momentum MeV/c

Figure 19

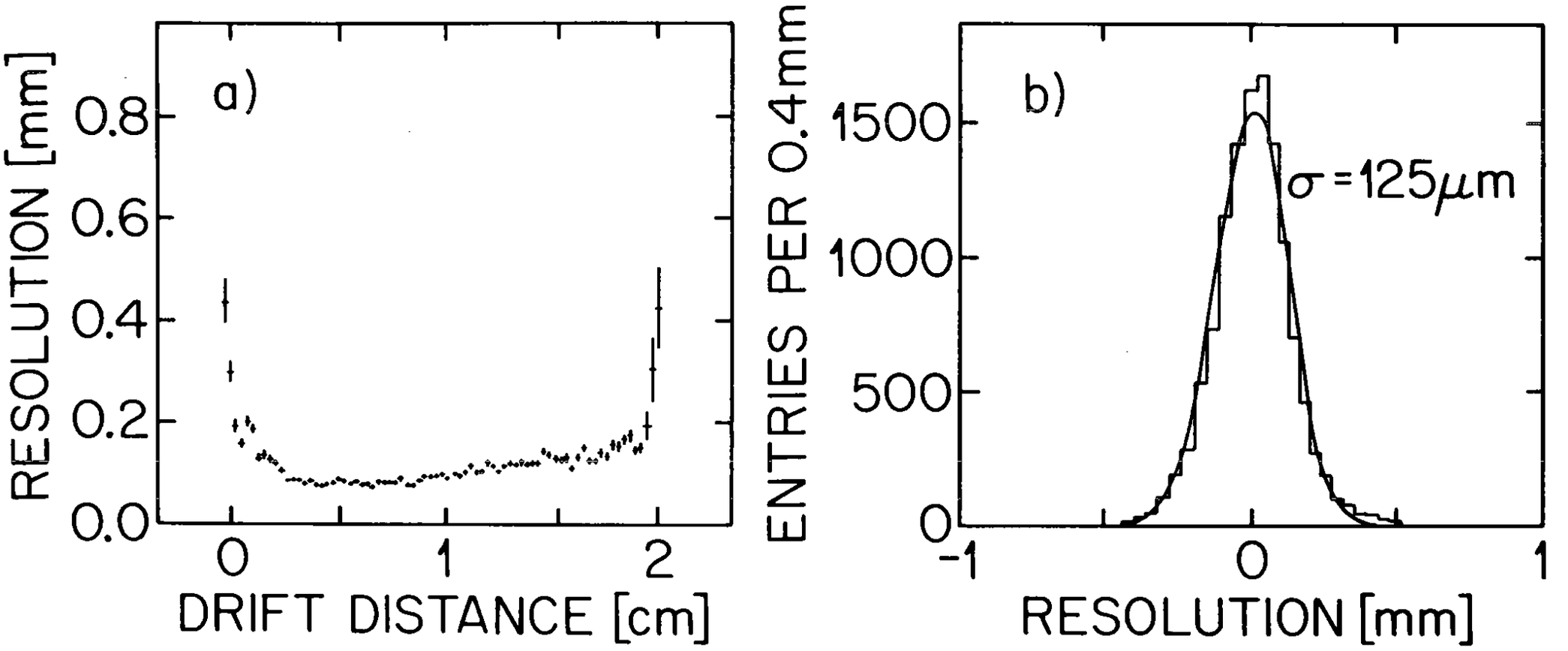
a)
RESOLUTION [mm]
0.0
0.2
0.4
0.6
0.8
0
1
2
DRIFT DISTANCE [cm]
b)
ENTRIES PER 0.4mm
0
500
1000
1500
σ = 125μm
-1
0
1
RESOLUTION [mm]

Figure 20

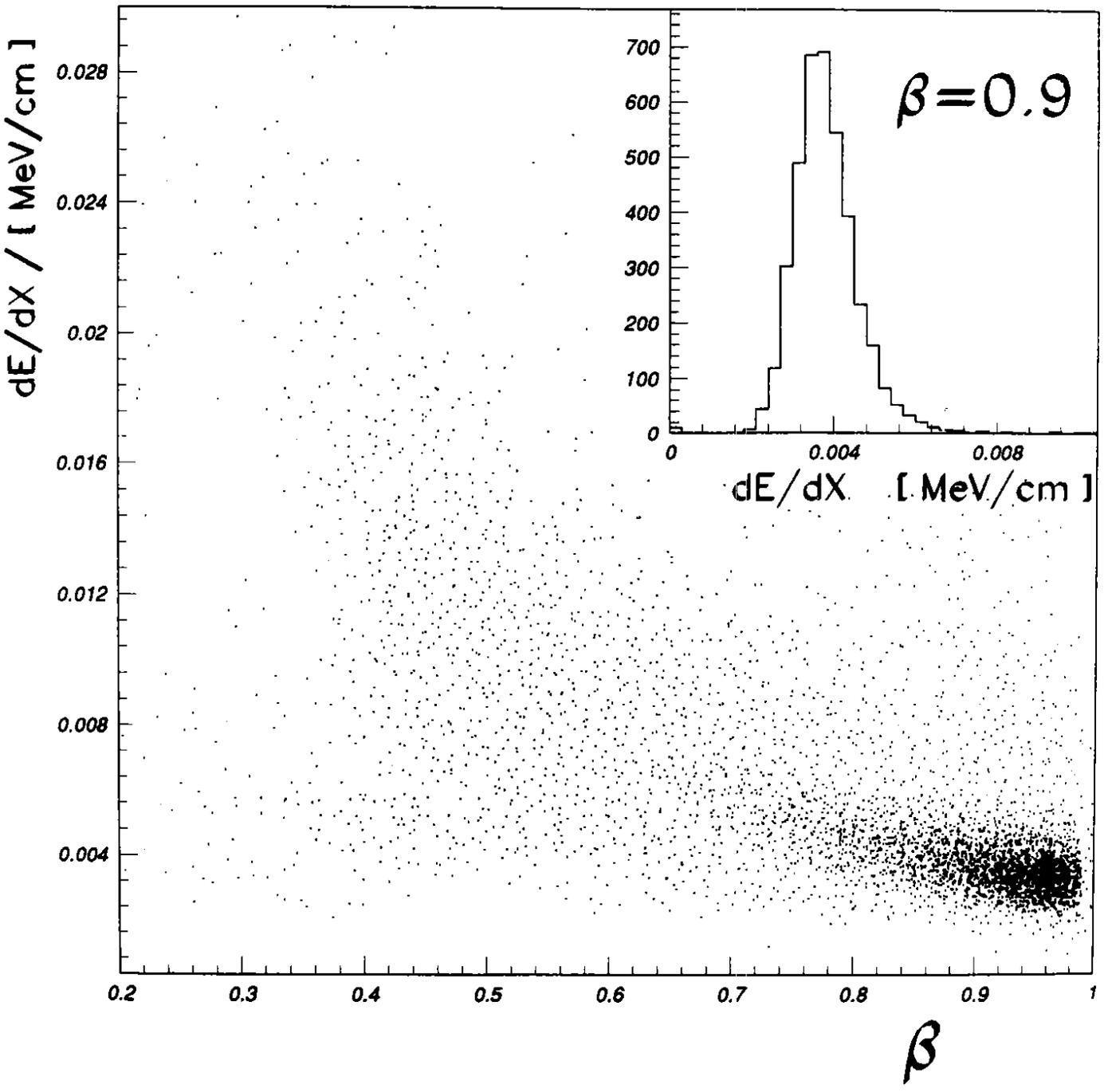
dE/dX / [MeV/cm]
0.028
0.024
0.02
0.016
0.012
0.008
0.004
0.2
0.3
0.4
0.5
0.6
0.7
0.8
0.9
1
β
β=0.9
700
600
500
400
300
200
100
0
0
0.004
0.008
dE/dX [MeV/cm]

Figure 21

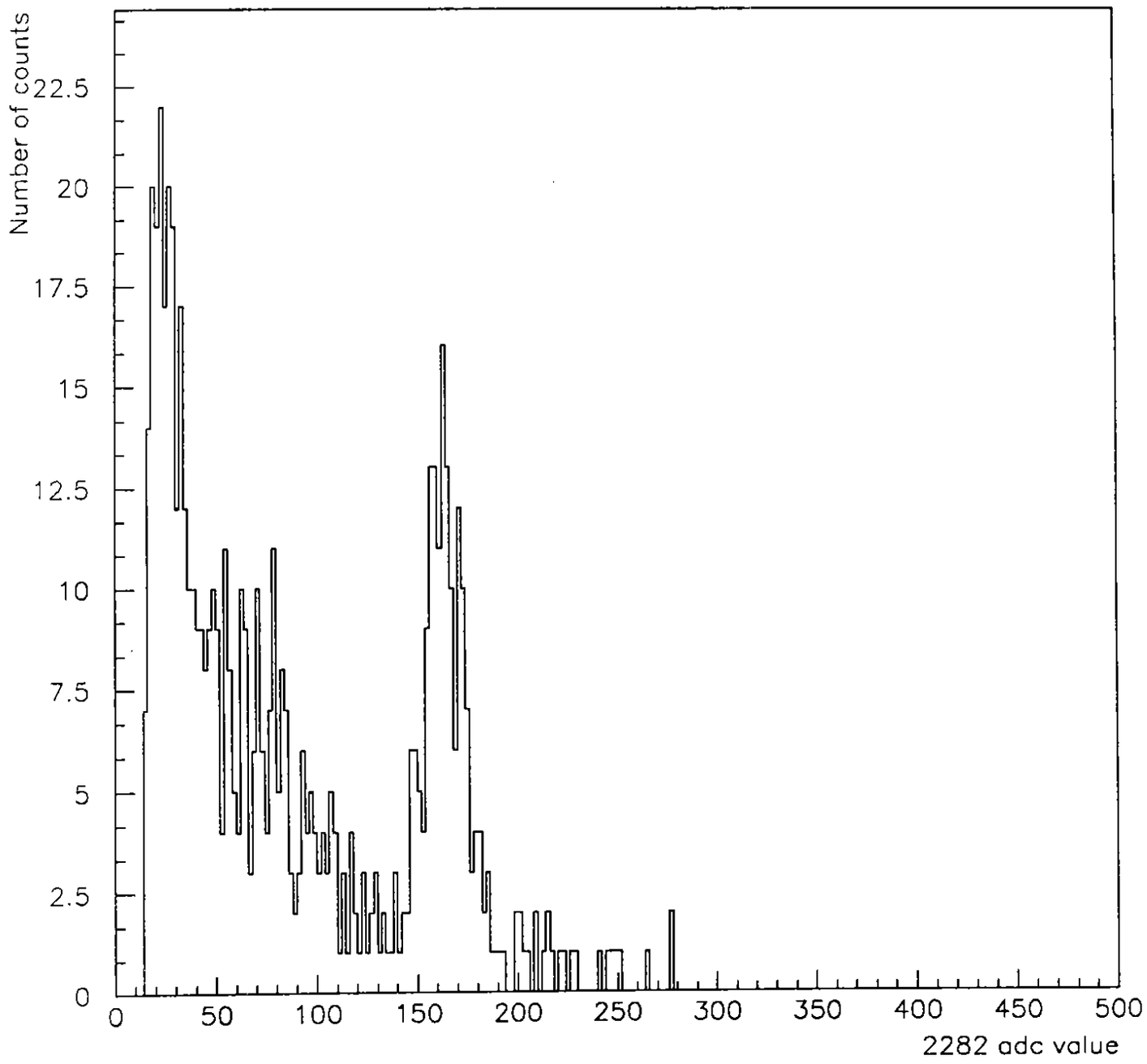
Number of counts
22.5
20
17.5
15
12.5
10
7.5
5
2.5
0
0
50
100
150
200
250
300
350
400
450
500
2282 adc value

Figure 22

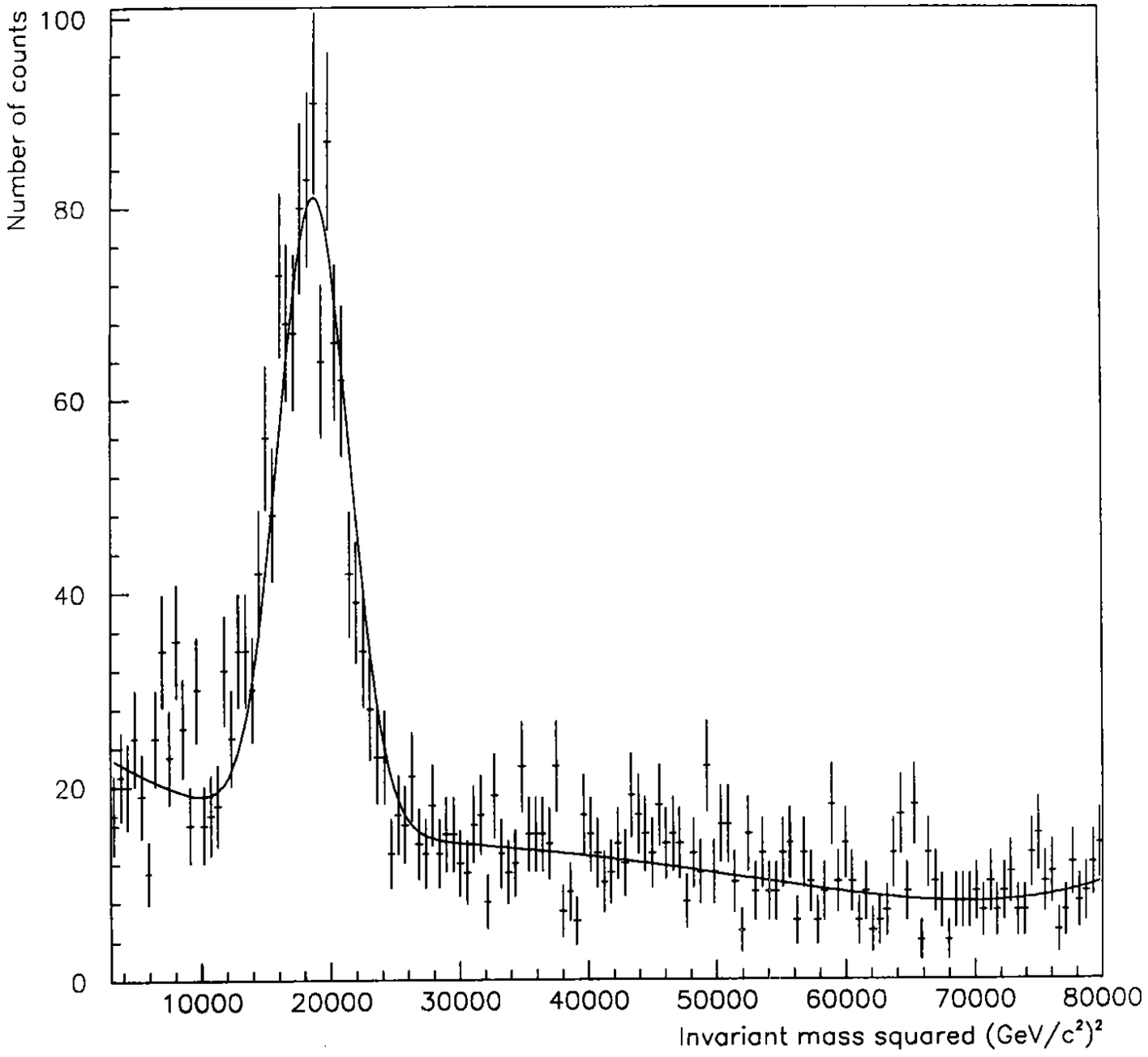
Number of counts
100
80
60
40
20
0
10000
20000
30000
40000
50000
60000
70000
80000
Invariant mass squared (GeV/c²)²

Figure 23

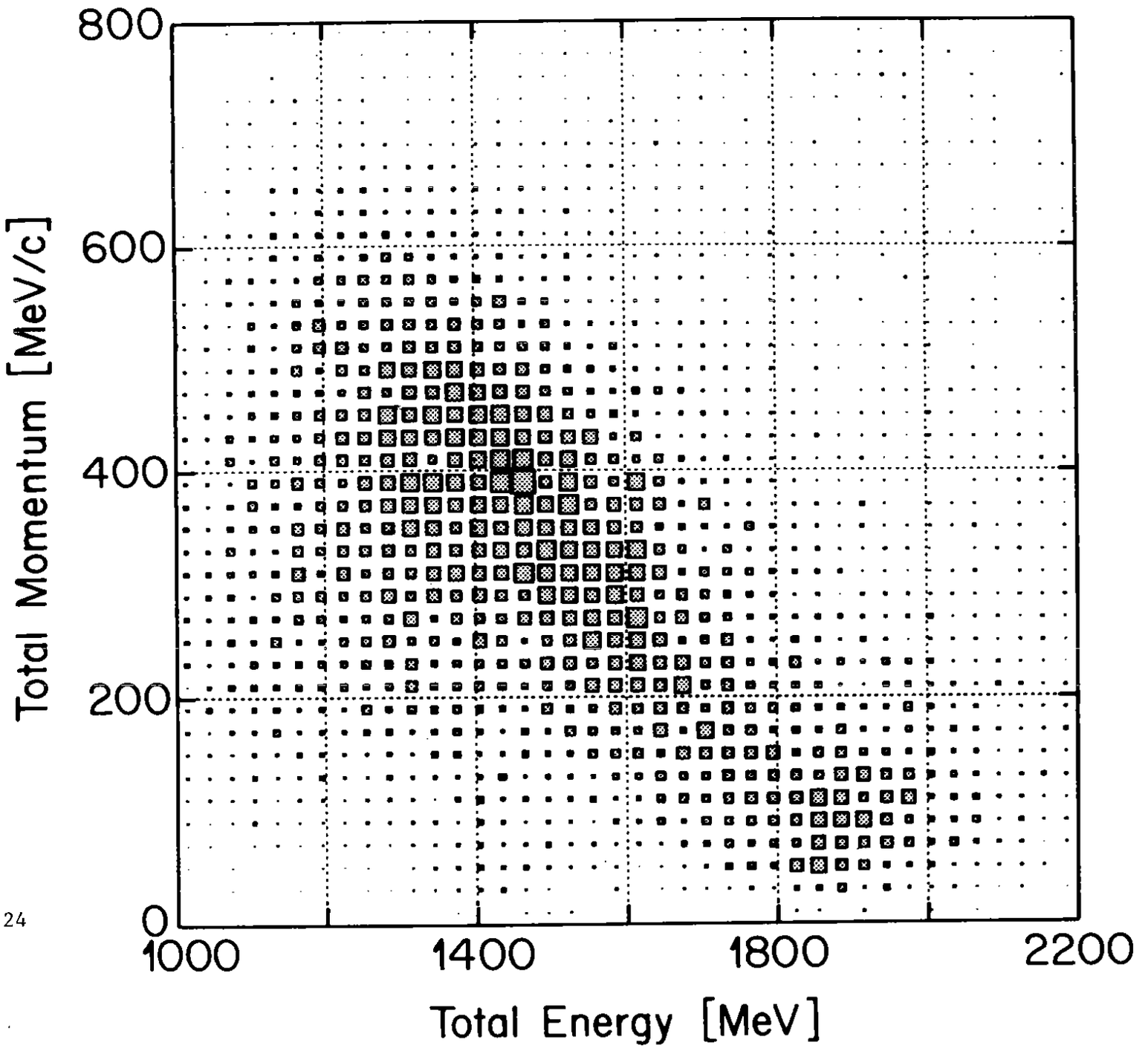
800
600
400
200
0
Total Momentum [MeV/c]
1000
1400
1800
2200
Total Energy [MeV]

Figure 24

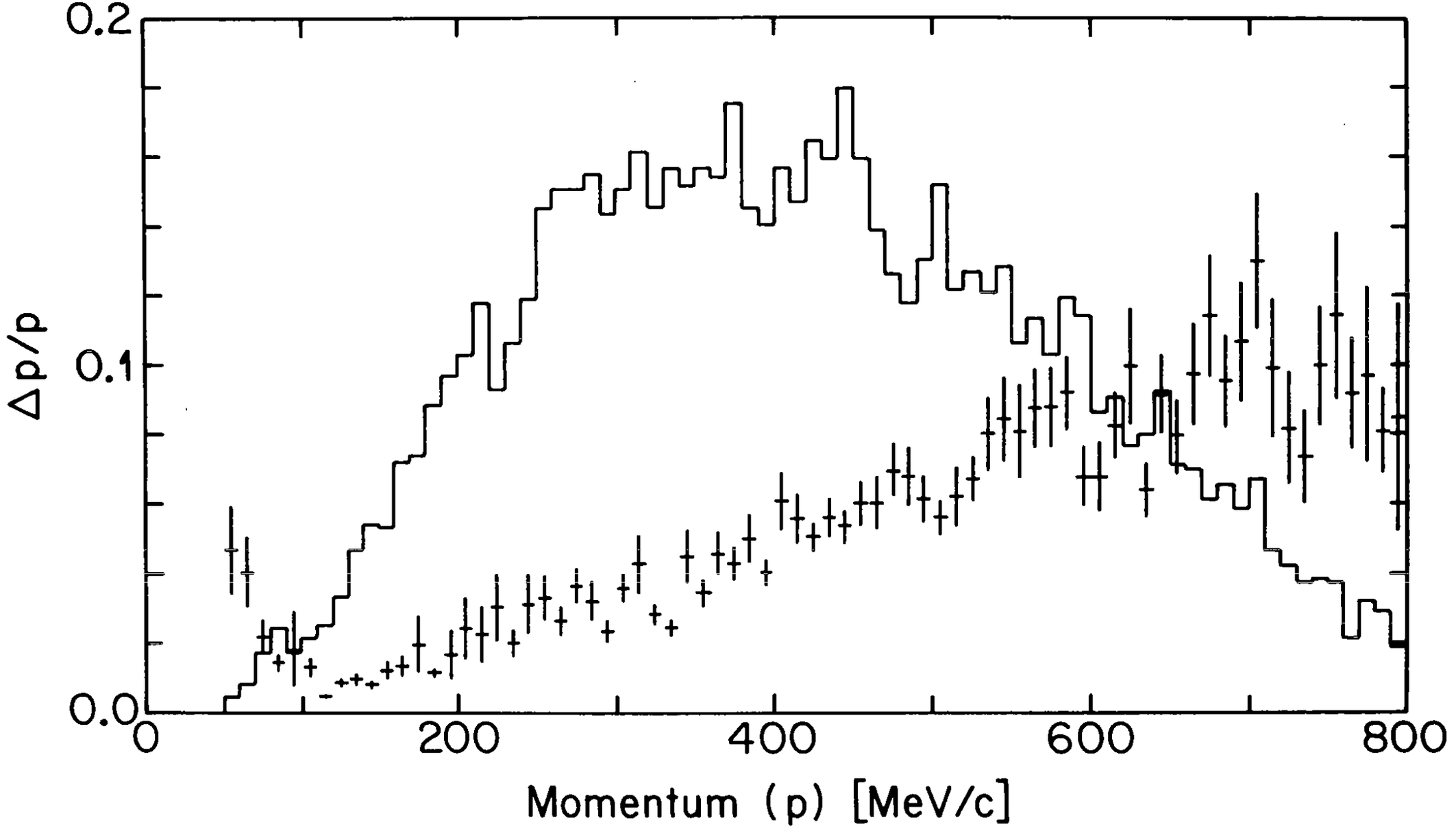

Figure 25

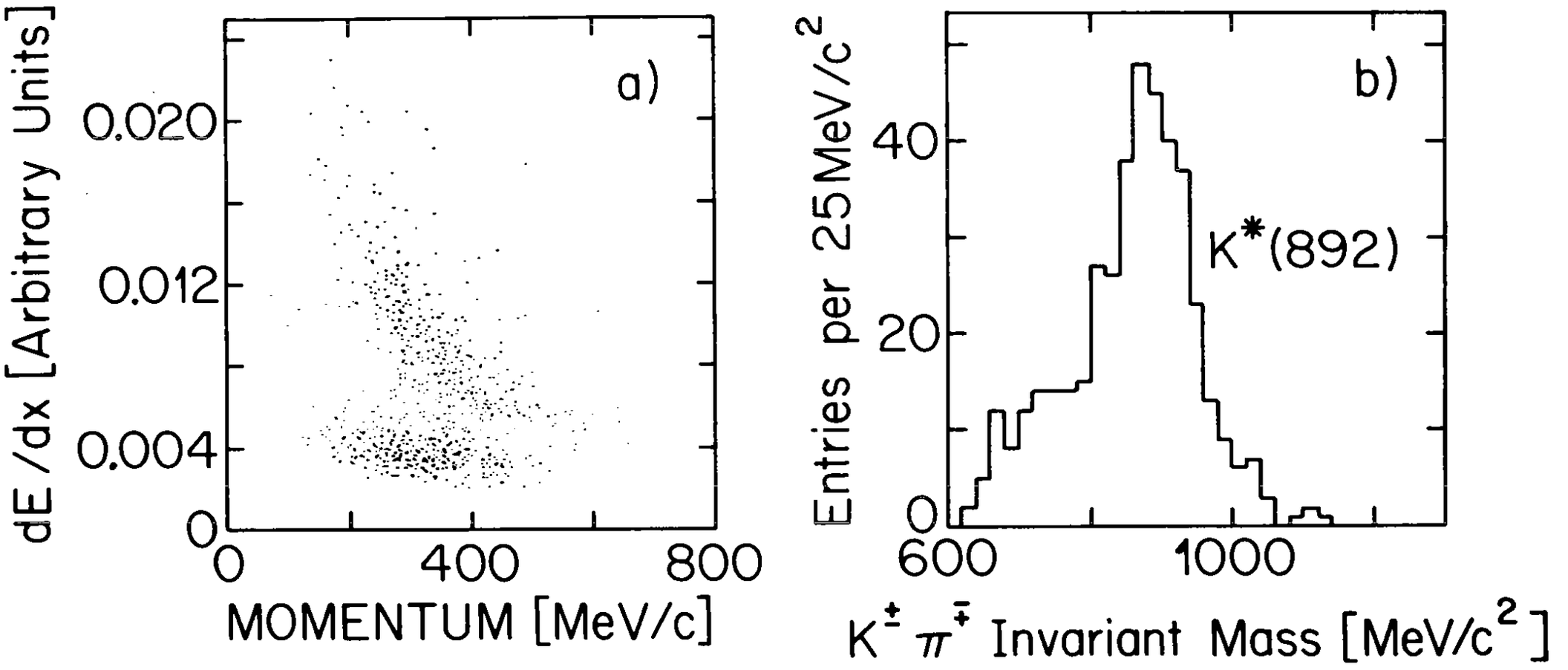
a)
dE/dx [Arbitrary Units]
0.020
0.012
0.004
0
0
400
800
MOMENTUM [MeV/c]
b)
Entries per 25MeV/c^2
40
20
0
600
1000
K*(892)
$K^{\pm}\pi^{\mp}$ Invariant Mass [MeV/c^2]

Figure 26

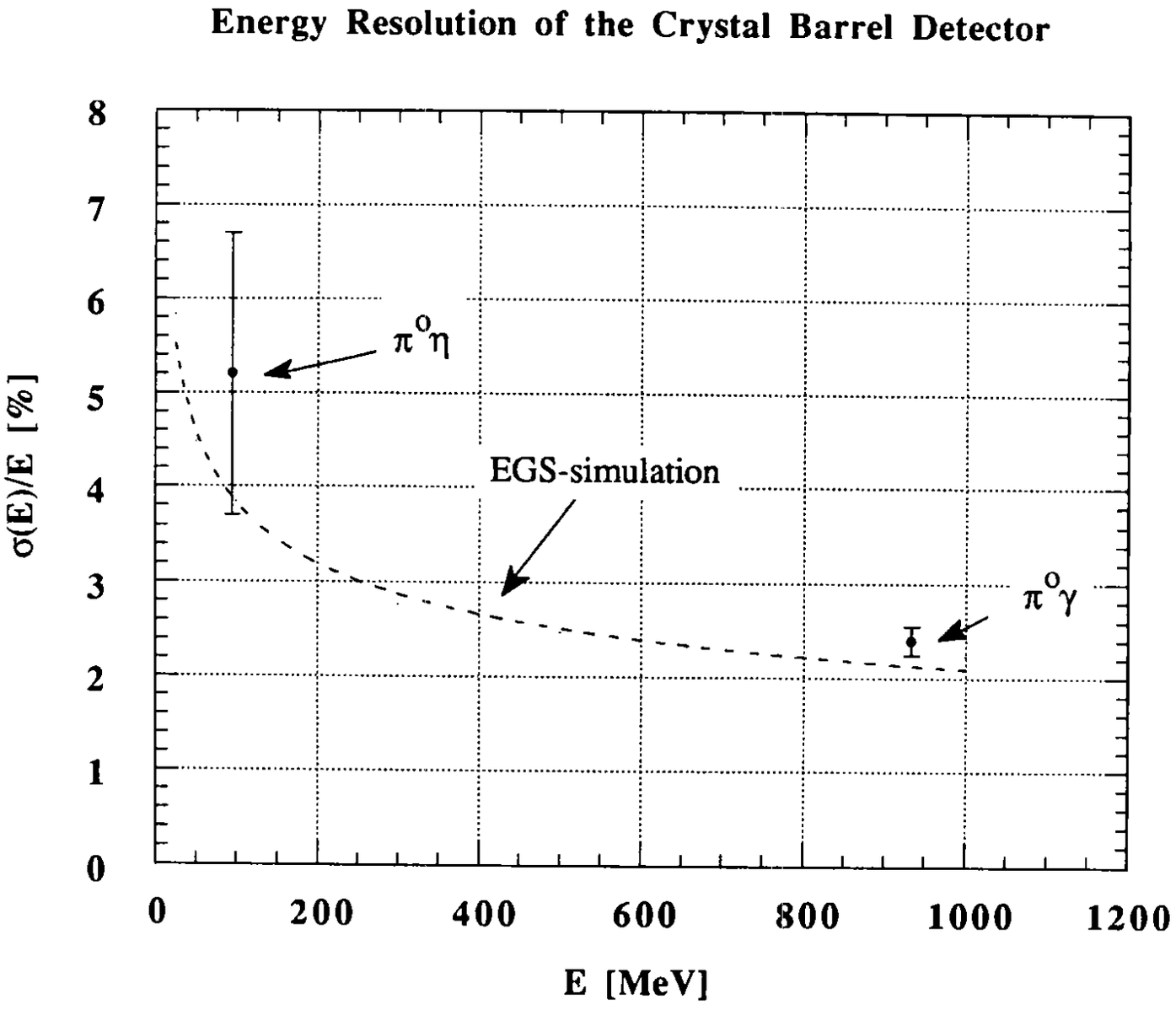
Energy Resolution of the Crystal Barrel Detector
σ(E)/E [%]
E [MeV]
π°η
EGS-simulation
π°γ
0
1
2
3
4
5
6
7
8
0
200
400
600
800
1000
1200

Figure 27

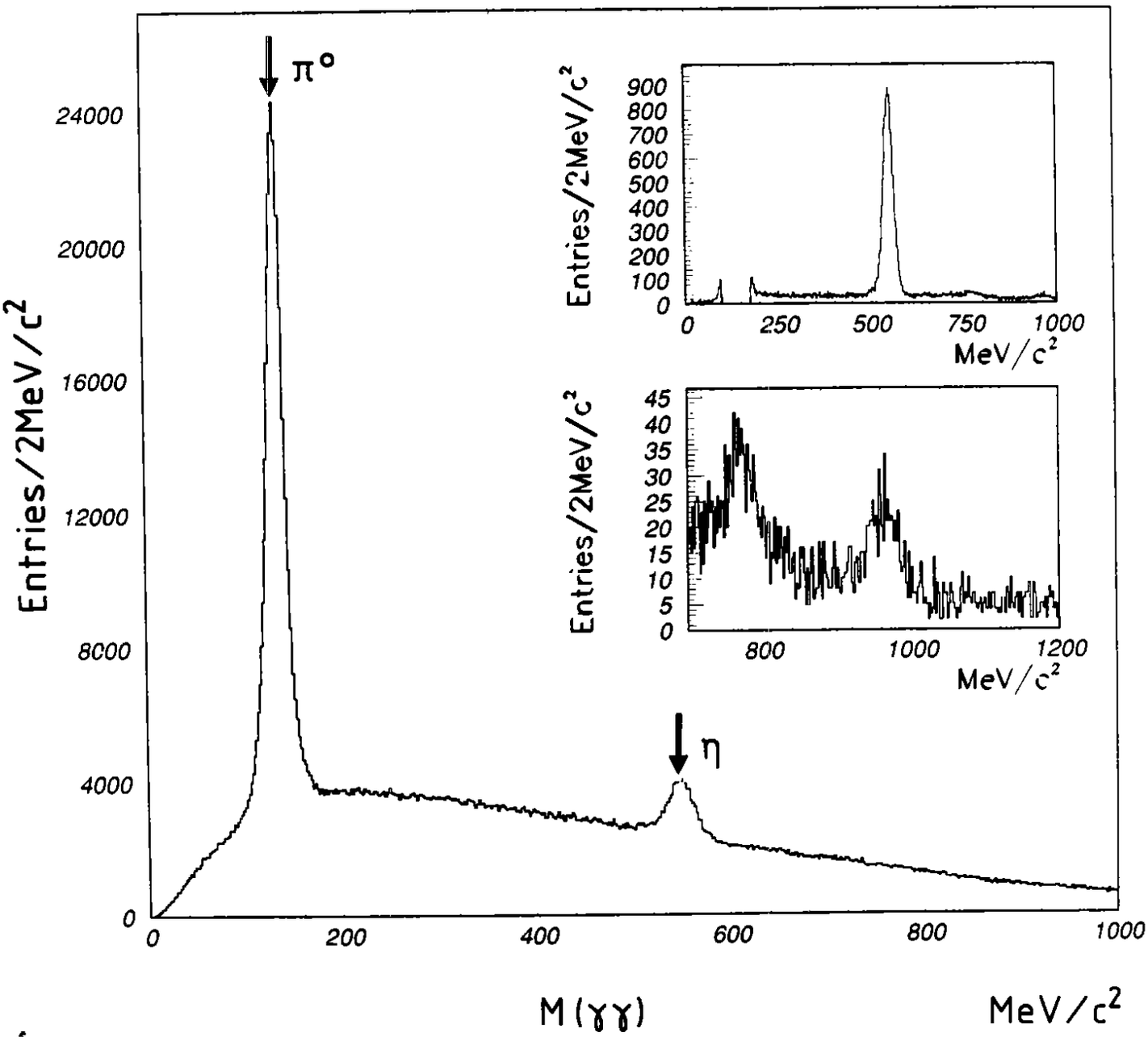
π°
η
Entries/2MeV/c²
M(γγ)
MeV/c²
0
4000
8000
12000
16000
20000
24000
0
200
400
600
800
1000
Entries/2MeV/c²
MeV/c²
0
100
200
300
400
500
600
700
800
900
0
250
500
750
1000
Entries/2MeV/c²
MeV/c²
0
5
10
15
20
25
30
35
40
45
800
1000
1200

Figure 28